2021-11-22

Spatiotemporal variability in field characterization of gas migration around energy wells

Fleming, Neil A.

UNIVERSITY OF CALGARY

Spatiotemporal variability in field characterization of gas migration around energy wells

by

Neil A. Fleming

A THESIS

SUBMITTED TO THE FACULTY OF GRADUATE STUDIES

IN PARTIAL FULFILMENT OF THE REQUIREMENTS FOR THE

DEGREE OF MASTER OF SCIENCE

GRADUATE PROGRAM IN GEOLOGY AND GEOPHYSICS

CALGARY, ALBERTA

NOVEMBER, 2021

Abstract

Fugitive methane gas migration outside the surface casing (GM) presents potential concerns for atmospheric greenhouse gas emissions, risk of explosion or asphyxiation, and groundwater quality impacts from the energy industry. The surface expression of gas migration, measured as an elevated concentration or efflux of natural gas (mostly methane), is relied upon for detecting well integrity failures resulting in GM. These measurements are complicated by spatiotemporal variation. This thesis presents two related field studies that investigate the presence and cause of this spatiotemporal variability in the surface expression of gas migration, and discuss the effects this may have on detection and impact assessment of wells with GM.

Firstly, the issue of variable gas migration test results is demonstrated by comparing historic GM tests conducted by multiple industry parties across six wells over 18 years. Testing method comparison indicated that GM detection is affected by measurement depth and spatially heterogeneous distributions of migrating gas at the well pad scale.

Next, field investigation at a case-study well in East-Central Alberta characterized the spatiotemporal variation in GM using repeated soil gas efflux measurements in combination with meteorological and soil parameters. The observed methane concentrations and effluxes were focused along preferential flow pathways within one meter of the wellhead, with temporal variation at second, hourly, and daily time scales. Methane efflux and concentrations were negatively correlated with wind speeds and air temperature. Total well pad scale emissions attributed to GM were estimated to be 350 g CH_4 d^{-1} (or 0.5 m^3 d^{-1}). Subsequent high-resolution CH_4 concentration measurements recorded temporal variability, both at ground surface and in the soil. Magnitude-order variations in effluxes and surface concentrations indicate potential error when using snapshot measurements to determine GM emissions or conducting risk assessments.

Together, these findings indicate that at this case study site, the presence of GM was reliably detected with established methods. Detection was improved with repeated measurements, greater in soil depths, or more sensitive detectors. Quantification of risks, emission rates, and tracking of temporal trends was only reliably assessed by long-term measurement. Consideration of findings may improve methods used in commercial measurement and future scientific study.

Laypersons Summary

Oil and gas well integrity failures resulting in fugitive methane gas migration outside of the well casing present environmental and safety concerns and are a financial liability. Field tests to identify and/or measure the rate of gas migration, and risk assessments, are challenged by variation in measured gas concentrations spatially across the well pad. Soil moisture and weather also cause changes to measured concentrations over time. Reliable detection and risk assessment depends on measuring representative concentrations or gas emissions around a well. However, methane concentration and emission rate measurements are highly affected by different testing approaches and parameters (e.g., testing depth, number of measurements conducted, and detector sensitivity).

This thesis compiles the results of two related field studies which recorded field-scale variations in gas migration, both as measured concentrations and emission rates. The results showed that gas concentrations will vary spatially across a well pad, and over time. Weather events such as rainfall and high winds negatively affected measured concentrations and emission rate estimation. Reliable detection of gas migration, and assessment of related risks and impacts, will be improved by considering this potential variability. Gas migration testing may benefit from more measurements spatially across the well pad to capture high-concentration zones, and/or by measuring with more sensitive detectors or in the soil at depth. Because of the natural variations in concentration and emission rates over time, long term measurements are needed to accurately estimate emission rates or quantify maximum potential soil gas concentrations. These findings have relevance to future gas migration detection efforts, and for quantifying emissions and risks related to gas migration.

Acknowledgments

This work was co-funded by the Petroleum Technology Alliance of Canada and the Natural Science and Engineering Research Council of Canada's Partnership Program. Research was also funded by the Canadian First Research Excellence Fund. I am thankful for the independent scholarships which allowed me to focus my efforts on this research, including the SPE Canadian Education Foundation Scholarship, Alberta Graduate Excellence Scholarship, John O. Galloway Memorial Scholarship and the University of Calgary Graduate Studies Scholarship, and the training and support through the Redevelop program.

The outcomes of this study would not have been possible without contributions from several parties in the energy industry. Firstly, I extend my gratitude to our anonymous industry partner who has provided access to a study well referenced throughout Chapters 3 and 4 of this thesis. I also wish the thank Aurora Land Consulting Ltd., CG Engineering Ltd., and The City of Medicine Hat who volunteered their time and expertise in development of the results presented in Chapter 2.

There are many individuals who I wish to thank for their support through this project. Firstly, I thank my academic supervisor, Cathy Ryan, for her advice and guidance, while giving me the freedom to independently learn. It has been a pleasure working in a research group led by someone who values the development of both good science and a good work-life balance. Secondly, I wish to thank my examination committee, who have generously offered to review my thesis and have contributed their insights and expertise to the work in this thesis throughout.

The academic success and enjoyment of my last few years has been thanks in large part to my colleagues for their willingness to share advice, insights, and days in the field. First and foremost, I wish to thank Tiago Morais who has been by my side every step of the way with an incredible enthusiasm for long days of fieldwork, commitment to the goals of the project, and logical approach to all the challenges we have faced. Several other members of the 'Gas and Groundwater' group, Evangeline Eldridge, Patrick Lagasca, Navreet Suri, Mary Zhang, and Shelly Alexander have been involved with various field work and project advice. Special thanks also go to Jason Abboud and Celia Kennedy for devoting their time and expertise to getting this

work started. Other volunteers in the field, including Dylan Cunningham and Joseph Leadley, contributed their expertise and effort to this project. Masaki Hayashi, Aaron Mohommed, Evan Sieben, and Jesse He lent equipment and insights that were invaluable to the project.

Thanks goes to Uli Mayer and Julia Soares from the University of British Colombia for the use of their gas flux equipment and advice and training in its use, and patience and assistance when processing the data.

Technical university staff have been very supportive of this project and my academic development and general enjoyment of time at the U of C. Thank you to Mike Nightengale for your mentoring on lab analysis techniques and insights and expertise into the gas migration problem, and to Steven Taylor and Veith Becker for the isotope analysis and training. Eric Mott and Farzin Malekani, thank you for your support of field work, analyses, and contagious enthusiasm in all aspects of the research process and academic life.

Finally, I wish to thank my wife, Carly, and the rest of my family for their support and encouragement though this process. At one point or another you have all assisted in preparing tools for the field, encouraged early mornings and late nights of work, and endured rambling monologues on bubbles. Thanks all!

Preface

This thesis consists of an introduction followed by two chapters, each of which presents a different field component of the research program. The field work was developed in collaboration with co-authors. All co-authors have given approval for this work to be included in the body of this thesis. Two of the chapters are also published or accepted as journal papers, with minor formatting changes in this thesis for consistency. No changes were made that would change the interpretation of presented findings. Introductory concepts and a background relevant to the research chapters are presented in Chapter 1, while a conclusion section in Chapter 4 summarises important findings and outcomes.

Chapter 2 presents the bulk scientific effort of this thesis, documenting the results of a field monitoring case-study of gas composition and efflux around and industry well with gas migration. Funding and supervision were shared by Cathryn Ryan and Uli Mayer. Study conceptualisation and eventual manuscript editing was shared by all authors. Field work was conducted in collaboration with Tiago Morais, with occasional contributions from other student volunteers. I led the field work organisation, data analysis and interpretation, wrote the initial manuscript, and led all manuscript revisions. Chapter 3 has been published as:

Fleming, N., Morais, T., Mayer, K.U., Ryan, M.C. 2021. Spatiotemporal variability of fugitive gas migration emissions around a petroleum well. Atmospheric Pollution Research. 12(6). 101094

Chapter 3 presents results from time series measurements of methane concentrations at multiple locations around a case-study well with gas migration. This work was conducted in collaboration with T. Morais, and supervised by M.C. Ryan. I led the study conceptualisation, field work, data analysis, and wrote the initial manuscript. All authors shared in editing the manuscript. Chapter 4 has been accepted for publication as:

Fleming, N. Morais, T. Ryan, M.C. 2021. Low-Cost Sensors Provide Insight into Temporal Variation in Fugitive Methane Gas Concentrations Around an Energy Well [Accepted by SPE Journal 2021-09-13; SJ-0621-0083]

Appendix 1 presents a detailed problem definition and motivation for the field studies based on the comparison of gas migration testing techniques and results around six industry

wells, using data collected from multiple industry partners. Study supervision and conceptualisation was shared by Celia Kennedy, and Cathryn Ryan. I conducted field work in collaboration with Tiago Morais and various industry partners. I analysed the data and led the presentation of this work. This work was presented at Geoconvention 2019 as:

Fleming, N., Morais, T., Kennedy, C., Ryan, M.C. 2019. Evaluation of SCVF and GM measurement approaches to detect fugitive gas migration around energy wells. Presented at Geoconvention 2019. Calgary, Canada. May 13-17 2019.

Table of Contents

Abstract ii
Laypersons Summary iii
Acknowledgments iv
Preface vi
Table of Contents viii
List of Tables xi
List of Figures xii
List of Abbreviations xiv
Chapter 1: Introduction 1
1.1 Motivation 1
1.2 Background 2
1.2.1 What is gas migration and surface casing vent flow? 2
1.2.2 Causes and occurrences of gas migration 3
1.2.3 Potential impacts 5
1.2.4 Relevant policy and regulation 9
1.2.5 Relevant characteristics of gas movement in saturated porous media 11
1.2.6 Relevant characteristics of gas movement in unsaturated porous media 13
1.2.7 Previous study of spatial and temporal variability in migrating gases 13
1.3 Problem Definition 15
1.4 Objectives and Thesis Organisation 17
Chapter 2: Spatiotemporal variability of fugitive gas migration emissions around a petroleum well 19
2.1 Abstract 19
2.2 Introduction 20
2.3 Materials and Methods 25
2.3.1 Field site description 25
2.3.2 Methane concentration measurements using standard industry practices 28
2.3.3 Soil gas sampling and analysis 29
2.3.4 Soil gas efflux measurements 32
2.3.5 Environmental measurements 34
2.3.6 Descriptive statistics of CH_4 and CO_2 concentration and efflux analysis 35

2.3.6.1 Regression modelling 35
2.3.6.2 Geostatistical interpolation 37
2.4 Results 38
2.4.1 Methane concentration surveys: 38
2.4.2 Gas efflux survey results 38
2.4.3 High frequency efflux measurement 41
2.4.4 Multivariate regression modelling of high-resolution methane efflux and concentration measurements 43
2.4.5 Soil Gas analysis results 46
2.5 Discussion 48
2.5.1 Gas source and mixing implications 48
2.5.2 Spatial distribution of migrating gases 49
2.5.3 Total CH_4 emissions and other impacts 51
2.5.4 Temporal variability in measured effluxes and concentrations: 56
2.5.5 Wind influences on variations in measured efflux 59
2.5.6 Methane oxidation in the unsaturated zone 61
2.5.7 Implications for gas migration testing and future scientific study 63
2.6 Conclusions 67
Chapter 3: Low-cost sensors provide insight into temporal variation in fugitive methane gas concentrations around an energy well 70
3.1 Abstract 70
3.2 Introduction 71
3.3 Materials and Methods 76
3.3.1 Study well description. 76
3.3.2 Sensor measurement of methane concentration. 78
3.3.3 Meteorological data collection during monitoring period. 81
3.3.4 Data processing. 81
3.4 Results and Discussion 82
3.4.1 Meteorological conditions over the monitoring period. 82
3.4.2 Time series methane concentrations response. 85
3.4.3 Change in observed distribution of methane concentrations and implications in gas movement behavior associated with a precipitation event. 88
3.4.4 Temporal variability patterns as a function of depth and location. 90

3.4.5 Methane concentration correlation to meteorological factors. 92
3.4.6 Implications for gas migration detection and risk assessment. 97
3.5 Conclusion 103
Chapter 4: Conclusion 105
4.1 Summary 105
4.2 Methane emissions and other risks resulting from gas migration 107
4.3 Implications for detection and quantification of gas migration outside the surface casing 110
References 112
Appendices A-1
Appendix A Problem Definition: A Field comparison of gas migration testing methodologies A-1
Appendix B Supplementary information for Appendix A: Field comparison of gas migration testing methodologies B-14
Appendix C Supplementary information for Chapter 2: Spatiotemporal variability of fugitive gas migration emissions around a petroleum well C-16
Appendix D Supplementary information for Chapter 3: Low-cost sensors provide insight into temporal variation in fugitive methane gas concentrations around an energy well D-18
Appendix D.1 Sensor description and field installation D-18
Appendix D.2 Sensor calibration.... D-3
Appendix D.3 Baseline noise and sensor response tests.... D-5
Appendix D.4 Supplementary field data and discussion D-9
Appendix E Supplementary field site characterization data E-1
Appendix E.1 Hydraulic Conductivities E-1
Appendix E.2 Soil gas concentration surveys E-3
Appendix F Barometric efficiency applications to migrating free-phase gas monitoring . F-1

List of Tables

Table 2.1 Descriptive statistics of Oct 11-27th, 2019 high resolution efflux measurement series with chamber locations described in distance (m) and direction.....42

Table 2.2 Parameters most influencing the statistical model for the first three steps of forward stepwise multivariate generalized additive modelling of pre-closure CH_4 chamber concentrations at each long-term location. 45

Table 2.3 Pearson correlation matrix of soil gas compositions at the 30 cm depth around the gas migration test well.....46

Table 2.4 Estimated total GM-related CH_4 emissions at this study site. Values are average effluxes (with upper, lower 95% confidence interval where available).....53

Table 2.5 Previously reported literature values for emissions resulting from well integrity failure, and comparison with other anthropogenic and natural CH_4 sources/sinks. 54

Table 3.1 Pearson correlation coefficients (r) between methane concentrations at each sensor (where the proximal arrays labelled as West or East of energy well,.....93

Table 3.2 Detection success rate (% of measurements that would have been above a given detection limit lower cut-off), for one-minute-frequency daytime measurements during working hours (07:00 to 18:00) over 19 days. 98

List of Figures

Figure 1.1 Histogram of Surface Casing Vent Flow (SCVF) rate (top) and cumulative total daily emissions with respect to rank ordered flow rate (bottom) for all open (reported but not successfully repaired) SCVF reports in Alberta as of 2018-05-30.. 7

Figure 2.1 Conceptual model of gas migration (GM) and surface casing vent flow (SCVF) (After Bachu, 2017) 22

Figure 2.2 The maximum recorded combustible gas concentration as ppm CH_4 (log scale) from all available gas migration testing conducted at the study well.....27

Figure 2.3 a) Overview of Alberta with all petroleum wells with open (i.e., detected but not repaired) reports of external gas migration as of 2018-05-30 b) Full scale and c) close-up plan view schematic of the efflux monitoring network at the study well pad 28

Figure 2.4 Plan view of efflux survey results for CH_4 (top row) and CO_2 (bottom row) measured in µmol m^2 s^{-1} on Aug 20, 2019 (PM; left hand side) and Sep 25. 2019 (AM; right hand side)...40

Figure 2.5 Time series of measured chamber pre-closure CH_4 concentrations (µmol mol^{-1}), CH_4 effluxes (µmol m^{-2} s^{-1}), and CO_2 effluxes (µmol m^{-2} s^{-1}) for three locations. 41

Figure 2.6 Wellhead chamber time series of CH_4 efflux from Oct 11-27th, 2019 with raw data (black dots), 20-point rolling median smoothing (yellow line) and multivariate regression modelling results (blue). 43

Figure 2.7 Selected scatterplot distributions of soil gas results at the 30 cm depth across five sampling events (% composition by volume), with lighter colors corresponding to increasing radial distance from the energy well. 46

Figure 3.1 Boxplot showing the relative occurrence of C1 (methane), C2 (ethane), and C3+ in combustible soil gas compositions. 78

Figure 3.2 Case study site cross section conceptual diagram showing the methane migration along the wellbore and underneath a low-permeability layer (After Forde et al., 2019a). 81

Figure 3.3 Water level in meters below ground surface (m below ground surface), and selected meteorological data from the nearest public weather station 84

Figure 3.4 One-minute frequency soil methane concentration boxplots (log ppm CH_4) plotted with depth and separated by sensor array location (East, West and Distal Control) 86

Figure 3.5 Time series of hourly averaged methane concentrations (ppm) around an energy well with gas migration observed between October 3-22, 2020.. 88

Figure 3.6 Methane concentration (ppm) time series plotted with one-minute measurement frequency over 24 hours for three depths 5 cm from the East side of the casing of an energy well with gas migration.....91

Figure A1 Maximum combustible gas concentrations (reported in ppm as CH_4) from each individual GM test conducted using eight different testing methods across six separate industry parties between 2000 and 2018 for six energy wells with gas migration……A-6
Figure A2 Boxplot showing the minimum, first quartile, median, 3rd quartile, and maximum recorded methane concentration test values (ppm CH_4) for all tests conducted at the same "cut-and-capped" energy well (Test well 3; Figure A1)..... A-9

Figure A3 Plan view soil-surface combustible gas concentration as ppmv CH4 above background air concentration around a surface-abandoned industry well with known GM (Test Well 3; Figure A1). Surveys were conducted on a two by two m grid, repeated one day apart (on November 2 and 3, 2019 for the left and right figure, respectively). Inverse Distance Weighting spatial interpolation shows 'hotspot' zones of higher concentration.....A-10

Figure A4 Comparison of CH_4 concentration around a single energy well measured using three different GM measurement methods for two different sample sets, including A) data from 12 measurement locations B) which included four measurements within 30 cm of the well casing (in addition to those at 2, 4 and 6 m distances from the well; AER, 2021).....A-11

List of Abbreviations

Abbreviation	Definition
AER	Alberta Energy Regulator
BCOGC	British Colombia Oil and Gas Commission
BGS	Below Ground Surface
GM	Gas Migration
ND	Non-Detect
SAP	Sustained Annular Pressure
SCVF	Surface Casing Vent Flow
ppm	Parts Per Million

Chapter 1: **Introduction**

1.1 Motivation

Gas migration outside the surface casing (GM) occurs when a well integrity failure results in the movement of natural gas from a subsurface source to the ground surface outside the outermost casing of a well, with corresponding negative impacts. Atmospheric emission of methane is an environmental concern since it is a potent greenhouse gas (e.g., IPCC, 2013). Groundwater quality impacts are a concern for well water users (e.g., Osborn et al, 2011), and in some cases gas migration can cause land use impacts (e.g., Noomen et al., 2012). Further, wells with GM cannot be legally abandoned (depending on the jurisdiction), presenting liabilities for the energy industry and the public purse (e.g., BCOGC 2019; AER 2021; Schiffner et al., 2021).

In preference to more easily obtained concentration measurements, GM emissions (i.e., effluxes) are currently rarely measured outside of academic settings due to technical difficulty in measurement and an absence of regulatory requirement. There is also uncertainty on the total number of wells with GM (Abboud et al., 2020). This leads to uncertainty in total GM contributions to upstream oil and gas greenhouse emissions. The behavior of free phase methane migrating through soils at sites with GM also has important implications for testing procedures since most GM detection and risk assessment is based on the measurement of methane concentrations around the well. Knowledge gaps exist in quantifying the emission rates and behaviors from these sources and validating existing and recommended testing procedures. Continued work is also needed to relate the conceptual understanding of gas migration, developed primarily through shallow controlled injection field projects (Cahill et al., 2017, 2018; Soares, 2019; Chao et al., 2020), numerical modelling (Nowamooz et al., 2015; Roy et al., 2016;

Schout et al., 2019), and laboratory studies (Chamindu Deepagoda et al., 2016; Van de Ven et al., 2020; Van de Ven & Mumford, 2020), to circumstances of GM around operational petroleum wells.

Concentrations and effluxes of methane around wells with gas migration have been observed to vary spatially and over time (Yin et al., 2014; Forde et al., 2019a), however the extent and causal mechanisms of this variation around industry wells has not been fully examined, nor has this observed variation been related back to perceived impacts on successful GM detection by industry practitioners. GM management decisions derived from standard industry testing procedures require an understanding of the potential spatiotemporal variability in the actual concentrations and effluxes before reliable interpretations can be made regarding methane concentrations or efflux, comparisons of GM testing approaches, comparisons of GM between wells, and/or comparisons at a single well over time.

1.2 Background

1.2.1 What is gas migration and surface casing vent flow?

Energy wells are constructed to produce hydrocarbons such as oil, liquid, or gas at surface, commonly via a production pipe or tubing surrounded by a series of progressively larger nested pipes, known as well casings (Dusseault & Jackson 2014). Fluids that are present at ground surface outside of the production casing are a sign of well integrity failure. Migrating fluids are commonly free-phase natural gas originating from intermediate-depth formations (Szatkowski et al., 2002; Tilley and Muehlenbachs, 2012). This gas is composed primarily of methane (CH_4), with minor amounts of ethane (C_2H_4), propane (C_3H_6) and other volatile hydrocarbons, with fresh or saline water vent flows occasionally reported also (Dussault &

Jackson, 2014; Bachu 2017). For the purpose of this section, the term ‘gas’ is used to refer to this free-phase migrating natural gas. Similarly, the term ‘fugitive’ gases (or ‘fugitive methane’) are meant to refer to gases that do not travel up the production casing, as intended by the well construction. Well integrity failures include surface casing vent flows (SCVF; where fugitive gases leak through the surface casing directly into the atmosphere), and fugitive gas migration (GM; where gases migrate from a gas-charged stratigraphic interval and exit at ground surface outside of the outermost well casing).

1.2.2 Causes and occurrences of gas migration

Migrating gas is not only the symptom, but can also be the initial cause of well integrity issues. For instance, gases can cause micro-channeling during primary well cementing (Bol et al., 1991). They can also exploit pathways between the cement and casing, cement and formation, or through natural or induced fractures/annuli in the cement or formation. After cement setting (and subsequent cement shrinkage), these pathways can provide an imperfect seal between the surface and subsurface environment (Bol et al., 1991; Dusseault et al., 2000; Vidic et al., 2013; Dussault & Jackson, 2014). The occurrence of GM and SCVF is highly dependant on both geologic factors (such as the presence and depth of a gas-charged formation; Jackson, 2014; Bachu, 2017) and well drilling and completion factors (such as the cement grade and weighting used to cover these formations; Dusseault et al., 2000). Since the migrating gas source is often not from the producing oil/gas formation (Szatkowski et al., 2002; Tilley and Muehlenbachs, 2012; Bachu, 2017), the recent increase in the use of horizontal drilling and high-volume multi-stage hydraulic fracturing technology to exploit low-permeability reservoirs is thought to have little direct influence on the occurrence of GM (though an overall increase in

drilling activity in a region would be related; Vidic et al., 2013; Dussault & Jackson, 2014). GM and SCVF occurrence have been correlated to well factors such as age, depth, deviation from vertical, and fluid production type (Watson & Bachu, 2009; Bachu 2017). While the causal mechanisms through which GM occurs are increasingly well understood, the variability in geological setting and drilling conditions lead to difficulty in predicting GM occurrence on a case-wise basis (Vidic et al., 2013; Montague et al., 2018; Sandl et al., 2021). This uncertainty necessitates direct testing for the presence or absence of well integrity failures.

In Alberta, Bachu (2017) reports that 0.73% of all ~ 450,000 wells as of 2013 had recorded cases of GM, though a recent review by Abboud et al. (2020) estimated that GM tests have only been required by regulations on 3.5% of Alberta's >450,000 petroleum wells, and therefore the actual number of wells with GM may be higher. Though typically addressed only for petroleum wells in literature, this type of leakage can occur in any drilling activity that may extend into the depths where gas zones may be present (which, in certain regions of the province of Alberta are < 200 m below ground surface; Rowe & Muehlenbachs, 1999; Hoch, 2005; Bachu 2017). For example, wells for water supply or disposal, and emerging industries such as geothermal heat exchange are not necessarily exempt from issues of active gas migration and surface casing vent flow that are commonly associated with the petroleum industry (D'Aniello et al., 2020). Failure to properly address the potential for GM and SCVF in these wells could represent an underestimation of the potential risks and impacts associated with these industries.

GM and SCVF are ideally resolved though well repair, typically where the micro-annuli are plugged with squeeze cementing or similar technologies (Dusseault & Jackson, 2014).

Repairing well integrity failures that result in gas migration incurs a financial cost of at least $CAN 150,000 per well, though this cost substantially increases if gas migration is initially not detected and repaired and the well must be re-entered post-decommissioning to complete the repair (Dusseault et al., 2014; Trudel et al., 2019).

1.2.3 Potential impacts

The potential impacts of SCVF and GM are similar, though in the case of GM the gas is presumed to have migrated through, and potentially interacted with, a zone of useable groundwater. The potential impacts of these well integrity failures largely fall within three categories:

i) Atmospheric emissions: Methane, the primary component of GM and SCVF, is a greenhouse gas with a global warming potential 28 times more potent by mass compared to carbon dioxide over a period of 100 years (IPCC, 2013). The global warming potential of CH_4 is 84 times that of CO_2 over a period of 20 years, representing a disproportionate short-term effect (IPCC, 2013). Global efforts have recognized anthropogenic methane emissions as an important contribution to atmospheric greenhouse gas increases leading to climate change. Within Alberta, there is specific focus on decreasing methane emissions from the upstream petroleum sector, with a 45% intended reduction of 2012 emissions by 2025 (Government of Alberta, 2015). Methane also impacts air quality, specifically in urban areas, where it may contribute as a precursor to tropospheric ozone which is associated with negative respiratory effects, though GM may be a relatively small factor compared to other sources (West et al., 2006; Jerrett et al., 2009; Anenberg et al., 2012). Methane emissions from SCVF and GM are poorly quantified globally, including in Alberta (Abboud et al., 2020) and Pennsylvania (Kang et al., 2016), but where

reported, emission rates from individual wells are, on average, thought to be relatively low compared to other anthropogenic and natural sources (Schmitz et al., 1993; Erno & Schmitz, 1996; Kang et al., 2014; Townsend-Small et al., 2016).

Methane has been recognized as an important overall contributor to global anthropogenic greenhouse gas emissions, and estimated sources from the upstream oil and gas industry are significant (representing 26% of Canada's total greenhouse gas emissions in 2018; Environment and Climate Change Canada, 2018). Emission measurements indicate a disparity between industry-reported 'bottom-up' (measured and reported emissions) and 'top-down' (satellite or aerially based measurements), showing some emissions are poorly quantified and under-reported (Vidic et al., 2013; Johnson et al., 2017). In addition, the statistical distribution of emissions is typically heavily skewed, with infrequent large values. These 'super-emitters' account for a large majority of total emissions, and within any single source the emissions are concentrated within a small spatial area or time period which may be poorly characterized with short-term and spatially discrete measurements (Lan et al., 2015; Lavoie et al., 2015; Riddick et al., 2020). This statistical distribution is also seen for reported SCVF's in Alberta, where the relatively numerous low-flow SCVF's contribute a proportionally minor volume to the total daily methane emissions caused by SCVF's (Figure 1.1). Spatially discrete emission detection and quantification at a well pad scale will also be complicated by the presence of surface equipment (with potential emission contributions) and likely preferential migration pathways around this equipment in the subsurface (Erno and Schmitz, 1996; Fox et al., 2019). Taken together, this indicates that adequate quantification of fugitive emission sources, including GM and SCVF, and rapid

identification and repair of high-emission sources, will allow for the largest positive impact towards reducing methane emissions from these sources.

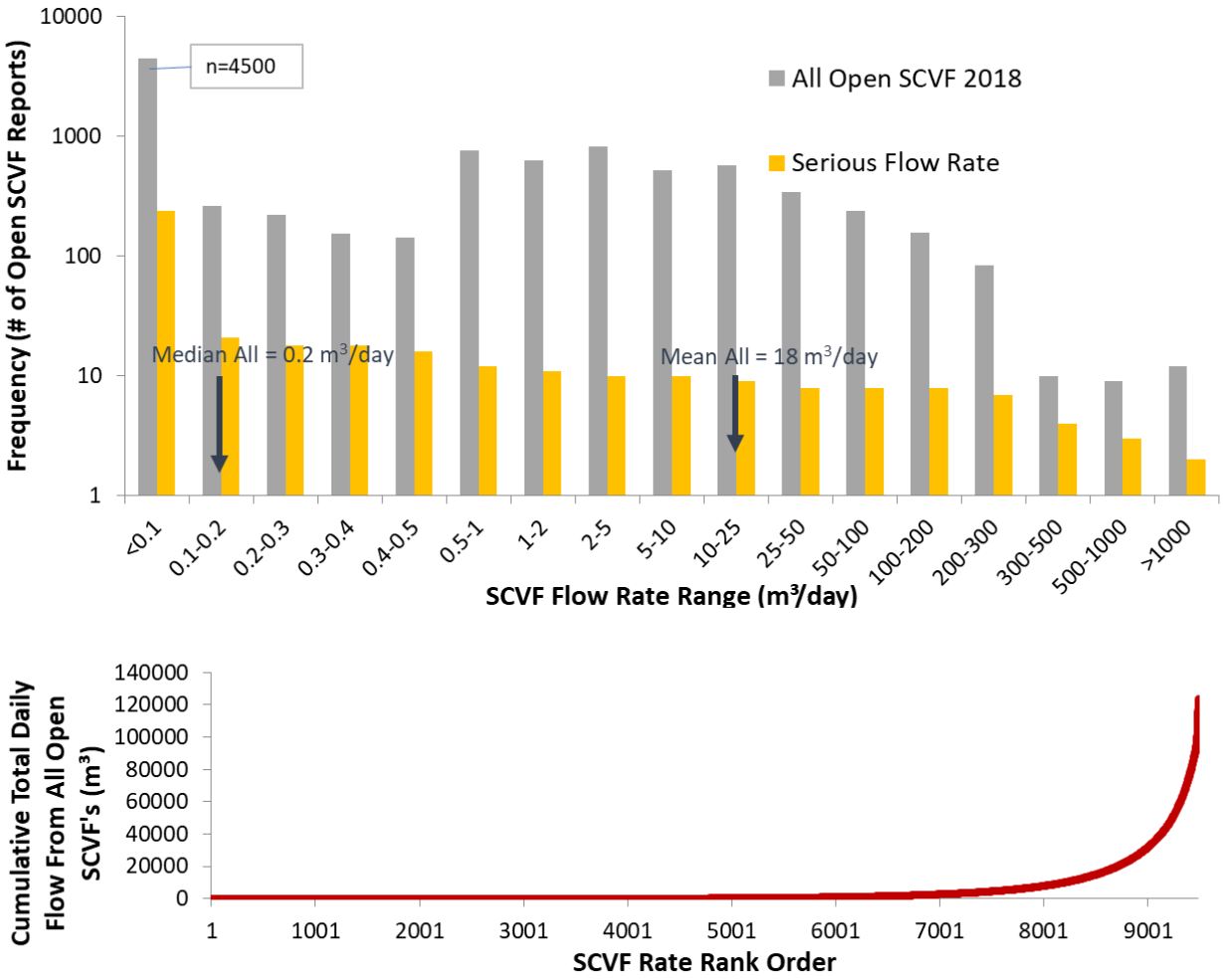

Figure 1.1 Histogram of Surface Casing Vent Flow (SCVF) rate (top) and cumulative total daily emissions with respect to rank ordered flow rate (bottom) for all open (reported but not successfully repaired) SCVF reports in Alberta as of 2018-05-30. Data on the 9493 SCVF's was obtained from the Alberta Energy Regulator Vent Flow/Gas Migration Digital Data Submission database **(**AER 2018). SCVF's are defined by the regulator as 'serious' based on a flow rate > 300 m^3/d, or due to the presence of H_2S or non-freshwater liquid (AER 2021).

ii) Groundwater quality: Dissolved methane can alter the chemical conditions of groundwater including master variables such as Eh and pH, potentially mobilizing metals, form hydrogen sulfide gas, or later exsolve when groundwater is pumped for residential or commercial use (Kelly et al., 1985; Gorody, 2012; Cahill et al., 2017). Peer-reviewed studies have recorded gas-migration resulting from oil and gas activity impacting groundwater, and show that wellbores can provide the necessary migration pathways to introduce natural gas into shallow groundwater where geochemical changes will occur (Kelly et al., 1985; Osborn et al, 2011; Tilley & Muelenbachs, 2012; Roy et al., 2016). It is important to note that methane itself is naturally ubiquitous in many groundwaters (such as in Alberta, the St. Lawrence Lowlands. and Pennsylvania; Pinti et al., 2013; Humez et al., 2016; Tilley & Muehlenbachs, 2011; Vidic et al., 2013). Methane itself does not pose a clear hazard to drinking water quality, with no stated drinking water quality guideline in Canada and limited peer-reviewed evidence of low-concentration health effects (Vidic et al., 2013; Health Canada, 2019). Widespread public concern around the invasion of usable groundwater by methane may be related with the risk of explosion (see below), and due to conflation with other potential groundwater quality impacts from the oil and gas industry (potentially related to hydraulic fracturing; Vidic et al., 2013; Dusseault et al., 2014; Barth-Naftilan et al., 2018).

If unoxided, the dissolved methane may eventually be introduced into the atmosphere. Where groundwater is pumped to the surface for use, the dissolved CH_4 will begin to exsolve and should these gases accumulate, explosive or asphyxiating gas mixtures may develop in pumphouses, residences, or other facilities (Alberta Government, 2006; Engelder &

Zevenbergen, 2018). Exsolved gases would also contribute to atmospheric emissions impacts as described above.

iii) Land use impacts: The potential for asphyxiating or explosive gas mixtures necessitate safely guidelines which prevent structures being built near migrating gases, and excess methane and/or carbon dioxide may displace soil oxygen and impact plant or crop health (Williams & Aitkenhead, 1991; Noomen et al., 2012; Sihota et al., 2013; Engelder & Zevenbergen, 2018). Subsurface sources of migrating gas may accumulate in structures and build to concentrations that may cause explosive or asphyxiating hazards (Sihota et al., 2013). Methane gas at concentrations between 5-15% v/v is explosive in a mixture with air (Molofsky et al., 2021). Concerns related to explosive methane concentrations near wellheads are currently addressed through setback regulations stipulating the distance between structures and facilities such as decommissioned wells (e.g., Directive 079; AER, 2014). Plants require soil oxygen, and therefore significant displacement of oxygen by CH_4, or its oxidation product CO_2, may cause impacts to plant vitality (Brady & Weil, 2002). Visually apparent impacts to plants depend on the individual plant susceptibility, making impacts of gas migration potentially obvious in croplands with otherwise uniform appearance (Jackson & Attwood, 1996).

1.2.4 Relevant policy and regulation

As of the release of this thesis, in Alberta GM testing is required within 90 days of drilling rig release and on all abandonments in the required testing area (Figure 3.3 a), and outside of this area on all cased-hole abandonments lacking a surface casing vent assembly (AER 2021, AER 2003). Other jurisdictions may have other stipulations, such as requiring testing only

when GM is indicated by drilling problems or sensory evidence such as odour, bubbling or vegetation impacts (BCOGC, 2019). Current Alberta regulation places priority to repairing 'serious' cases (non-freshwater liquid SCVF, SCVF gas flow rates >300 m^3/d, any presence of H_2S, and GM deemed to have potential to impact the environment or human health). These cases must be repaired within 90 days of discovery, while non-serious cases may be addressed at the time of decommissioning/abandonment (AER, 2003).

In Alberta the surface casing installation is currently required to a depth below usable groundwater (defined as <4000 mg/L total dissolved solids; AER Directive 008), with cement completion across the full depth (AER Directive 009; AER, 2021). Beginning in 2011, the surface casing was mandatorily vented to the atmosphere using a surface casing vent assembly (thereby preventing pressure build-up within the surface casing annulus; ERCB, 2011). In jurisdictions without a vented surface casing (or older wells in AB), SCVF would manifest as Sustained Annular Pressure (SAP), also known as Sustained Casing Pressure, which may induce more frequent and/or increased GM rates (Dusseault & Jackson, 2014; Lackey & Rajaram, 2019) or explosions (Engelder et al., 2018).

Tests for SCVF or SAP are comparatively simple when a surface casing vent assembly or external fitting exists, since a pressure or gas flow measurement can be made directly from the casing vent or valve. GM flows out of the soil are typically unperceptively low to human senses and common gas flow meters. Therefore, GM detection has historically relied on measurement of anomalous methane concentrations in soil gases around a well, or associated indications such

as bubbling or visually obvious vegetation impacts (Noomen et al., 2012; BCOGC, 2019; AER 2021). Current testing requirements for GM in Alberta (and similar in other jurisdictions) refer to methods developed in the 1990's developed to assess the presence or absence of GM, with no intention or capacity to quantify magnitude of leakage or associated risk (Drilling and Completions Committee, 1993; Abboud et al., 2020; AER 2021). The current recommended approach for GM detection in Alberta (and largely replicated in similar jurisdictions including British Colombia, Saskatchewan, Northwest Territories, and Newfoundland & Labrador) involves a single methane (or 'combustible soil gas') concentration measurement at 50 cm depth at locations 0.3, 2, 4, and 6 m radially from the wellhead in four directions, for a total of 14 methane concentration measurements. (The measurement pattern thus forming a 'bulls-eye' or cross pattern centered around the wellhead). Operators or service companies are permitted to use other techniques, including combustible gas detection at ground-surface. Factors affecting costs and feasibility of subsurface testing for gas migration include the requirement of ground-disturbance permitting and locating subsurface infrastructure for any subsurface testing below a specified depth (30 cm in Alberta; Pipeline Act, 2020).

1.2.5 Relevant characteristics of gas movement in saturated porous media

As illustrated by many previous authors, the movement of migrating gas, or indeed any fluid, requires a gas source, driving force, and migration pathway (e.g., Roy et al., 2016). Isotopic and compositional fingerprinting of migrating gases frequently identify their source as intermediate level gas-bearing formations such as overlying shales or coals rather than the producing zone of hydrocarbon wells, with some exceptions (Rowe & Muehlenbachs, 1999; Tilley & Muehlenbachs, 2012; Bachu, 2017). These intermediate-depth gas-bearing formations

may be covered in the well annulus by a lesser grade of cement than the producing formation and are generally less well characterized compared to producing or shallow formations due to low economic potential (Dussault & Jackson, 2014; Hammond, 2016). In the case of gas migration, the driving force for the upwards migration of gas from these typical intermediate gas-bearing formations is buoyancy due to the density differences between water and free gas (Roy et al., 2016; Woods and Norris, 2016; Van de Ven et al., 2020). Groundwater flow direction is predicted to have relatively little impact on the migration pathway of vertically travelling free-phase gases due to the large difference in magnitude between buoyancy and lateral groundwater movement forces (Cahill et al., 2017). Capillary barriers in the saturated zone, however, strongly control the movement of buoyant gases due to the higher entry pressure required for gas to travel through smaller pore spaces (Gurevich et al., 1993; Van de Ven et al., 2020; Chao et al., 2020). For this reason, free-phase gas may accumulate beneath, and disperse laterally under, a low-permeability barrier such as a shale layer or clay-rich glacial till (Woods and Norris, 2016; Forde et al., 2018). This interaction of capillary and buoyancy forces has been observed to result in episodic release of gas through ebullition, despite a constant gas source at depth (Van de Ven et al., 2020).

Preferential migration pathways will develop where larger connected pore spaces exist, such as in natural or drilling-induced fractures or, more commonly for GM, in the annulus that may exist between the casing and cement or the cement and borehole wall (Gurevich et al., 1993). These micro-annuli formed in the cement of petroleum wells are through to commonly present the most likely migration pathway, often due to issues during the primary cementing of the wellbore or during cement shrinkage (Dusseault & Jackson, 2014). The combination of

upward, buoyant gas movement, and a higher-permeability migration pathway along the wellbore is attributed to the frequent observation in anecdotal and published reports of the most obvious indications of GM (i.e., bubbling, highest gas concentrations and effluxes) within < 1 m of the well casing (Erno & Schmidt 1996; Lyman et al., 2017). The exception to this may be in regions of clay till or other prominent low-permeability stratigraphy, where capillary barriers may drive the primary migration pathway further from the well casing (Forde et al., 2019; Chao et al., 2020).

1.2.6 Relevant characteristics of gas movement in unsaturated porous media

Within the unsaturated zone, diffusion of gases is much more important in comparison to the saturated zone since methane diffusion rates are ~ 10 000 faster in air compared to water (Rumble et al., 2020). The different molecular weights of individual gas species can cause moderate gas movement due to relative density effects, where lower density gases (e.g., CH_4) may migrate vertically upwards through soils at a higher rate than denser gases (e.g., CO_2) (Chamindu-Deepagoda et al., 2016). Pressure differences between regions of soil gas, and between soil gas and the atmosphere, also induce advective gas movement. This advective movement may be impacted by varying meteorological and subsurface conditions including barometric pressure changes (Forde et al., 2019b) atmospheric temperature (Nachson et al., 2011), and wind-induced pressure fluctuations (Poulsen & Møldrup, 2006).

1.2.7 Previous study of spatial and temporal variability in migrating gases

Temporal variability in some SCVF rates have been well documented since at least 1996 (Erno & Schmitz, 1996) and recent advances in high-resolution flow measurement and recording clearly indicate that some flow rates will vary over the period of hours to days (Dusseault &

Jackson, 2014; Riddick et al., 2020). Spatial and temporal variability in gas transport through groundwater and soils is well documented in many fields in the earth and biological sciences, including landfill emission studies (e.g., Börjesson & Svensson 1997; Poulsen, & Møldrup 2006), ecological studies of forests and peatlands (e.g., Tokida et al., 2007; Baldocchi et al., 2012), and others including controlled injection experiments (e.g., Cahill et al., 2018; Ulrich et al., 2020). Seepage of natural gases from deep geologic sources through apparently natural pathways have been shown to occur at discrete locations, and to be spatially and temporally variable (Tang et al., 2008; Frederick et al., 2017; Oliveira et al., 2018). More recently, authors have begun to document spatial and temporal variability in measured GM fluxes and soil concentrations around petroleum wells (Yin et al., 2014; Forde et al., 2019a; Schout et al., 2019; Riddick et al., 2020).

Barometric pressure decreases have been shown to cause increasing methane effluxes out of peatlands, landfills, and during artificial injection experiments of methane into the unsaturated zone, where decreasing barometric pressure causes a pressure differential between the soil gas and atmosphere and therefore increased gas efflux (Tokida et al., 2007; Abbas et al., 2010; Forde et al., 2019b). These authors report that barometric variations in soil gas efflux are more significant in areas with thicker unsaturated zones. Pressure variations produce a zone of penetration of atmospheric air, on top of an oscillation zone where gases are not displaced or mixed with atmospheric air. The thicknesses of these oscillation zones are proportional to the total unsaturated zone thickness (Abbas et al., 2010; Forde et al., 2019b).

Daily variations in soil gas movement can also be caused by diurnal variations in vegetative gas production (Raymond & Jarvis, 2000), microbial activity (Börjesson & Svensson, 2000), and temperature (Nachshon et al., 2011).

Finally, the dissolution and oxidation of migrating gases in the saturated zone (Roy et al., 2016; Forde et al., 2018) and oxidation of methane within the unsaturated zone (McMahon et al., 2018) can also contribute to decreased methane effluxes into the atmosphere and a modified compositional and isotopic signal. While this is preferable from an atmospheric emission perspective, decreased surface emissions may obscure the presence of GM, contributing to poor detectability while allowing continued groundwater impacts (McMahon et al., 2018).

1.3 Problem Definition

Anecdotal reports from industry practitioners have indicated that the results of gas migration tests can be variable, with potential impacts due to the gas migration testing method and other factors. However, there is limited documentation of this variation in the publicly available scientific literature. In addition, while it is suggested in regulation that different gas migration testing methods may be used by industry practitioners (AER, 2021), there is relatively little current documentation on the methods employed for gas migration testing in commercial (non-academic) settings.

A preliminary assessment at the beginning of this thesis work sought to fill these knowledge gaps by:

i) Comparing historic gas migration test results conducted by different industry testing parties, at six different wells with documented gas migration.

ii) Documenting the incidence of variable gas migration test results in the academic record.

iii) Investigating any potential relationships between the gas migration testing method and the measured methane concentration and pass/fail result of the test. This included dependence on depth of investigation below ground surface.

A detailed account of the comparison methodology, supporting field investigations, and the conclusions based on these findings are presented in Appendix A, with additional information in Appendix B. Briefly, the work conducted in support of the problem definition documented:

i) Variation in gas migration test results, both as the maximum recorded methane concentration and occasional differences in the pass/fail test outcome. These variations were seen between different gas migration testing parties (suggesting a method dependant mechanism), and for tests conducted by the same testing party over time (suggesting a method-independent mechanism).

ii) Statistically significant dependence on testing party for both the gas migration test maximum measured methane concentration and the pass/fail outcome, suggesting that some testing methods more frequently fail to detect gas migration.

iii) Increased measured methane concentrations with greater in-soil depths of investigation.

1.4 Objectives and Thesis Organisation

The objectives of this thesis are to conduct a field-based examination of the spatial and temporal variability of gas migration at the well-pad scale, including factors that may impact the successful detection and representative measurement of migrating gases in commercial and scientific studies. Specifically, work in this thesis seeks to:

i) Document incidence of variability in gas migration test results, and the investigate the dependence of GM test concentrations on test methodology.

ii) Record second-to-daily scale temporal variability in gas efflux and concentrations in a field setting, and investigate how these variations may be related to environmental factors.

iii) Record the spatial distribution of compositional and isotopic changes to soil gas at the well-pad scale caused by the presence and in-soil processes of migrating gases.

Briefly, this thesis reports on two different field campaigns, followed by a summary of the most important conclusions and recommendations. Related publications and statement of co-author contributions have been articulated in the Preface. Observations of spatiotemporal variability of gas migration around a case-study petroleum well are discussed in relation to previous gas migration artificial injection experiments and the existing understanding of gas movement behavior in the saturated and unsaturated zones. Findings are presented in the context of perceived impacts on various commonly used scientific and commercial gas migration detection and quantification strategies.

Chapter 2 presents results from intensive migrating gas characterization around a single energy well, recorded through long-term and survey CH_4 and CO_2 efflux measurements, soil gas isotopic and compositional sampling, and comparison with auxiliary measurements. Statistical techniques were used to investigate explanatory relationships between environmental factors such as temperature and wind speed and the observed temporal variability in efflux and concentration.

Chapter 3 presents measurements using simple sensors to document temporal variations in continuous time-series measurement of methane gas concentrations in the soil around this same case-study well. Concentration temporal variability is observed and characterised at ground surface and five and thirty centimeter depths, and related to meteorological factors. These findings are related to potential outcomes of gas migration testing and risk assessments at each of these three depths.

A closing summary in Chapter 4 links the findings from these chapters and presents broad outcomes relevant to future commercial and scientific study of gas migration detection and impact assessment. Supporting information for the Problem Definition and Chapters 2 and 3 are provided in Appendices A, C and D respectively. Additional gas migration study site characterisation details are provided in Appendix E, and work using the calculated barometric efficiency from shallow piezometer measurements to characterise free gas content in the unconfined aquifer of the study site is provided in Appendix F.

Chapter 2: **Spatiotemporal variability of fugitive gas migration emissions around a petroleum well**

Fleming, N., Morais, T., Mayer, K.U., Ryan, M.C. 2021. Spatiotemporal variability of fugitive gas migration emissions around a petroleum well. Atmospheric Pollution Research. 12(6). 101094

2.1 Abstract

Well integrity failure resulting in migration of natural gas outside of the surface casing can cause atmospheric greenhouse gas emissions and groundwater quality impacts from existing and historic energy wells. Spatial and temporal variability in gas migration can result in errors in detection (i.e., presence/absence) and efflux estimations. This field-based case study used automated dynamic closed chambers to record repeated (~ every 18 minutes) CO_2 and CH_4 efflux measurements over a two-week period around a single petroleum production well in Alberta, Canada. Long-term efflux measurements supplemented soil gas compositional and isotopic characterization, along with surface concentration measurements. Effluxes were spatially concentrated around the wellhead and only occasionally detectable more than a few meters away. Estimated total emissions attributable to gas migration ranged from 48 - 466 g CH_4 d^{-1} (or 0.07 - 0.7 m^3 CH_4 d^{-1}). Methane effluxes and concentrations were temporally variable on second-to-hourly and diel scales. Multivariate stepwise regression analysis indicates that multiple meteorological factors, particularly wind speed and air temperature, were related to the temporal variability. Despite temporal variability, elevated concentrations and effluxes were consistently detectable around the well. Major soil gas composition suggests that gas migration near the wellhead causes advective displacement of soil gas, while more distal measurements are indicative of episodic and diffusion-dominated transport. Values of ^{13}C-CO_2 and ^{13}C-CH_4 samples were consistent with CH_4 oxidation within the unsaturated zone. Although these results

reflect a single well, the findings are salient to gas migration detection and emission estimation efforts.

2.2 Introduction

Energy well integrity issues are a topic of increasing focus among government and industry practitioners, spurred in part by increased drilling activity in regions now accessible due to multi-stage hydraulic fracturing and concern of the growing environmental and economic liability of inactive and abandoned wells (Jackson et al., 2013; Alboiu & Walker 2019; Schiffer et al., 2020). Well integrity issues include gas migration outside the surface casing (GM), where a subsurface source of natural gas typically migrates from a shallow or intermediate gas-charged stratigraphic interval to ground surface (Figure 2.1; Rowe & Muehlenbachs, 1999, Tilley & Muehlenbachs, 2012). The "surface casing" of energy wells is generally installed to a depth below the base of non-saline groundwater protection (typically 100-300 m; Dusseault and Jackson, 2014). The annulus between progressively smaller diameter casings is typically cemented between the casing and the borehole (e.g., Bachu, 2017; Alberta Energy Regulator, 2020). Leakage pathways which result in gas migration are generally understood to be due either to defects in the cement itself, or between the cement and the borehole or one of the casings (Dusseault and Jackson, 2014; Bachu, 2017). Fugitive, or migrating, gases are typically primarily methane (CH_4), often with minor amounts of ethane, propane, and other volatile hydrocarbons (Szatkowski et al., 2002; Tilley & Muehlenbachs, 2012).

Gas migration impacts can include atmospheric emissions, groundwater water quality perturbations, and land use interference. Methane is a greenhouse gas with a global warming potential 25 times more potent by mass than carbon dioxide over a period of 100 years (and 84

times that of CO_2 over a 20-year period; IPCC, 2013). Specific focus on decreasing methane emissions from the upstream petroleum sector is included in global efforts to decrease anthropogenic greenhouse gas emissions (IPCC 2013). For example, the Alberta oil and gas industry intends to reduce 2012 methane emission rates by 45% by 2025 (Government of Alberta). Specific concern for GM also arises since, in some instances, gases migrate through non-saline (i.e., total dissolved solids less than 4000 mg L^{-1}; Alberta Energy Regulator 2021) groundwater. Dissolved methane can alter chemical conditions of groundwater, specifically its redox state, perturbing the indigenous microbial community, potentially altering pH, mobilizing metals, forming hydrogen-sulfide gas, or later exsolving when groundwater is pumped to the surface for residential or commercial use (Cahill et al., 2017; Gorody, 2012; Kelly et al., 1985; Roy et al., 2016). Should these exsolved gases accumulate in pumphouses, residences, or other facilities, explosive or asphyxiating atmospheres may develop (Engelder & Zevenbergen, 2018). Finally, GM may cause impacts or limitations on land usage since excess methane and/or carbon dioxide may displace oxygen in soil gas and impact plant or crop health. GM also has the potential for generating a dangerous or explosive atmosphere, necessitating setbacks for built structures (Noomen et al., 2012; Sihota et al., 2013; Williams & Aitkenhead, 1991). Although gas migration has only been reported for 0.73% of all wells in the province of Alberta (n > 450,000 wells in total; Bachu, 2017), a recent review concluded gas migration testing has only been required in 3.5% of Alberta's energy wells (Abboud et al., 2020). Methane emission distributions are often heavily skewed by a small number of 'super-emitter' sources that comprise a large proportion of the total emissions (Brandt et al., 2014; Saint-Vincent et al., 2020; Zavala-Araiza et al., 2015). Previous work suggests that emissions specific to GM in Alberta

follow this same distribution, where a smaller number of wells have the highest GM emission rates and contribute disproportionately to total emission volumes (Erno & Schmitz, 1996).

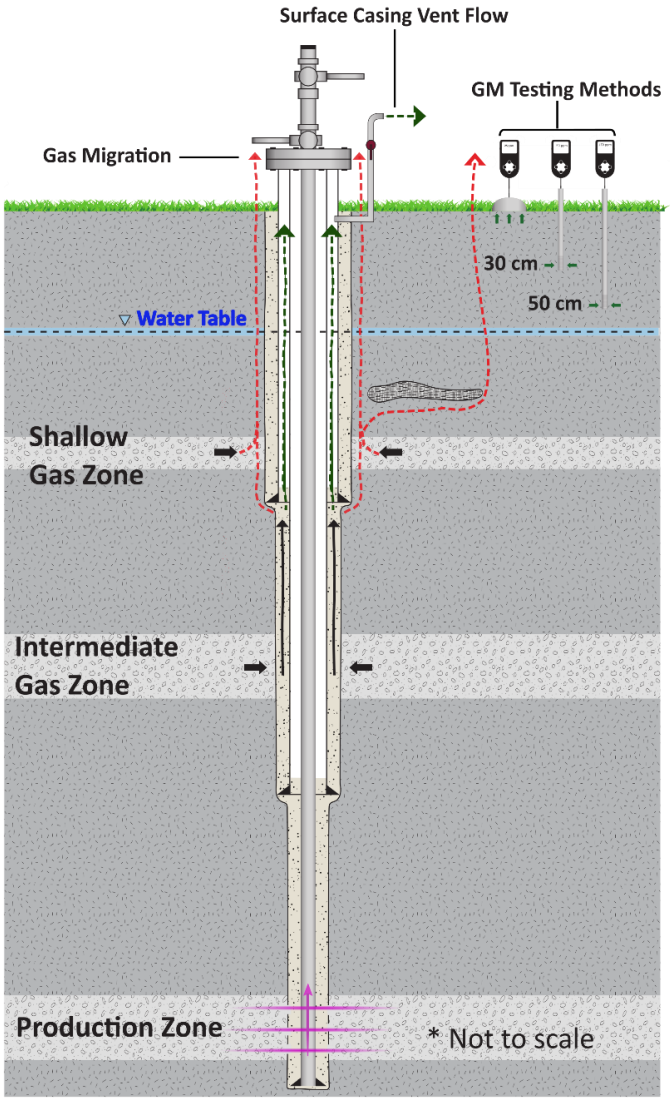

Figure 2.1 Conceptual model of gas migration (GM) and surface casing vent flow (SCVF) (After Bachu, 2017). Migrating gases (CH_4 and other light hydrocarbons) originate from an intermediate or shallow gas producing formation and travel to the surface either wholly outside the casing (GM; red) or also within the outermost casing annulus (SCVF; green). Common testing depths for detecting the presence of GM through combustible gas and/or CH_4 concentration measurements include ground-surface detection, or at a specified depth (usually >

30 cm threshold requiring ground disturbance permitting despite the ‘recommended’ 50 cm depth (Alberta Energy Regulator, 2021; Fleming et al., 2019).

A significant fraction of Alberta’s energy wells will require GM testing before they can be abandoned (Abboud et al., 2020). If GM is found, repair is required prior to legal abandonment, presenting an economic liability to industry (Alberta Energy Regulator, 2021). While requirements vary depending on jurisdiction, an effective and reliable approach to measure presence/absence of GM and estimate emission rates is needed to manage GM around petroleum wells. Tests for the presence/absence of GM are often conducted by sequential snapshot measurement of near-surface combustible gas concentrations at multiple points around a well, over a total GM test duration of less than one hour (Alberta Energy Regulator, 2021; Szatkowski et al., 2002). The recommended test point spacing by the Alberta Energy Regulator includes a total of 14 measurement points, with two within 30 cm of the wellbore and then at 2, 4, and 6 m away in a cross pattern. Measurement depths are recommended as 50 cm, though measurements are often completed at ground surface or some intermediate subsurface depth (< 30 cm) that does not require ground disturbance permitting (Figure 2.1; Alberta Energy Regulator, 2021; Fleming et al., 2019; Province of Alberta, 2020). The efficacy of the recommended gas migration testing method has not been fully validated (Abboud et al., 2020). Recent surveys of methane efflux measurements around industry gas wells (Forde et al., 2019a; Lyman et al., 2020; Riddick et al., 2020), and in field injection experiments (Cahill et al., 2017; Forde et al., 2018) have revealed substantial variability of measured concentrations and effluxes, both spatially and temporally on seasonal, diel, and short-term (30 minute) time scales, potentially complicating reliable detection and emission rate estimations.

Several causal mechanisms explain the spatiotemporal variability of migrating gases. Within the saturated zone, subsurface heterogeneity and the presence of capillary barriers will trap buoyant free gas and cause fingered lateral and vertical movement and eventual episodic release when free gas pressure and buoyancy forces overcomes viscous forces and capillary entry pressures (Gorody, 2012; Steelman et al., 2017; Van de Ven et al., 2020; Woods & Norris 2016). Dissolution and oxidation decrease migrating free phase gas quantities reaching the water table, to varying degrees depending on geochemical conditions and free-gas interfacial area (Cahill et al., 2017; Roy et al., 2016; Van de Ven et al., 2020). Heterogeneity in the unsaturated zone also leads to variable advective and diffusive gas effluxes (Ulrich et al., 2019). Barometric pressure decreases cause a pressure differential between the soil gas and atmosphere and therefore increased gas efflux across the soil-atmosphere interface, especially in thicker unsaturated zones (Forde et al., 2019b; Kovach, 1945). Wind-induced soil gas transport can be significant, where higher wind speeds (and related turbulence-induced pressure fluctuations) induce short-term variations in advective efflux (Poulsen & Møldrup, 2006; Poulsen et al., 2017; Redeker et al., 2015). Advective or diffusive mixing of migrating gases of deep subsurface origin (such as CH_4, C_2H_6, He) and gases of primarily atmospheric origin (O_2, Ar), produce identifiable soil gas mixtures (Frederick et al., 2017). Particularly in a thick unsaturated zone, microbial oxidation can consume enough methane to decrease or entirely obscure the GM surface expression, resulting in diagnostic carbon isotope fractionation (Forde et al., 2018; McMahon et al., 2018; Rowe & Muehlenbachs, 1999; Schout et al., 2019).

In summary, spatially and temporally variable CH_4 efflux and concentrations have been observed around energy wells, and field injection and laboratory studies have revealed some of

the causal mechanisms. While episodic subsurface migration and varying meteorological factors such as barometric pressure, wind speed, and temperature can explain some of the variation, there is limited temporal and spatial discretization of measurements of gas migration effluxes and concentrations around energy wells. In addition, temporal variability is not assessed in the context of the standard of practice for GM testing. Industry tests for the presence of GM and further quantification of emissions, as well as the need to quantify the GM contribution to atmospheric emissions, water quality perturbations, and land use impacts, will benefit from field-validation of the conceptual understanding of the behavior and spatiotemporal variability of migrating gases.

We present findings of spatiotemporal efflux and concentration variability around an established petroleum well known to have gas migration, with a view to recommending an effective field test for GM detection and efflux estimation. High-resolution efflux and concentration data and statistical analysis results relate external factors that may be driving changes in measured CH_4 efflux and concentration. Spatial efflux surveys and soil gas samples establish relationships and spatial trends in migrating gases and in-soil processes of oxidation, atmospheric mixing, and atmospheric displacement. The implications of these findings are discussed in terms of atmospheric methane emissions and the standard of practice for GM detection using currently practiced and proposed techniques.

2.3 Materials and Methods

2.3.1 Field site description

An industry partner provided access to an anonymous site with known gas migration outside the outermost casing, at a conventional (non-thermal) petroleum production well that was

drilled and completed using standard practices for non-horizontal wells after 1995. The status of this well is ‘suspended’ (i.e., idle, not actively producing oil or gas but with no decommissioning work completed). No additional methane emission sources beyond those attributed to GM are expected at the site. No SCVF was measured by the well operator, and no other surface and subsurface methane leakage sources are located near the well (verified through site inspection and spot concentration measurements performed by the authors). The well is located within Alberta Energy Regulator’s ‘Required Test Area’ where a high instance of GM has been identified (Alberta Energy Regulator, 2021; Figure 2.3a). Historic gas migration test results were provided by the operator for 14 GM testing events conducted by the site operator (8 tests) and service providers (6 tests) using industry-accepted methods (Alberta Energy Regulator, 2021) over >10 years (Figure 2.2). The GM measurement spacings generally followed the Alberta Energy Regulator’s ‘recommended’ method (described above). Specific details of historic sampling, including sampling equipment and measurement depth, were not provided, and may have differed depending on testing party (Alberta Energy Regulator, 2021; Fleming et al., 2019). The maximum methane concentration measured across all (n = 14) historic GM testing events averaged 18,000 ppm (std. dev. = 30,000 ppm), demonstrating substantial variation in maximum concentrations between test occasions.

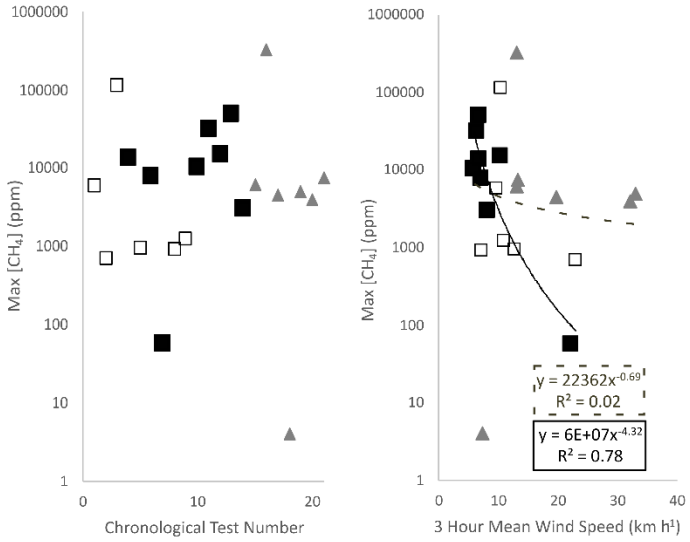

Figure 2.2 The maximum recorded combustible gas concentration as ppm CH_4 (log scale) from all available gas migration testing conducted at the study well. Historic tests conducted by one individual field operator are indicated as filled squares, and tests conducted by various service companies are empty squares. Tests conducted by the authors are shown as gray triangles. Results are shown in chronological order of testing date (left) and as a function of wind speed (using mid-day (11:00 to 14:00 hrs) data from the nearest weather station 10-20 km from study site; right). Trendlines are shown on all tests conducted (R^2=0.02; dashed line) and for those conducted by the same individual well operator (R^2= 0.78; black line).

A shallow water table ~0.6 m below ground surface (BGS; with +/- 0.3 m seasonal fluctuations) was identified by water monitoring wells hand-installed by the authors. The water table slope was consistent with an approximately southward groundwater flow direction. Slug and permeameter testing yielded a hydraulic conductivity at shallow depth (< 2 m) of $3x10^{-6}$ m s^{-1}. Fine silty-sand was observed down to two meters (the depth at which hand auger lithology samples were collected). Nearby water well records suggest unconsolidated sediments are present to about 10m depth, below which sedimentary bedrock occurs. Additional site details are reserved to protect site anonymity.

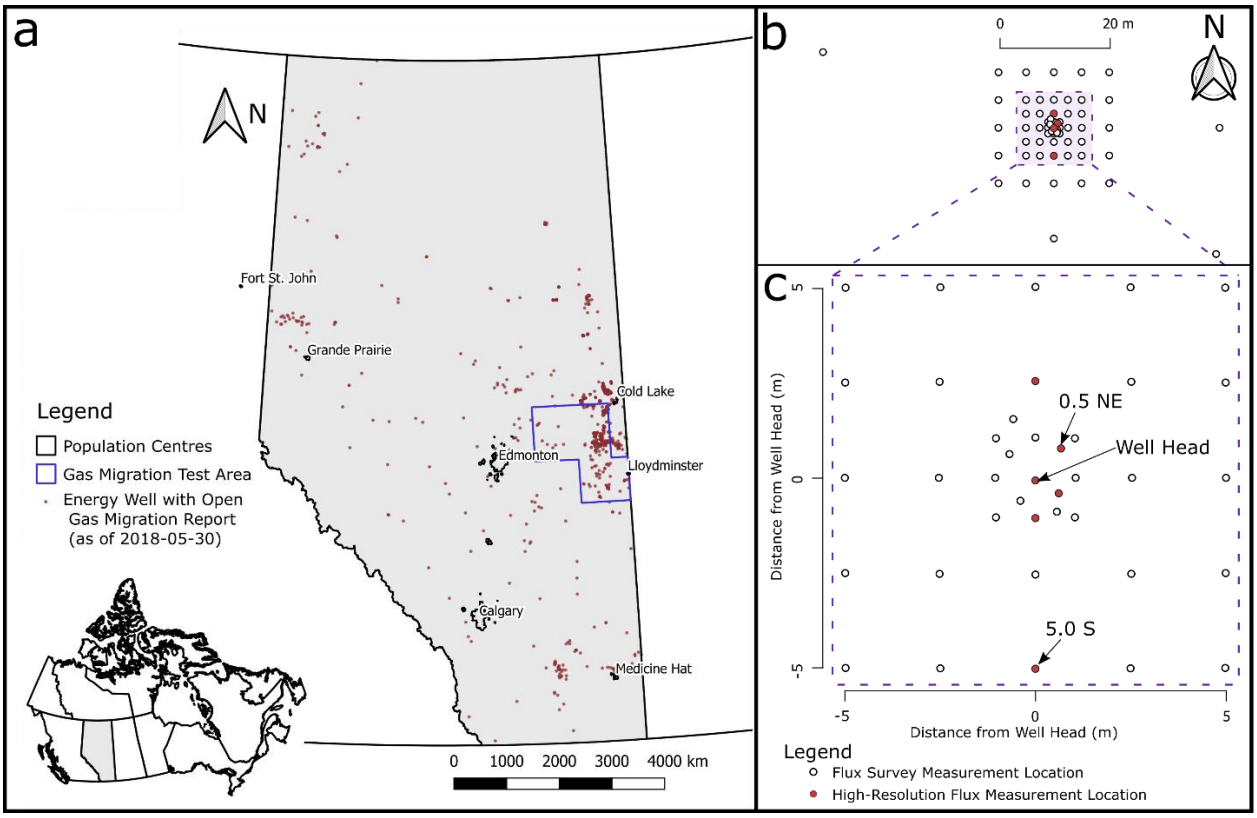

Figure 2.3 a) Overview of Alberta with all petroleum wells with open (i.e., detected but not repaired) reports of external gas migration as of 2018-05-30 (n = 1186), with the majority of these reported cases located on the eastern side of central Alberta in the region around Lloydminster and Cold Lake. The Alberta Energy Regulator Directive 20 gas migration Required Test Area outlined in blue is the only location provincially in which gas migration testing is currently mandated on all wells (Alberta Energy Regulator, 2021). Data from Alberta Energy Regulator (2018) and Statistics Canada (2016). b) Full scale and c) close-up plan view schematic of the efflux monitoring network at the study well pad, showing locations of flux survey chambers (open circles). The location of repeat sampling and high-resolution efflux measurements over a two-week period (October 11th-27th 2019 are shown as red circles, labelled by distance and direction from the wellhead).

2.3.2 Methane concentration measurements using standard industry practices

Combustible gas concentrations were surveyed with a handheld detector (GT-43, Gas Measurement Instruments Ltd.) on soil surface (using a bell probe) and at 30 cm depth (with a slide-hammer gas vapor probe; Retract-A-Tip Gas Vapor Probe, AMS Inc.) on five separate

occasions at recommended spacings (Alberta Energy Regulator, 2021). The handheld detector is representative of commonly available portable gas detectors in use, where multiple integrated sensors (thermal conductivity, semiconductor, catalytic bead) detect combustible hydrocarbon gases (CH_4, C_2H_6, etc.) across a wide range of concentrations (Szatkowski et al., 2002). The sensors are calibrated to CH_4, and the sensor response to all combustible gases is reported in concentrations of CH_4 by ppm, % of the Lower-Explosive Limit (LEL) of methane (~5% v/v), or % gas by volume depending on sensed concentration (Gas Measurement Instruments, 2016). Using the three integrated sensors, the reported measurement resolution for CH_4 is 1 ppm in the <10,000 ppm range, 1% LEL in the <100% LEL range, and 1% gas by volume in the 1% to 100% volume range (Gas Measurement Instruments, 2016).

2.3.3 Soil gas sampling and analysis

Soil gas samples were collected from shallow soil vapor wells on five occasions (Feb 22, Jul 11, Aug 22-23, Sep 25, Oct 27, 2019). The soil vapor wells were constructed using 6.4 mm (1/4”) ID polyethylene plastic tubing with a Luer stopcock-valve fitting (Masterflex) and geotextile filter cloth covering a 10 cm perforated screen at the bottom. Vapor wells were installed at depths of 10 cm and 30 cm below ground surface by insertion of pre-constructed soil vapor wells into diagonally drilled holes with soil allowed to collapse around the tubing. The 10 and 30 cm depths was selected based on inferred applicability to commercial gas migration testing procedures, with 30 cm being the maximum depth of observation permitted for subsurface sampling without the added expense of ground disturbance permitting (Province of Alberta, 2020). Previous attempts at installation of deeper soil vapor wells (0.5 and 1.0 m) resulted in saturation and clogging due to the shallow (0.3 to 0.8 m BGS over the observation

period) water-table at the site. Prior to sampling, 20 mL of stale gas was purged from the vapor well tubing using a syringe (representing more than 3 tubing volumes removed). Following purging, a 60 mL soil gas sample was collected and injected through the butyl septa of a 30 mL helium-flushed and partially evacuated glass vial until the vial was overpressured. Syringe withdrawal rates were < 2 mL s^{-1} to limit atmospheric contamination and influx along the tubing. Soil gas samples were also obtained on Oct 21, 2018 using a slide-hammer probe (Retract-A-Tip Gas Vapor Probe, AMS Inc.) and stored in fully evacuated vials (in contrast to helium-flushed vials in other sampling events), permitting analysis of the He content of soil gas).

Major gas species were analysed by injecting a 5 mL gas sample aliquot into a Scion 450/456 four-channel gas chromatograph fitted with four separate sample loops, analytical columns, and detectors. The dedicated fourth channel separated and quantified argon-oxygen, with a lower detection limit of 50 ppm argon. The fourth channel used an MXT-Molsieve 5A analytical column (30m x 0.53mm, 50um film thickness) held at a constant temperature of 30°C, a 50µl sample loop, hydrogen carrier gas (constant flow 1.0 mL/min), and a Thermal Conductivity Detector (Filament Temperature 250 °C). Certified gas standards were used to calibrate the gas chromatograph immediately prior to analyses. Analytical precision and accuracy for all gases is typically better than ±2.5% of the reported concentration, and the reported lower detection limit for alkanes (C1 to C5) is approximately 0.5 ppm. Isotope composition was measured using gas chromatography-isotope ratio mass spectrometry methods to determine $\delta^{13}C$ on CO_2, CH_4, and C_2H_6 (C2; ethane) on nine selected soil gas samples and six dissolved gas samples that met concentration thresholds (0.1% of the gas species of interest) (Humez et al., 2016). Two samples were analysed for $\delta^{2}H$ on CH_4 for additional gas source identification.

Analyses were performed on a ThermoFisher MAT 253 isotope ratio mass spectrometer coupled to Trace GC Ultra + GC Isolink (ThermoFisher). All samples are reported in ‰ notation with respect to VPDB for $\delta^{13}C$ and VSMOW for $\delta^{2}H$. Lab reported accuracies are ±0.5 ‰ $\delta^{13}C$ and ±2 ‰ $\delta^{2}H$. All compositional and isotopic analyses were conducted at the University of Calgary Applied Geochemistry and Isotope Science Laboratories.

The composition and isotopic signatures of soil gases have previously been used to interpret the origins and near-surface interactions of migrating gases. Helium is routinely used as a noble trace gas associated with deep geologic origin, such as around natural CO_2 and CH_4 seeps, fault zones, and in gas migration leakage scenarios (Annunziatellis et al., 2008; Frederick et al., 2017; Wen et al., 2016). Similarly, elevated concentrations of higher alkanes (ethane, C2; propane, C3; etc.), are indicative of deeper gas origins since these gases are not considered to be co-produced during microbial methanogenesis that might occur in wetlands or surface aquifers (Bachu, 2017; Kang et al., 2014; Whiticar, 1999). Isotope ratios of $\delta^{13}C$ on CH_4, C2¸and CO_2 can also all be used to distinguish gas sources since diagnostic isotopic fractionation will occur during the source formation of these gases (Tilley & Muehlenbachs, 2012; Szatkowski et al., 2002; Whiticar, 1999) and during their transport over geologic time (Hendry et al., 2017). In shallow groundwater and soil gas, argon can originate from both atmospheric sources, and the ultimate geogenic source of most argon on Earth, where ^{40}Ar is produced in the subsurface through the radioactive decay of ^{40}K. However, any Ar in younger groundwater and soil gas systems (<20,000 years) can be presumed to originate from atmospheric sources due to the negligibly low abundance and long half life of the ^{40}K source (Almon and Magaritz, 1990). Therefore, Ar is used here as a noble gas tracer in shallow soil and groundwater systems,

alongside other primarily atmospheric gases such as N_2 and O_2 (Almon and Magaritz, 1990; Martin et al., 1995; Frederick et al., 2017). Carbon dioxide can co-occur with CH_4 as a component of migrating subsurface natural gas, be produced during the microbial oxidation of methane, or during natural biologic respiration in soils (Romanak et al., 2014; Whiticar, 1999). Isotopic $\delta^{13}C_{CO2}$ values, and soil gas compositional trends, are used here to infer CO_2 origins (Risk et al., 2013; Romanak et al., 2014; Sandau et al., 2019).

2.3.4 Soil gas efflux measurements

Near-surface gas concentrations and effluxes were measured in two efflux survey and sampling events (Aug 20, 2019 and Sep 25, 2019) and one high-resolution long-term sampling event (Oct 11-27, 2019). Automated long-term and survey chambers measured spatial and temporal distributions of carbon dioxide and methane effluxes using the same equipment and approach previously described (Forde et al., 2018; Sihota et al., 2013). Soil efflux collars (20 cm tall, 200 mm internal-diameter SDR pipe segments) were installed in the soil to approximately 15 cm depth more than 24 hours before the initial survey measurements. During the two-week intensive measurements, a multiplexer (LI-8150, LI-COR Inc) switched between six long-term dynamic closed chambers (LI-8100-104, LI-COR Inc.) with chamber concentrations analyzed at 1 Hz with an infra-red gas analyzer (Li-8100, LI-COR Inc.) and an ultra-portable greenhouse gas analyzer (model 915-0011, Los Gatos Research Inc.). During each survey event, an efflux survey chamber (LI-8100-103, LI-COR Inc.) connected to the same two analysers was manually moved between 51 different collar locations (Figure 2.3b). A custom wellhead collar (16 cm radius from the outermost well casing, total ground surface area 0.44 m^2) measured GM effluxes in the previously identified high-efflux zone immediately outside the surface casing (Figure C1). This

custom collar fully encircled the well and was sealed against the intermediate casing below the wellhead. The long-term chamber closure times ranged from 15 to 90 seconds, switching sequentially between all 6 chambers with appropriate pre- and post-purge times, at around 18 minutes per cycle (Table C1).

Conservative CH_4 and CO_2 effluxes were calculated with linear curve fitting of chamber closure time vs. concentration in SoilFluxPro (LI-COR Biosciences; Forde et al., 2018; Sihota et al., 2013). The minimum detectable efflux (MDF) was calculated with conservative detector analytical accuracies taken to be $\Delta C = 0.2$ ppm for CH_4 and $\Delta C = 1$ ppm for CO_2, which is consistent with similar measurements at controlled injection gas migration study sites (Table C1; Christiansen et al., 2015; Forde et al., 2019a, 2019b). Manufacturer-reported instrumental accuracies are < 2 ppb for CH_4 (Los Gatos Research) and <1 ppm for CO_2 (LI-COR Inc).

The pre-closure concentrations of CH_4 and CO_2 within each chamber during each efflux measurement were taken as conservative estimates of the ground-surface concentrations at that moment and location. Use of these concentration 'initial values' from each automated efflux measurement as a proxy for measured concentrations using standard GM detection methods was validated by direct comparison between the two approaches using the same analyser. Immediately before each Aug 20, 2019 efflux survey measurement, the pre-closure concentrations were recorded within the chamber, and using the same gas analysers with a custom-fit bell-probe held against the soil surface adjacent to the outside of the collar. This procedure imitates standard industry practice for ground-surface concentration measurement (e.g., DP-IR, Gas Measurement Instruments Ltd.; Irwin, INFICON; etc.). The moderately good

positive correlation between the two methods (Spearman Rank R^2 = 0.48, m=0.85 on n= 48 measurement) at concentrations of < 3 ppm, validates use of initial chamber concentrations as a conservative estimate of ground-surface concentrations that would be obtained with industry-practiced detection techniques.

2.3.5 Environmental measurements

Soil moisture sensors (HydraProbe, Stevens Water Monitoring Systems Inc.) recorded hourly averaged temperature, electrical conductivity, water content, and apparent dielectric content to a datalogger (CR1000, Campbell Scientific Inc.) between July and November 2019 at six locations (depths of 5 and 30 cm, and distances of 1.0, 2.5, and 6.0 m East of the wellhead). Soil temperatures were also monitored using small sensors (TidbiT, Onset Computer Corporation) affixed with wire into countersunk holes in a softwood post at soil depths of 0, 0.1, 0.3, 0.5, 1.0 and 1.5 m BGS at locations 1.0 m East, and 6.0 m East of the wellhead between July 9 and November 18, 2019. Three additional temperature sensors were installed at 0.25 m North of the wellhead (immediately outside the wellhead efflux chamber) at depths of 0, 0.1 and 0.3 m for the duration of the October 11-27 measurement period. Water levels were recorded hourly in two piezometers with screens centered 1.0 m BGS, located 1.25 and 10 m South of the wellhead.

Precipitation and wind speed data were retrieved from the nearest public weather station (10 to 20 km away; exact distance withheld for confidentiality reasons) (Alberta Agriculture and Forestry). During this period, there was good regional correlation (averaging 0.86) between the 2 m height average wind speeds for the five nearest publicly available weather stations within a 50 km radius of the study site. Atmospheric pressures and temperatures were recorded hourly on-site (Barologger Edge, Solinst Canada Ltd.). Earth tide data (cm vertical displacement) over the

measurement period was estimated with site-specific coordinates using open software (Milbert, 2018). Change rates of water level and barometric pressure were calculated using a weighted five-hour central difference with three-hour rolling median smoothing (selected as the shortest window that eliminated hour-to-hour noise and produced visually smooth change rates).

2.3.6 Descriptive statistics of CH_4 and CO_2 concentration and efflux analysis

2.3.6.1 Regression modelling

Data processing and statistical analysis were conducted in the software package R (R Project version 4.0.2) with figures generated primarily using the ggplot2 package (R Core Team, Wickham, 2016). Linear interpolation was used to match the environmental data (typically recorded hourly) to times of efflux measurement. Thirteen environmental factors from the auxiliary data were considered for potential explanation of temporal variation in effluxes and concentration at each of the six chamber locations. These factors included: relative humidity, absolute barometric pressure, atmospheric temperature, approximate barometric pressure change rate, piezometer water level, approximate water level change rate, soil temperature at 0.05 m and 0.3 m BGS, soil water content at 0.05 m and 0.3 m BGS, temperature difference between the atmosphere and 0.3 m soil depth, vertical earth tide displacement, and wind speed.

Stepwise generalized additive regression models were used to identify the most important environmental predictors of temporal efflux and concentration variation by assessing the statistical relationships to the explanatory environmental factors (Hastie, 2019; Hastie & Tibshirani, 1990; Oliveira et al., 2018). Generalised additive regression models consider the combined (i.e., additive) linear or nonlinear (i.e., generalised) statistical relationships between multiple predictor variables (e.g., wind speed, atmospheric temperature, barometric pressure) and

a response variable such as CH_4 efflux (Hastie & Tibshirani, 1990). In contrast to multivariate linear regression, this method is advantageous for natural systems since it allows for nonlinear relationships between predictor and response variables to be described by a smooth function (Chen et al., 2019). In this analysis, parameter relationships could be represented as either linear, or a 2^{nd} or 3^{rd} order smoothed curve.

The relative statistical importance of each explanatory variable was assessed by building the model sequentially (i.e., in a forward stepwise fashion), with a single predictor variable being added at each step (Oliveira et al., 2018). Beginning with no explanatory factors, at each step the chosen algorithm sequentially added the single predictor variable which caused the largest increase to model performance. Continuous addition of all predictor variables may eventually lead to addition of irrelevant variables, overfitted models of excessive complexity, and weaker general predictive capacity. Excess model complexity was prevented here by optimising model performance towards the lowest possible Akaike Information Criterion (AIC) at each step (Akaike, 1974). A decreased AIC is produced by a model with better fit to the data, analogous to an increase in the model R^2. An increased AIC is produced by a model with greater complexity, such as a model with extraneous parameters or a statistical relationship described with a 2^{nd} order curve when a linear fit is adequate (Hastie, 2019). Following this algorithm, the stepwise addition of model parameters stopped when further model fit would be achieved at the expense of excessive complexity. This type of statistical model analysis allows for identification of relationships between explanatory and response variables in complex data series with multiple potential interactions, however the results must be compared to existing scientific literature to ensure they are sensible (Chen et al., 2019).

2.3.6.2 Geostatistical interpolation

The relationship between flux magnitude and distance from the wellhead was first assessed through the Spearman rank correlation coefficient. The Spearman correlation describes non-linear relationships by correlating the relative rank rather than absolute magnitude. Total methane gas emissions from gas migration were then estimated by interpolating the CH_4 effluxes from August and September spatial surveys across the 20 m by 20 m measurement grid using Empirical Bayesian Kriging and Inverse Distance Weighting methods in ArcMap (ESRI). These two methods of spatial efflux interpolation were chosen for comparison based on their previous application in the related field of landfill gas emissions (Abichou et al., 2006; Börjesson et al., 2000; Spokas et al., 2003;), and elsewhere in the environmental geosciences (Annunziatellis et al., 2008; Cardellini et al., 2003). In this application, both kriging and IDW methods rely on the assumption that locations more closely spaced will have more similar effluxes than locations further apart (Börjesson et al., 2000). Inverse distance weighting is a deterministic method where the flux value at each interpolation location is calculated based on nearby measured values, weighted directly by the distance to the measurement points. Kriging can more optimally relate a predicted value to nearby measured points using a semi-variogram that most closely describes the site-specific distance-efflux relationship for all measured data. The predicted values in the kriged interpolation are based on both the distance and direction to the measured points, which may account for anisotropy and a non-uniform relationship between distance and efflux (Spokas et al., 2003).

The geospatial mean of the interpolated surfaces were used to generate an estimate of total methane emissions related to gas migration across the gridded area (Abichou et al., 2006),

and the error associated with the interpolation using a 95% CI in the case of the kriged interpolation. Emissions attributable to gas migration were also estimated with the previously published practice using the arithmetic mean efflux of all points measured within a 3 m radius of the wellhead, applied to the area within this radius (Erno & Schmitz, 1996). Finally, total emissions from directly within the wellhead chamber were calculated using the ground-surface area of the wellhead chamber, 0.42 m^2, multiplied by the mean efflux rate.

2.4 Results

2.4.1 Methane concentration surveys:

Combustible gas concentrations measured using the handheld sensor were highest, and generally consistently detected, at ground surface only within one meter of the wellhead (Figure C2), while subsurface (30 cm depth) combustible gas was detected at higher concentrations and further distances (Figure C3). These gas concentrations had a similar spatial distribution and concentration range to the industry-provided GM test results (Figure 2.2), which also showed highest concentrations near the wellhead. Concentration measurements indicated that the only source of elevated combustible gas was from within the soil, with no indication of emissions from SCVF or other internal well integrity failure. During repeated site visits, there were no consistent sensory indications of the presence of GM, including an absence of visually obvious vegetation stress such as stunted, dead or discolored plants.

2.4.2 Gas efflux survey results

Higher CO_2 effluxes were also observed around the wellhead, especially during the September efflux survey (Figure 2.4). Methane effluxes were substantially greater immediately around the wellhead, and some positive effluxes (emitting CH_4 from the soil into the

atmosphere) were detected up to 10 m from the wellhead. Many effluxes (66% and 36% of measurements in August and September respectively), including some within meters of the wellhead, were less than the detection limit (0.02 μmol CH_4 m^{-2} s^{-1}). Several sampling locations in September registered low-rate negative effluxes indicating CH_4 consumption occurred in the soil zone.

Considering data from both surveys, there was an inverse Spearman rank correlation with distance from the wellhead and CH_4 efflux across the entire measurement grid, and poor inverse correlation with distance and CO_2 efflux (r = -0.73, -0.17 for CH_4 and CO_2 respectively). Spearman correlation analyses were preferred to Pearson correlations since the former more appropriately described the nonlinear decline in effluxes with radial distance from the well. The estimated total CH_4 emissions from gas migration varied depending on measurement period and the method used (Table 2.4). There was a 62% increase in mean GM-related methane efflux in the wellhead chamber between the October dataset considering all measurements across the two-week measurement period (n=1215) and a subset when only considering times with wind speeds less than 3 km h^{-1} (< 0.83 m s^{-1}, thus reducing the observations to n =243; Table 2.4; Figure C12).

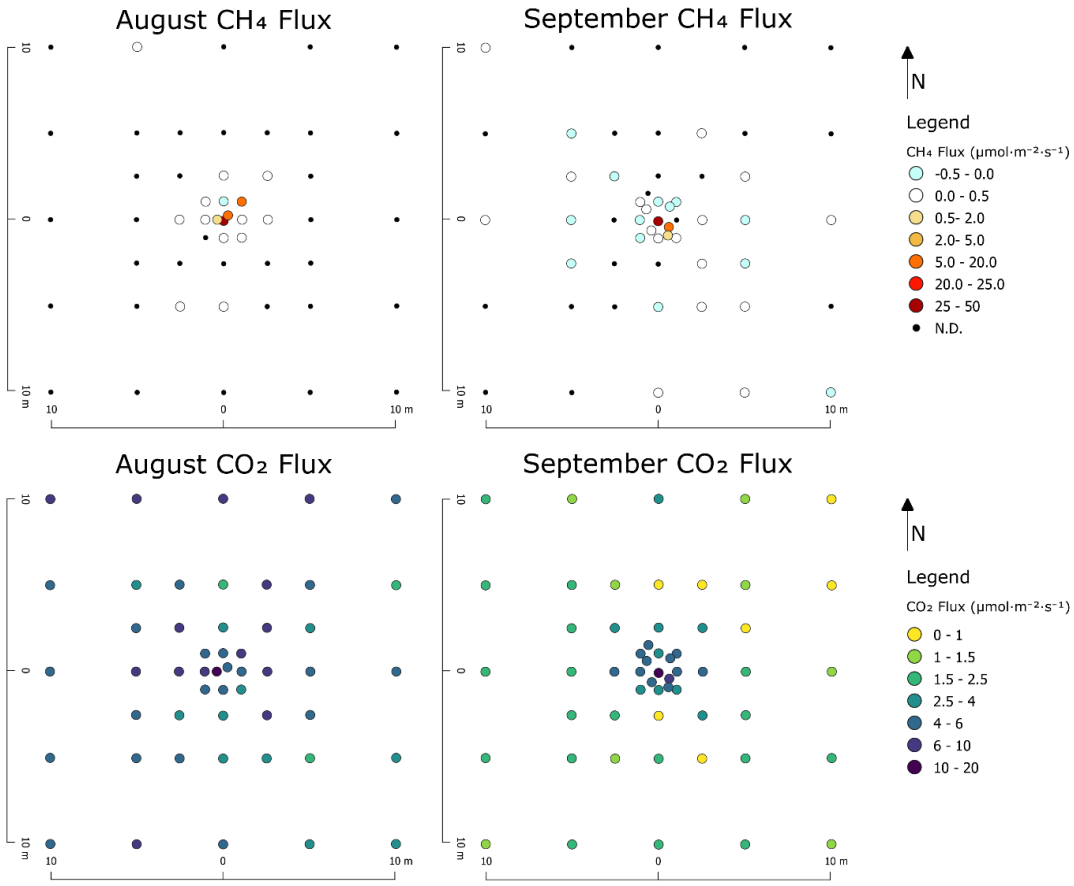

Figure 2.4 Plan view of efflux survey results for CH_4 (top row) and CO_2 (bottom row) measured in µmol m^2 s^{-1} on Aug 20, 2019 (PM; left hand side) and Sep 25. 2019 (AM; right hand side). Detection limits are generally 0.08 µmol m^2 s^{-1} CO_2 and 0.02 µmol m^2 s^{-1} CH_4. The horizontal distance from the wellhead is shown in scale bars.

2.4.3 High frequency efflux measurement

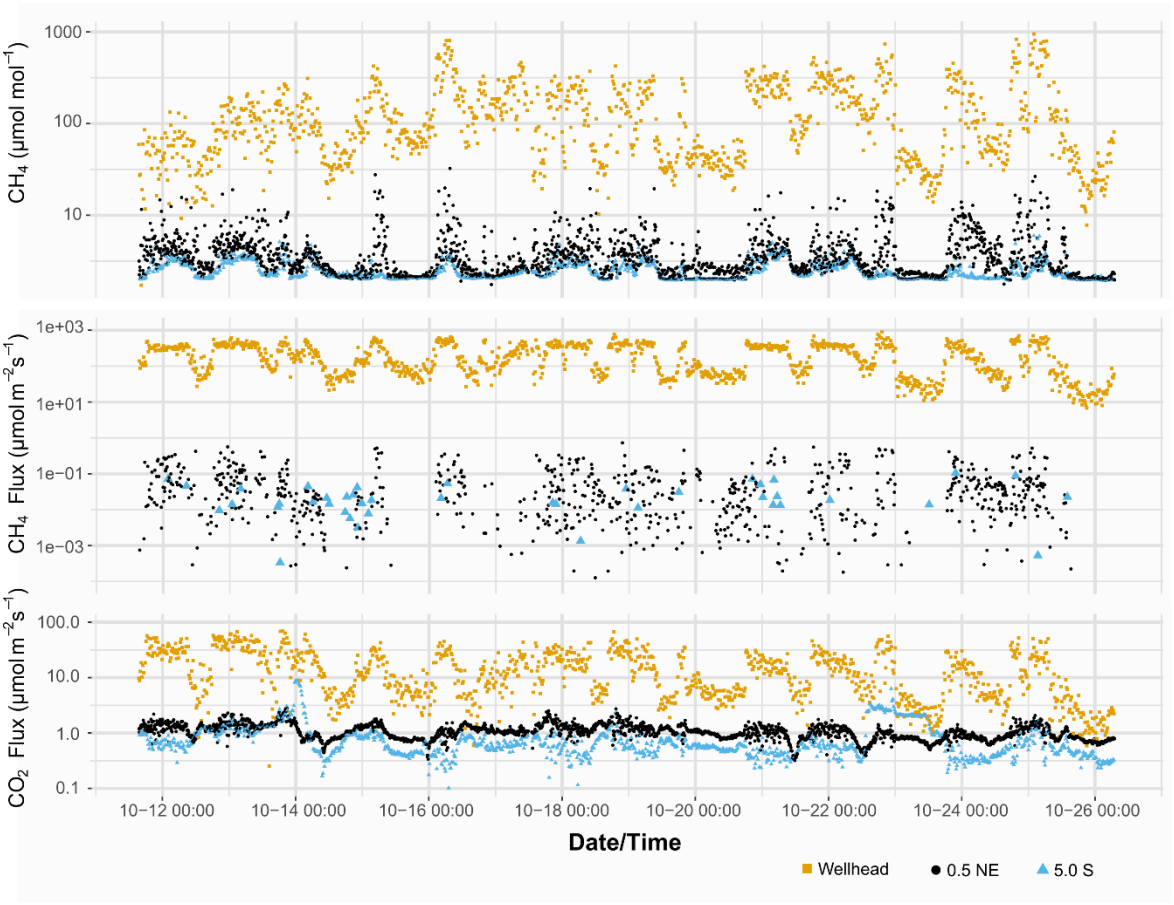

Figure 2.5 Time series of measured chamber pre-closure CH_4 concentrations (µmol mol^{-1}), CH_4 effluxes (µmol m^{-2} s^{-1}), and CO_2 effluxes (µmol m^{-2} s^{-1}) for three locations with high resolution measurement: at the wellhead (yellow squares), 0.5 m NE (black circles) and 5.0 m South of the wellhead (blue triangles).

The initial CH_4 concentrations at the wellhead chamber were always above the values at 5.0 m South of the wellhead, though the difference fluctuated from 10 to > 100 ppm CH_4 and the distinction was less clear during some periods (e.g. mid-day; Figure 2.5). Initial concentrations of CH_4 for other long-term chambers, including two located only 0.5 m from the wellhead, were approximately similar to the 5.0 South location, though slightly higher during peak flux periods

(Table 2.1). Initial CH_4 concentrations at 5.0 South ranged between minimum and maximum values of 2.0 and 5.5 ppm CH_4, (5^{th} percentile 2.07 ppm, 95^{th} 4.33 ppm). Despite the higher CO_2 efflux at the wellhead, the pre-closure CO_2 concentration was not substantially different between chambers, ($R^2 > 0.9$) (Figure C5).

Table 2.1 Descriptive statistics of Oct 11-27^{th}, 2019 high resolution efflux measurement series with chamber locations described in distance (m) and direction from the gas migration petroleum well. Confidence intervals calculated at 95% with bootstrapping methods and presented as (lower, upper).

	---------- CH_4 Efflux----------			-- CO_2 Efflux --	CO_2 Efflux: CH_4 Efflux Linear Correl. Coeff (R)	CH_4 Concentration	Total Obs.
Chamber Location	Mean	SD	Detectable Obs.	Mean		Mean	n
	------- µmol m^{-2} s^{-1} ------		%	- µmol m^{-2} s^{-1} -	--	--- ppm ---	---
Wellhead	219 (210, 230)	197.2	100	16.4 (15.5, 17.3)	0.86	146 (138, 153)	1212
0.5 SE	1.25 (1.14, 1.35)	2.3	93	1.97 (1.93, 2.02)	0.51	6.22 (6.00, 6.42)	1216
0.5 NE	0.04 (0.04, 0.05)	0.8	47	1.08 (1.06, 1.09)	0.15	3.72 (3.62, 3.82)	2431
1.0 S	0.07 (0.06, 0.08)	1.0	40	1.27 (1.24, 1.30)	0.12	3.94 (3.74, 4.14)	1215
2.5 N	0.01 (0.00, 0.01)	0.3	11	0.87 (0.85, 0.89)	0.12	2.65 (2.60, 2.69)	1215
5.0 S	0.00 (0.00, 0.01)	0.3	8	0.84 (0.79, 0.89)	-0.19	2.48 (2.45, 2.51)	1214

2.4.4 Multivariate regression modelling of high-resolution methane efflux and concentration measurements

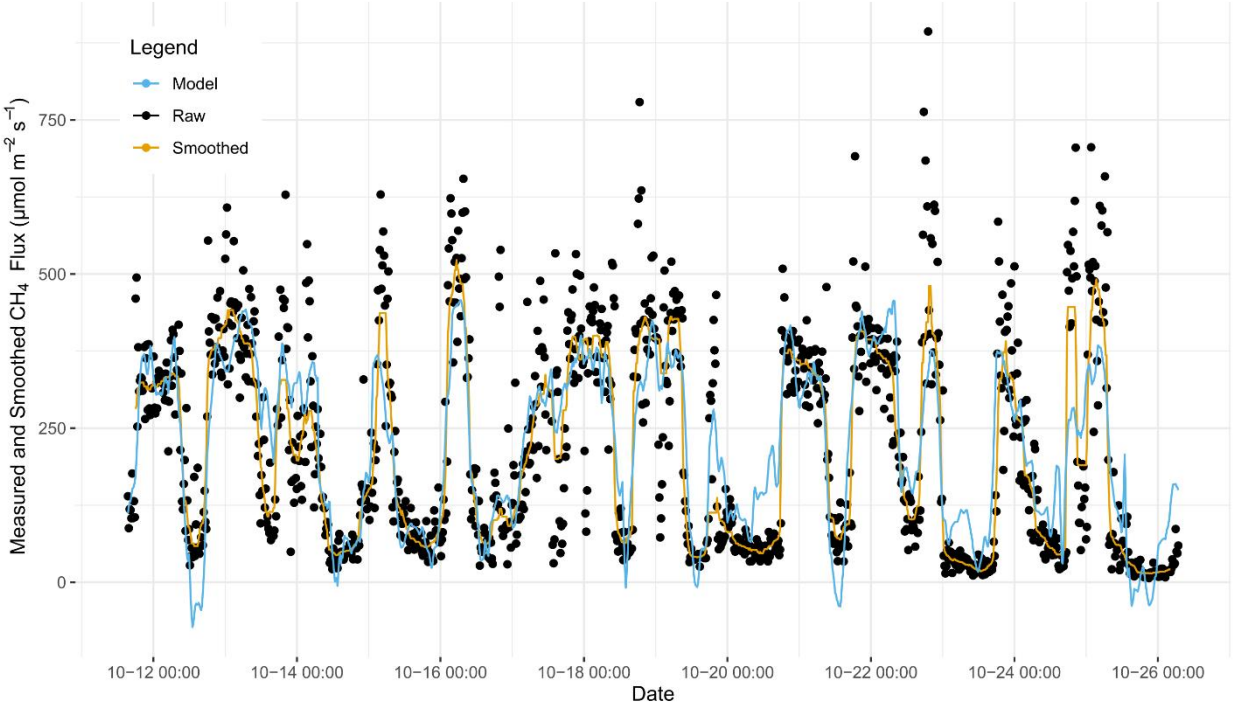

Figure 2.6 Wellhead chamber time series of CH_4 efflux from Oct 11-27th, 2019 with raw data (black dots), 20-point rolling median smoothing (yellow line) and multivariate regression modelling results (blue).

The two-week high resolution efflux monitoring period showed strong temporal variability, including diel variation with higher measured pre-closure concentrations and effluxes generally occurring overnight (Figure 2.5), and differences between consecutive measurements and stepped efflux behavior during chamber closure (Figure C6). Stepwise multivariate regression modelling results indicate that the quasi-diel patterns in observed gas migration concentrations and effluxes at the wellhead over the October 11-27th measurement period were most strongly related to varying wind speed and atmospheric temperature. Minor model

contributions by other factors, including temperature at 30 cm depth, were considered in a final regression model including eight of the 13 possible environmental factors that explained 63% of the temporal variation in wellhead CH_4 efflux (and 81% of smoothed efflux; Figure 2.6, Table C3). Wind speed was the most important parameter, and could explain 44% of the variation in measured CH_4 efflux at the wellhead (59% of smoothed efflux). Wellhead chamber CH_4 efflux was negatively correlated with wind speed (Pearson Correlation R = -0.72) and atmospheric temperatures (Pearson Correlation R = -0.49).

At all chamber locations, wind speed was the most important single predictor of temporal variation in CH_4 pre-closure concentration, and therefore first added factor to the stepwise model (Table 2.2). Wind speed was also the most important single addition to model R^2 at four out of the six chamber locations (Table C5). Other common relevant factors for CH_4 concentration models included change in barometric pressure, atmospheric temperature, and shallow soil water content or temperature. Compared to the CH_4 concentration regression models, the CH_4 efflux regression models (Table C3, Table C4) had less consistency in significant factors across all modelled chamber locations. However, wind speed and atmospheric temperature, or the differential in temperature between the atmosphere and soil, were assigned the highest priority by the model at 5 of 6 locations. Other lower priority (but statistically significant) factors included in the regression models for CH_4 efflux included groundwater levels and soil water contents (Table C4).

Table 2.2 Parameters most influencing the statistical model for the first three steps of forward stepwise multivariate generalized additive modelling of pre-closure CH_4 chamber concentrations at each long-term location. Model formulae are in the form: $[CH_4]$ = Parameter$_1$ + Parameter$_2$ …. The Akaike information criterion (AIC) is listed below the formulae at each step, with a decreasing AIC indicating an incrementally increasing goodness of fit. Environmental parameters abbreviations are: U_wind (windspeed), Wat.Cont_0.3 (30 cm depth soil water content), T_soil_0.05 (soil temperature at 5 cm depth), Baro_dP_dt (approximated barometric pressure change rate), T_atm (atmospheric temperature), E_tide (vertical component earth tide displacement).

Chamber Location	Model Step:1	Model Step:2	Model Step:3
Wellhead	U_wind ; 15200	Wat.Cont_0.3 + U_wind ; 15059	Baro_dP_dt + Wat.Cont_0.3 + U_wind ; 14985
0.5 SE	U_wind ; 6451	Baro_dP_dt + U_wind ; 6423	Baro_dP_dt + s(U_wind, df* = 2) ; 6405
0.5 NE	U_wind ; 11258	T_soil_0.05 + U_wind ; 11139	Baro_dP_dt + T_soil_0.05 + U_wind ; 11112
1.0 S	U_wind ; 6368	s(U_wind, df = 2) ; 6326	E_tide + s(U_wind, df = 2) ; 6308
2.5 N	U_wind ; 2816	T_soil_0.05 + U_wind ; 2708	T_soil_0.05 + s(U_wind, df = 2) ; 2676
5.0 S	U_wind ; 1789	T_atm + U_wind ; 1542	T_atm + Wat.Cont_0.3 + U_wind ; 1480

*df refers to the degrees of freedom of the smooth fitting function (1 if not indicated)

2.4.5 Soil Gas analysis results

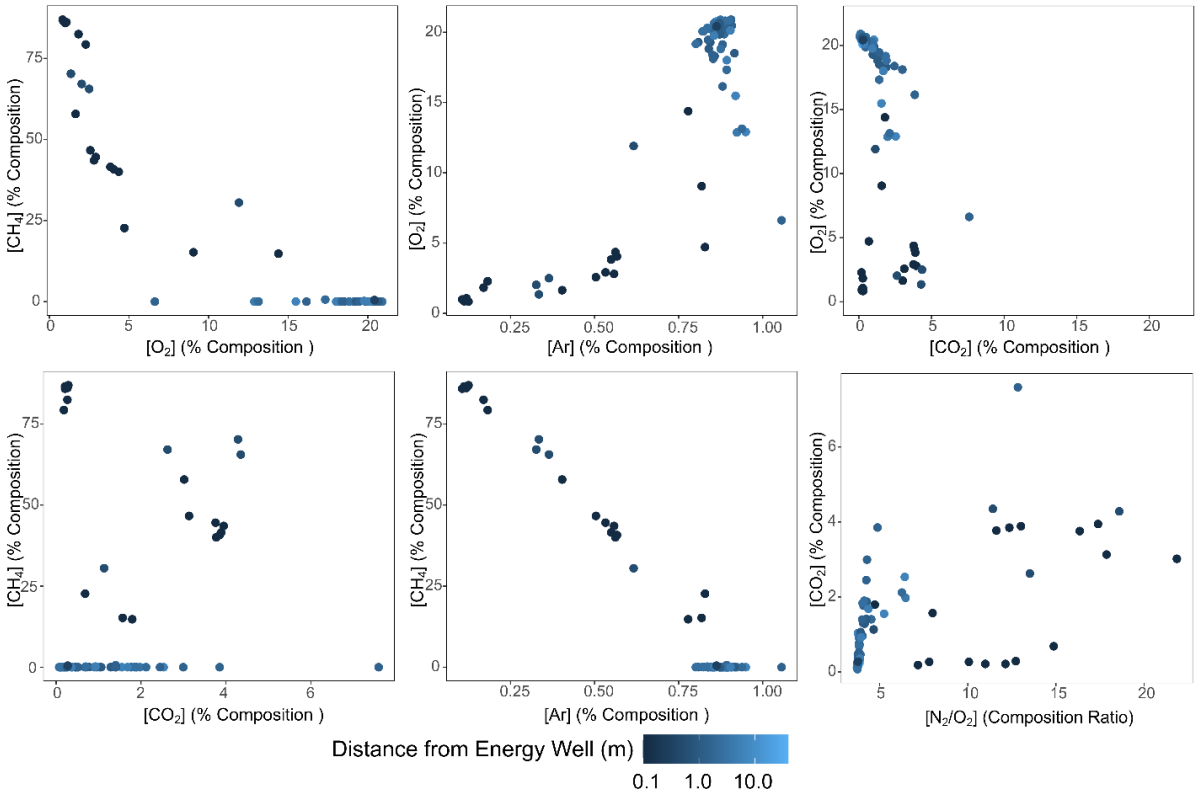

Figure 2.7 Selected scatterplot distributions of soil gas results at the 30 cm depth across five sampling events (% composition by volume), with lighter colors corresponding to increasing radial distance from the energy well.

Table 2.3 Pearson correlation matrix of soil gas compositions at the 30 cm depth around the gas migration test well.

	Ar	N_2	O_2	CO_2	CH_4
Ar	1	0.99	0.85	-0.12	-0.99
N_2		1	0.87	-0.15	-1.00
O_2			1	-0.51	-0.91
CO_2				1	0.21

The highest CH_4 concentration measured was 87% v/v, collected immediately outside the surface casing at a depth of 30 cm in November (i.e., early winter); this sample also contained CO_2 at 0.289 % v/v and He at 306 ppm. Across all samples, there was a relatively linear negative relationship between CH_4 and Ar (Figure 2.7). The O_2-Ar and O_2-CH_4 relationship was non-linear, with proportionally lower O_2 concentrations in most samples relative to direct mixtures of atmospheric and migrating gases. Further from the well, the soil gases contained generally lower concentrations of CH_4 and trace He, and higher concentrations of Ar, O_2, and N_2. Moderately positively correlations between CH_4 and CO_2 (Table 2.3) indicate CO_2 may be associated with migrating gases; however, the highest concentration CH_4 samples have lower concentrations of both CO_2 and Ar in comparison to samples with slightly lower CH_4 concentrations (Table C2). Several samples of soil CH_4 concentrations within < 5 m from the wellhead were as low as < 5 ppm CH_4. Some subsurface gas samples with deep gas signatures (including elevated CH_4, C2 and higher alkanes, and He) were detected up to 10 m from the well. Near the wellhead, soil gas samples had a high CH_4 content and low N_2 and Ar. CH_4 correlated very well with He (R^2 = 0.99) and the total concentration of higher alkanes, sum C_2-C_5, (R^2 = 0.87). Isotopic analyses of high concentration CH_4 samples nearest the wellhead had signatures of $\delta^{13}C_{CH4}$ = -60.7 ‰, $\delta^{13}C_{C2H6}$ = -45.0 ‰, $\delta^{2}H_{CH4}$ = -232 ‰, consistent with previous soil gas analyses conducted by the well owner (not shown). All soil gas samples (n=9) with CH_4 concentrations high enough for isotopic analysis (> 0.1% v/v CH_4) were within 0.5 m from the wellhead (Table C2). Analyses of $\delta^{13}C_{CO2}$ on these same gas samples ranged from -64.2 to -42.7 ‰. The $\delta^{13}C_{CH4}$ value rose as the concentration of CH_4 decreased relative to CO_2 (Figure C7).

2.5 Discussion

2.5.1 Gas source and mixing implications

Trends and ratios in the isotopic composition and concentration of fixed gas indicators can be combined to infer mixing between two end-members soil gas sources and redox processes (Frederick et al., 2017; Romanak et al., 2014; Sandau et al., 2019). The presence of He and higher alkanes with methane, in addition to the carbon isotope ratios of $\delta^{13}C_{CH4}$, $\delta^{13}C_{C2}$ and $\delta^{2}H_{CH4}$, are diagnostic of migrating deeper or intermediate-zone thermogenic gases (Annunziatellis et al., 2008; Frederick et al., 2017). Isotopic and compositional 'fingerprints' of SCVF or GM gases can be compared with compositional depth profiles of gases sampled during drilling in nearby wells to estimate the stratigraphic source of the gas. Comparison of the isotope values of methane and ethane at this study well to four published isotope depth profiles in the region (Rowe & Muehlenbachs, 1999; Szatkowski et al., 2002), indicate that the source of migrating gases at this study well may be ~300-400 m BGS.

While the saturated soils observed at the site provide conditions suitable for shallow natural (biogenic) CH_4 production (Romanak et al., 2014; Tokida et al., 2007; Whiticar, 1999), several results suggest there is not a significant biogenic CH_4 source at this site. Firstly, ethane, propane, higher alkanes, and helium are indicative of a deeper thermogenic methane, and gases are not co-produced during biogenic methane production (Kang et al., 2014). Similarly, the carbon isotope composition of CH_4 (and CO_2 near the wellbore) indicate a non-biogenic source (Kang et al., 2014; Szatkowski et al., 2002; Romanak et al., 2014; Whiticar, 1999). Though the well pad is located near wetland areas, the maximum recorded methane efflux rates are higher

than previously published rates in natural wetland settings (Tokida et al., 2007; Kang et al., 2014).

Considering the above observations and findings by previous authors, at this site CH_4, C2-C5, and He are interpreted to originate from a deeper gas migration source, while N_2, Ar and O_2 are interpreted to have primarily atmospheric origins (Annunziatellis et al., 2008; Frederick et al., 2017; Sandau et al., 2019). Since Ar is biologically inert, it provides a 'tracer' of atmospheric gases. The generally linear Ar-CH_4 relationship suggests a two end-member mixing model between methane and Ar, with dilution and displacement of atmospheric gas near the wellhead (Frederick et al., 2017). The non-linear correlations between O_2 and other gas species reflects its biological consumption and production.

2.5.2 Spatial distribution of migrating gases

Elevated CH_4 concentrations and efflux around the wellhead indicated a preferential migration zone. During the long-term measurements, the average CH_4 efflux at the 0.44 m^2 chamber encircling the wellhead was approximately two orders of magnitude greater than the next highest measured location at 0.5 m SE (Table 2.1). While the wellhead chamber extended > 15 cm beyond the edge of the surface casing, concentration surveys repeatedly indicated that the highest measured surface CH_4 concentrations (and therefore likely also the highest efflux) occurred immediately outside the casing (Figure C2). The observed spatial distribution supports the dominance of vertically acting buoyancy forces on gas transport in the saturated zone, and a higher gas permeability near the well in both the saturated and unsaturated zones (Van de Ven et al., 2020). Fracturing or disturbance of the rock within the formation during drilling, and the subsequent cementation challenges, are generally understood to result in micro-annuli between

the cement and casing or cement and formation, causing the zone along the well casing to be a preferential migration pathway with lower capillary entry pressure to migrating free-phase gas (D'Aniello et al., 2020; Dusseault & Jackson, 2014).

Excluding the subset of highest effluxes and concentrations immediately adjacent to the wellhead, effluxes at ground surface, and surface and in-soil gas concentrations, were not uniformly lower with increasing radial distance (0.5 to 5 m) from the interpreted preferential migration pathway immediately outside the outermost casing. Spatial variability in gas effluxes and concentrations measured at the soil surface are known to exist due to subsurface heterogeneity and lateral migration underneath capillary barriers in the saturated zone (Forde et al., 2019a; Steelman et al., 2017; Van de Ven & Mumford, 2020) as well as preferential gas movement in the unsaturated zone (Chamindu Deepagoda et al., 2016; Mitton, 2018). This spatially variable distribution of migrating gases, with higher effluxes and concentrations closer to the well, rapidly decreasing to low or intermittently non-detectable values, confirms findings by several previous authors (Erno & Schmitz, 1996; Forde et al., 2019a; Lyman et al., 2020; Smith et al., 2019).

The rate and shape of concentration increase curves within the closed efflux chambers over time (Figure C6) varied spatially. Advective efflux was suggested by rapid linear concentration increases at high efflux locations, regardless of concentration gradients, while a low-rate exponential concentration increase indicative of diffusive efflux was observed at collars more distal to the preferential migration pathway (similar to finding by Forde et al., 2019a; Sihota et al., 2013). Occasional stepwise concentration increases suggest ebullition events

(Figure C6). The total number of CH_4 efflux measurements above the minimum detectable efflux ranged from 100% at the wellhead chamber down to 8% at 5.0 South (Table 2.1), suggesting that the gas migration pathway outside the outermost casing can be characterized as a relatively continuous transport pathway, while further away the transport of gas through the saturated zone shifted to a transitional or discontinuous flow regime, as was observed by Van de Ven et al. (2020) in lab experiments. The spatial distribution of soil gas composition, detectable effluxes, and efflux curve behavior indicates primarily advection-driven gas transport from the gas source depth, along the well-casing preferential migration pathway to the atmosphere, with more intermittent and diffusive flow at greater distances from the wellhead (similar to observations by Chamindu Deepagoda et al., 2016).

Both heterogeneity in efflux patterns and short-term variation in effluxes over the two-hour spatial survey may have also introduced some apparent spatial variation since individual 90 second closures may have captured ebullition events or periods of higher efflux at some locations but not others. This spatial heterogeneity resulted in a poor spatial autocorrelation of CH_4 effluxes which introduced a large degree of uncertainty in the interpolated effluxes used to estimate total emissions (Table 2.4).

2.5.3 Total CH_4 emissions and other impacts

Total gas migration CH_4 emissions across the full measurement grid was estimated to be 466 g d^{-1} (non-detectable to 2590 g d^{-1} at 95% CI) in August and 229 g d^{-1} (non-detectable to 1750 g d^{-1} at 95% CI) in September using Bayesian kriging interpolation methods. Emissions averaged 129 g d^{-1} from the wellhead chamber over the 15-day high resolution measurement period (Table 2.4). While multi-day emissions directly around the wellhead reasonably predicted

GM emission magnitude, the sum of low-rate diffusive effluxes applied across the 20 m by 20 m measurement area centered on the well did contribute significantly to the total estimated emissions from GM. Poor spatial autocorrelation of CH_4 effluxes resulted in substantial uncertainty in interpolation and therefore large total emissions estimate error through kriging methods (Figure C8). Emission estimates at the lower and upper 95% confidence intervals were non-detectable to 2590 and non-detectable to 1750 g CH_4 d^{-1} for August and September, respectively. This uncertainty indicates the potential for error in estimates of total GM emissions at other sites when using point efflux measurements. Total GM emission estimates compared similarly when using Inverse Distance Weighting interpolation or the mean efflux applied to a three-meter radius around the well (after Erno & Schmitz, 1996), while Bayesian kriging estimates were higher (Table 2.4). High-resolution multi-day measurements were more likely than single sampling events to capture higher magnitude GM methane effluxes, which tended to occur over night during periods with low wind velocities, resulting in order of magnitude higher estimated effluxes for long-term chamber measurements compared to the snapshot survey measurements (Table 2.4).

Despite the uncertainty in emission estimates, the average of the two kriged spatial survey estimates, at 350 g CH_4 d^{-1} (or 0.5 m^3 d^{-1}, 3.6 t CO_2e y^{-1}), is within the range of values reported for energy wells with gas migration and comparable to other sources of anthropogenic methane emissions (Table 2.5). Direct comparison between these results and emission values presented in previous studies are complicated by differences in study design, since emissions measured through full-wellhead enclosures (e.g., Kang et al., 2014) or at cut-and-capped wells (Schout et al., 2019) may not be entirely due to GM, but also SCVF or other well integrity

failures. There is also an expected variation between wells due to differences in geology and well design, and jurisdictional differences in wellhead configuration (where surface casings in Alberta are vented to the atmosphere; Dusseault & Jackson, 2014).

Table 2.4 Estimated total GM-related CH_4 emissions at this study site. Values are average effluxes (with upper, lower 95% confidence interval where available).

Data Description	Average Emissions		Method	Comments
	g d^{-1}	m^3 d^{-1}		
		STUDY WELL		
August efflux survey	23	0.03	a	
	104	0.15	b	n=10 detectable efflux locations
	466 (0, 2590)	0.7 (0, 3.8)	c	
	118	0.17	d	
September efflux survey	15	0.03	a	
	84	0.12	b	n=8 detectable efflux locations
	229 (0, 1748)	0.34 (0, 2.6)	c	
	48	0.07	d	
October long-term measurement	129 (123, 135)	0.19 (0.18, 0.20)	a	Bootstrapped mean on n=1215 ground-surface emission measurements over 14 days
	1733	2.55	b	Mean of n=5 14-day long-term chamber mean efflux rates
Wind speed < 3 km h^{-1}	208 (199, 217)	0.31 (0.29, 0.32)	a	Mean wellhead ground-surface emissions, subset to times with wind speed < 3 km h^{-1}

[a] Ground-surface efflux in chamber directly around wellhead, [b] Arithmetic mean of all efflux measurements applied to a 3 m radius around the well (non-detectable and < 0 efflux treated as zero), [c] Bayesian Kriging Interpolation, [d] Inverse Distance Weighting Interpolation

Table 2.5 Previously reported literature values for emissions resulting from well integrity failure, and comparison with other anthropogenic and natural CH_4 sources/sinks. Unless otherwise stated, values are mean emissions (with upper, lower 95% confidence interval where available).

Data Description	Emissions		Method	Comments	Source
	$g\ d^{-1}$	$m^3\ d^{-1}$			
GAS MIGRATION AROUND PETROLEUM WELLS					
Mean ground-surface emissions (Western Canada)	2350	3.5	b	N =29 shallow oil and gas wells in Eastern Alberta and Western Saskatchewan. Average 3 m CH_4 emission for all measurements at each well across n=29 wells reported in their Table 2. Median = 1052 $g\ d^{-1}$, 1.55 $m^3\ d^{-1}$.	Erno & Schmitz, 1996
Mean ground-surface emission, natural gas storage wells (Utah)	100 (0, 300)	0.15 (0, 0.4)	b	Measurements conducted by Lyman et al., 2020. Dynamic efflux chamber measurement method	Smith et al., 2019
Mean wellhead emissions (Pennsylvania)	264	0.390	e	Measurements from 19 abandoned Pennsylvanian wells with existing above-ground wellhead. Median = 1.3 $g\ d^{-1}$, 0.0020 $m^3 d^{-1}$	Kang et al., 2014
1 abandoned well (Netherlands)	10392		e	Only one of 29 abandoned (cut-and-capped) wells surveyed was leaking. Efflux at 2 m depth in soil.	Schout et al., 2019
Mean abandoned onshore oil and gas well (UK)	43 (35, 51)	0.06 (0.05, 0.08)	-	Emissions based on diffusive modelling of methane concentration measurements. Mean of 104 wells.	Boothroyd et al., 2015
SURFACE CASING VENT FLOWS IN PETROLEUM WELLS IN ALBERTA					
Mean Surface Casing Vent Flow (Alberta)	8860	013	-	April 2018 database records on n= 9493 open reports. Median = 136 $g\ d^{-1}$, 0.2 $m^3\ d^{-1}$	Alberta Energy Regulator, 2018
NON-PETROLEUM SOURCES/SINKS					
Replacement/growing heifers/steers	183	0.27	-	Per-head direct emission through enteric fermentation, North America	IPCC 2019
Dairy cow	268	0.40			
Canadian landfill emissions to atmosphere, per capita	35	0.05	-	Based on the 2018 estimate of 12 Mt CO2e emitted to the atmosphere as CH4, with per-capita values calculated using July 1st, 2019 population of 37,589,262	Environment and Climate Change Canada, 2020.
Alberta soil consumption capacity	-124	-0.2	-	Per m^2 ground area. Ideal laboratory conditions. Up to 40-50% oxidation efficiency	Stein & Hetteriatchi 2001
Methane biofiltration	-1900	-2.8	-	Per m^3 bulk substrate. Actively aerated system	Gunasekera et al., 2018

[b] Arithmetic mean of all efflux measurements applied to a 3 m radius around the well (non-detectable and < 0 efflux treated as zero), [c] Bayesian Kriging Interpolation, [d] Inverse Distance Weighting Interpolation, [e] All efflux at and around the wellhead

Gas migration emissions are thought to typically represent only a small contribution of total emissions in the perspective of other vented and fugitive methane emission sources at the well pad scale, and more broadly within the upstream oil and gas industry (Schiffner et al., 2020; Schout et al., 2019; Smith et al., 2019). For example, an estimated 3.9 % of average per-well emissions at a gas storage facility measured by Smith et al. (2019) were due to emissions from gas migration outside the surface casing. While likely comparatively low in the perspective of other sources within the upstream oil and gas industry, relatively poor quantification of the absolute number of wells with GM complicates quantification of industry-wide contributions of methane emissions through GM (Abboud et al., 2020). In addition, representative emission averages are difficult to obtain from limited measurements in an emission distribution that is characteristically heavily skewed by a small number of 'super emitters' (Brandt et al., 2014; Erno & Schmitz, 1996; Saint-Vincent et al., 2020; Zavala-Araiza et al., 2015). Nonetheless, GM at this study well was repeatably detectable using efflux and concentration-based approaches at varying time scales, despite a comparatively low emission rate in perspective of industry-wide sources. This indicates that 'super-emitting' GM wells most significant from an emissions standpoint will be reliably detected in similar field settings. Placed within the larger context of anthropogenic emissions, the annual methane emissions from this study well were equivalent to the operation of ~1 Canadian passenger vehicles (at 3.26 t CO_2e y^{-1}) or the direct emissions through enteric fermentation over the full-life of < 2 North American beef cattle (IPCC 2019; Natural Resources Canada).

Legal requirements for well decommissioning (abandonment) in Western Canada stipulate that GM (and other well integrity failures such as surface casing vent flow; SCVF) are

repaired to non-detectable rates, at expense averaging at least $CAN 150 000 per well, and with an anecdotally high rate of unsuccessful repair attempts (Alberta Energy Regulator 2021; Dusseault et al., 2014). This repair cost is an economic disincentive for operators to repair and decommission non-producing wells with GM, therefore contributing to a backlog of suspended energy wells that may otherwise be decommissioned (Abboud et al., 2020; Alboiu & Walker, 2019; Schiffner et al., 2020). More widespread and increasingly rigorous testing approaches may provide insight into the liability of suspended wells with GM, while remediation of all but super-emitter wells may contribute proportionally low reductions in overall methane emissions in the broader perspective of anthropogenic emissions.

From a GM detection perspective, surface efflux and concentration measurements most easily detect those wells which are more significant sources of atmospheric emissions, such that the highest impact wells will be most readily detected. This, however, may not be true of subsurface and groundwater impacts due to the complexity of subsurface migration pathways and geochemistry, and the potential for greater methane dissolution with lower rate or more episodic gas migration due to greater interfacial area between free phase gas and groundwater (Cahill et al., 2017; Van De Ven et al., 2020). The desired testing sensitivity and future standards of GM testing must consider desired risk mitigation, be it atmospheric emissions, groundwater impacts, or simply any presence of GM.

2.5.4 Temporal variability in measured effluxes and concentrations:

Measured CH_4 and CO_2 efflux and pre-closure concentrations of CH_4 at locations < 1 m from the well varied by up to 50% between individual measurements (taken ~18 minutes apart; Figure 2.5). Previous authors have found, both conceptually and experimentally, that the

interaction of buoyancy and capillary forces of migrating free-phase gas in porous media will result in fingered and continuous or discontinuous migration pathways, causing spatially variable and potentially intermittent gas emission at the surface despite a continuous gas source at depth (Ahlfeld & Dahamani, 1994; Gorody, 2012; Van de Ven et al., 2020). This conceptual and laboratory understanding is supported by these field data of intermittently detectable observations, 'stepped' closed chamber concentration increases (Figure C6), and substantial variations in efflux magnitude between measurements < 1h apart, as has been observed by other authors (Sihota et al., 2013; Forde et al., 2019a; Lyman et al., 2020).

In addition to this described irregular variation attributed to episodic ebullition and gas movement in the saturated zone, a quasi-diel cycle in efflux and concentration by up to one order of magnitude was identified with higher measured CH_4 and CO_2 initial chamber concentrations and effluxes occurring at night, and greater magnitude of variation nearest the wellhead (Figure 2.5). Decreased initial chamber concentrations during the daytime were correlated with periods of higher wind speeds, as suggested by the stepwise regression modeling results (Table 2.2), and as observed in previous gas migration studies at the well pad scale, and field-scale vadose zone gas injection experiments (Yin et al., 2014; Ulrich et al., 2019). Wind speed was also inversely correlated with historic gas migration concentration tests (Figure 2.1; Figure 2.2) suggesting it has a similar effect in efflux chambers and the industry standard of practices. Increased wind velocity has been shown to erode the methane concentration boundary layer, thereby decreasing measured methane concentrations at and near the ground surface (Chamindu Deepagoda et al., 2016; Ulrich et al., 2019).

Regression models suggest multiple other factors were also related to varying initial CH_4 concentrations, including soil temperature and barometric pressure change for chambers near the well, and air temperature and absolute barometric pressure for chambers further away (Table 2.2). Despite the relatively thin vadose zone, the regression model also indicated a moderate relationship to changes in barometric pressure, particularly for suppressing higher modelled effluxes and higher concentrations during periods with the highest rate of barometric pressure increase, leading to a modest increase in the model R^2 for the CH_4 concentrations at several locations (Table C3, Table C5). This observation is consistent with pressure-differential induced movements of soil gas within the unsaturated zone, as previously observed in multiple fields of research including artificial gas migration experiments, landfill gas emission, and natural methane-producing ecosystems such as peatlands (Börjesson, & Svensson, 1997; Forde et al., 2019b; Nachshon et al., 2011). There was no indication that falling barometric pressure triggered ebullition events as observed by Tokida et al. (2007).

Other observed statistical relationships to methane efflux and concentrations were to the water level and rate of water level change, and the related variable of soil water content. This is consistent with advective movement of gas during filling and emptying of pores, and altered gas movement pathways and lower effective gas permeability in the soil at higher soil water contents. Temperature-related factors included the atmospheric temperature, potentially leading to greater diffusion rates at higher temperatures, and the differential between soil and atmospheric temperatures since this may induce a convectively driven advective efflux (Nachshon et al., 2011).

2.5.5 Wind influences on variations in measured efflux

Regression modelling results also indicate that variation in wind speed was the most important predictor for the variation in the measured CH_4 efflux at the wellhead chamber, where it contributed to 11% of the final model R^2 fit. Measured CH_4 and CO_2 efflux and wind speed are negatively correlated at multiple chamber locations (Figure C11), where lower measured effluxes occur during times of higher wind speeds. These observations are similar to previous studies using dynamic closed chambers (e.g., Oliveira et al., 2018; Seo et al., 2020). This trend of lower measured efflux at higher wind speeds largely conflicts with conceptual understandings of greater ground-surface gas exchange at higher wind speeds caused by pressure pumping and a Bernoulli effect of reduced pressure (Poulsen & Møldrup, 2006; Poulsen et al., 2017; Redeker et al., 2015). While these reported data may be due to a strong correlation to some unconsidered factor accounting for true variation in efflux at this site, lower observed efflux is most likely explained by measurement bias with site infrastructure and the equipment used (Maier et al., 2019). Experimental error involving flushing of gases within the chamber due to an imperfect isolation during chamber closure is considered unlikely. This wind-efflux relationship was observed across all six independent chambers, and spot-checked concentration increase curves did not indicate any air flushing during chamber closure (Figure C6; Figure C11).

Firstly, winds may flush soil gases around structures, removing the migrating soil gases from within the collars (5 cm depth at the wellhead, 15 cm depth elsewhere). Previous authors suggested that higher wind caused lower measured radon efflux and radon entry into structures due to flushing of the soil with atmospheric air, especially around above-ground structures that will induce pressure gradients within the soil (Kovach, 1945; Riley et al., 1996). This may

present a potential problem for future use of chamber-based methods of CH_4 emissions through well pad soils. Larger flux collars (as used here), or larger or custom chambers or tents may be necessary to encircle the surface facilities (including the well casing or full wellhead) that are expected to represent preferential gas movement pathways (e.g., Kang et al., 2014; Lebel et al., 2020; Riddick et al., 2020).

Another explanation for the observed wind-efflux relationship is a bias towards under-estimating effluxes during high-wind periods due to more rapid breakthrough times at higher wind speeds and the closed chamber's attenuation of atmospheric pressure variations. In a laboratory experiment of gas breakthrough with varying wind speeds, Poulsen et al. (2017) noted that the breakthrough times of soil gas during windy periods was as low as 1 to 2% of wind-free conditions. Episodic arrivals of methane and other gases through ebullition at the water table will therefore break through to the ground-surface boundary layer more rapidly in times of higher wind speed, increasing the chance that an ebullition event will not be captured by the discrete 90 second chamber measurements during higher-wind periods. At a shallow peatland, Redeker et al. (2015) observed that a high wind event of less than 10 minutes caused substantial gas exchange that temporarily raised peatland CO_2 effluxes until the soil had been flushed with atmospheric air, at which point the efflux was suppressed for several tens of minutes until pre-wind efflux rates re-established. The vents on the dynamic closed efflux chambers used in this study are specifically designed to limit any pressure fluctuations caused by wind under the intent to limit measured effluxes to those caused by diffusive mechanisms while avoiding the over-estimation of effluxes caused by a venturi-induced pressure drop within a chamber with open vents (Xu et al., 2006). Therefore, the vented chambers used in this study inhibit one of the primary modes of

gas exchange across the ground surface. Since the effluxes at sites with shallow water tables are decreased after a higher wind event, the chamber measurements at this site may have been biased towards under-estimating the effluxes during periods of higher winds (Maier et al., 2019). This bias may have contributed to the 62% increase in average wellhead CH_4 efflux for low-wind (< 3 km h^{-1}) periods compared to the full time series (Table 2.4).

2.5.6 Methane oxidation in the unsaturated zone

Several previous authors have also suggested quasi-diel variations in CH_4 efflux may be explained by the strong, exponential dependence of CH_4 oxidation rates on higher temperatures, even when the magnitude of temperature variation in some previous studies were relatively small (Börjesson, & Svensson., 1997; Mikkelä et al., 1995; Stein & Hettiaratchi, 2001; Tang et al., 2008). During this field experiment, the magnitude of daily atmospheric temperature variation was up to 15 ℃ (from -5 to +10 ℃), leading to soil temperatures variations of up to 4 ℃ (from 2 to 6 ℃) at the 5 cm depth and <1 ℃ (around an average 3 ℃) at the 30 cm depth (Figure C9). Variable oxidation rates caused by these diurnally fluctuating soil temperatures were unlikely to have caused a substantial proportion of the variation in observed efflux at the wellhead. The regression model fit indicated that soil temperature variation gave a relatively limited contribution to model performance at most chamber locations (Table C3, Table C5). In addition, there was no indication of increased CO_2 efflux coinciding with decreased CH_4 efflux at higher temperatures, as would be expected if the soil microbes were producing CO_2 at higher rates during higher daytime temperatures. This observed oxidation effect is expected to be more prevalent away from the primary gas transport zone. The relative importance of oxidation in decreasing measured concentrations would be lower along the high-efflux preferential flow

pathway due to less contact time, lower surface area, and lower soil O_2 where atmospheric gases have been displaced (Forde et al., 2018; Gunasekera et al., 2018).

Although variable oxidation rates do not appear to contribute substantially to the diel variation in effluxes, there is good evidence that some CH_4 is being oxidized to CO_2 within the unsaturated zone, in support of observations of previous research at gas migration sites (Erno & Schmitz, 1996; Forde et al., 2018, Schout et al., 2019). Soil $\delta^{13}C_{CO2}$ averaged -53 ‰, indicating some CO_2 was being formed through biodegradation of thermogenically sourced CH_4, or a mixed thermogenic-biogenic source (Table C2, Figure C7; Risk et al., 2013; Romanak et al., 2014). Higher CO_2 effluxes and soil CO_2 concentrations are observed within meters of the wellhead preferential flow pathway (Figure 2.4; Figure 2.7). At the elevated concentrations observed, this CO_2 may be derived from some combination of natural in-soil biologic respiration, production of CO_2 during oxidation of CH_4, and transport of deeper CO_2 as a component of the migrating gases (Romanak et al., 2014). The samples with highest migrating gas concentrations of CH_4 and He, collected from immediately outside the well casing, did not have the highest concentration of CO_2. In addition, the N_2/O_2 ratio is commonly higher than ten for samples near the well, compared to the atmospheric value of 3.7, which is consistent with the consumption of atmospheric O_2 (Figure 2.7; Romanak et al., 2014). Samples with O_2 concentrations that are depleted relative to atmospheric concentrations also have higher CO_2 concentrations. At the lower O_2 concentrations, the trend between O_2 and CO_2 is steeper than -1, indicating that methane oxidation is more important than natural biologic respiration in the production of CO_2 near the wellhead. More distal to the well, the N_2/O_2 ratio and the trend of O_2 to CO_2, are more consistent with a biologic respiration source (Figure 2.7; Sandau et al., 2019; Romanak et al.,

2014). Biologic respiration is likely contributing to measured CO_2 concentrations and effluxes with a mixed or natural source, with increasing importance of biologic respiration further from the well. These combined compositional and isotopic indicators suggest that CH_4 oxidation within the unsaturated zone is leading to the elevated CO_2 concentrations and effluxes within meters of the wellhead.

While perturbations to the natural geochemical conditions, including anaerobic soils and inhibition of plant growth may develop, microbially mediated oxidation of CH_4 is favorable from an explosion hazard and emissions standpoint since these reactions will eventually yield CO_2, with substantially lower global warming potential (Hoeks, 1972; IPCC 2013). Systems to enhance this microbial methane oxidation may therefore be exploited as one potential option to decrease emissions from low-rate gas migration sources. Passively or actively managed in-soil oxidation or biofiltration systems could therefore be investigated as a medium or long-term strategy to address low-rate emission sources. However, the capacity of natural, actively, and passively managed systems to continue oxidizing CH_4 during soil conditions sub-optimal for microbial growth (including low temperatures or low moisture contents) will need to be investigated further (Stein and Hettiaratchi. 2001; Gunasekera et al., 2018).

2.5.7 Implications for gas migration testing and future scientific study

Potential sensory indications of GM may include visual observations of bubbling through ponded water, vegetation impacts (including discolored, stunted, or dead plants), and "auditory, olfactory, or other evidence of possible gas migration" (BCOGC, 2019; Nooman et al., 2012). In Alberta, GM impacts on vegetation have been recorded historically and additional GM test points are recommended at locations of apparent vegetation stress surrounding a well (Alberta

Energy Regulator, 2021; Bachu, 2017). Other sensory indications are not formally referenced by Alberta's provincial regulator. Throughout the field campaigns at this study site, conclusive sensory indications of GM were absent. Vegetation impacts were not observed despite soil oxygen contents at the 30 cm depth routinely approaching < 5% v/v O_2 (Figure 2.7). This may be explained in part by lessened requirements of soil O_2 by willow (Salix sp.) and other wetland vegetation at this site, with relevance to other sites with shallow water tables (Jackson & Attwood, 1996). These observations support previous arguments by Forde et al. (2019a) and Sandl et al. (2021) that reliance on sensory GM indications may be unreliable or insufficiently conclusive (especially at lower emission rates in similar field settings), and likely lead to under-quantification of the total number of wells with GM.

These high-resolution and survey efflux data document increased episodicity and less advection-driven gas movement further from the well casing, leading to increasingly lower and more irregularly detectable concentrations and effluxes (Figure C6; Chamindu Deepagoda et al., 2016; Van de Ven et al., 2020). Preferential flow pathways have often been observed along the well casing, as in this study, though Forde et al. (2019a) suggest that soil heterogeneity may, in some cases, lead to undetectable GM nearby the well while gas is detectable at further distances. Spatiotemporal variability at this site caused intermittently non-detectable values of both surface concentration and measured efflux within meters of the casing. With application to GM detection, both efflux and concentration measurements were highly sensitive to measurement location, requiring measurement at sufficient spatial density to capture any preferential gas flow pathways both close to and further from the wellhead. Surface CH_4 concentrations, despite being in the % gas range in the shallow subsurface, were at times limited to 10's of ppm in the

wellhead chamber, indicating that sensitive detectors in the ppm range are vital to distinguish the presence of wells with GM, especially if using surface detection methods (Ulrich et al., 2019). Wind speed was shown to be strongly inversely related to temporally variable pre-closure chamber CH_4 concentrations, a conservative proxy for ground-surface concentrations, and historic GM survey results. This suggests withholding GM testing during times of high wind speeds may increase the likelihood of detecting GM, especially if using ground surface measurements. The observed temporal change in maximum methane concentrations may also have implications for risk assessments of sites with GM near public structures or surface developments, such as where urbanisation has encroached on legacy infrastructure (Alberta Energy Regulator, 2014). Risk assessments could be improved by performing concentration-based measurements during circumstances that are expected to produce the highest possible concentrations at a site (e.g., low wind speeds), or through long-term measurements.

Geological factors and soil heterogeneity may drive spatial variations at this site (e.g., Forde et al., 2019a; Steelman et al., 2017). Differences in well construction and operating practices, and local geology, may drive differences in spatiotemporal gas migration behavior and emission rates between this site and at other sites (Bachu, 2017; Forde et al., 2019b; Kang et al., 2014). Short-term temporal variability in measured concentrations may have been caused by some combination of variable wind, temperature, episodic gas migration, and other factors, leading to a range in measured values of concentration or efflux at any one location over time. Despite this variation, methane concentration as a screening tool (i.e., pass/fail) for the presence of GM was resilient to temporal variability at this well with a thin unsaturated zone. Therefore, the concentration or efflux value from any ‘snapshot’ measurement may be a good indication of

the presence of gas migration and relative magnitude of emissions only. Attempts, whether in industry or academia, to attribute a single efflux or concentration value to a well for the purposes of total emission quantification, risk classification, or assessment of trends in leakage rate over multiple years, must consider the error associated with estimates based on short-term measurements. In addition, the reported total emission rate depends substantially on the estimation method used (Table 2.4). Effluxes, like concentration measurements, were also shown to be spatiotemporally variable and impacted by a variety of environmental factors.

Accurate measurement of total gas migration emission rates may require multi-day measurements to account for variation induced by episodic gas movement and meteorological factors, including the apparent decrease in observed effluxes at higher wind speeds when using the dynamic closed chamber approach. While not considered in this work, soil frost and recent strong rainfall are currently listed in legislation as complicating factors for gas migration detection in Alberta, showing a precedent in regulations for recommending consideration of other environmental factors significant to gas migration detection work such as wind speed and barometric pressure change (Forde et al., 2019b; Alberta Energy Regulator, 2021). We recommend future work directly comparing the influences on measured gas efflux and concentration by these various environmental factors, as well as assessing the resiliency of different testing methodologies to the observed spatiotemporal variation.

2.6 Conclusions

This study recorded multi-day shallow subsurface transport dynamics, and instances of spatial and temporal concentration and efflux variations for established conditions of gas migration around a petroleum well, where:

i) Efflux and concentration values varied spatially, with the highest CH_4 effluxes and concentrations focused within < 1 m of the wellhead. Gas species and isotopic composition, and efflux patterns, suggested deep gas (including thermogenic CH_4, C2-C5, and He) displaced atmospheric air and soil gas.

ii) Compared to measurements around the casing, detectable methane effluxes and concentrations as near as 0.5 m away from the wellhead were more temporally irregular. Methane effluxes 5 m South of the preferential migration pathway were routinely below detection limits.

iii) Two-week high-resolution efflux data recorded moderate temporal variability among individual measurements at a single location, and a diel variation with higher CH_4 and CO_2 initial concentrations and effluxes occurring at night. Multi-component stepwise regression modelling results show wind speed and atmospheric temperature were important predictors of temporal variation in surface concentration and measured efflux around the wellhead. Multiple factors were related to the observed temporal variation, and the correlated factors changed depending on measurement location.

Spatial variability, and short and medium-term temporal variability, may introduce error in estimates of total emissions and surface concentrations around sites with migrating gases.

Although the presence of gas migration could be reliably determined at this site, despite observed spatiotemporal variability, quantifying the efflux rate was challenging. The range of total GM-related emissions at this site was 48-466 g CH_4 d^{-1} (0.07-0.69-m^3 CH_4 d^{-1}) using different emission estimation methods, with a mean efflux of 129 g CH_4 d^{-1}; (0.19 m^3 CH_4 d^{-1}) from the preferential migration zone encircling the well casing. At this site, total emissions from gas migration were largest around the well casing, though effluxes at this location also varied temporally. Variation in emission estimates introduced by different estimation methods, and spatiotemporal emission variability, suggests that measurement and estimation methods to account for spatiotemporal variation may need to be considered for accurate GM emission estimation. This well had comparatively low methane emission rates in the broader context of the upstream petroleum industry. Reliable detectability of migrating gas at this site indicates that higher-rate GM sources most important from an emissions standpoint will be detectable using common GM test methods in similar field settings. Relative gas species composition and shifts in the $\delta^{13}C$ value of CH_4 and CO_2 were consistent with near-surface methane oxidation, suggesting this process could be enhanced to further decrease emissions. Consideration of factors causing spatial and temporal variability of migrating gases may lead to more representative measurements of surface concentrations and effluxes, and therefore improved detection and quantification of the risks and impacts associated with migrating gases around energy wells.

We conclude that at this case-study site, short-term concentration or efflux surveys at sufficient spatial density will be resilient to temporal variability for the purposes of detecting the presence of gas migration. GM detection surveys could be optimized by considering

meteorological factors, and long-term assessment is required for accurate estimation of total emissions.

Chapter 3: **Low-cost sensors provide insight into temporal variation in fugitive methane gas concentrations around an energy well**

Fleming, N. Morais, T. Ryan, M.C. 2021. Low-Cost Sensors Provide Insight into Temporal Variation in Fugitive Methane Gas Concentrations Around an Energy Well [Accepted by SPE Journal 2021-09-13; SJ-0621-0083]

3.1 Abstract

Effective measurement of the presence and rate of methane gas migration (GM) outside the casing of energy wells is important for managing social and environmental impacts and financial liabilities in the upstream petroleum industry. Practitioners typically assess GM by above-background methane gas concentrations in-soil or at-grade; however, factors influencing the potential variation in these measurements are not well represented in industry recommended best-practices.

Inexpensive chemoresistive sensors were used to record a one-minute frequency methane gas concentration time series over 19 days. Time series were recorded at three soil depths (0, 5, and 30 cm) at two locations <30m cm radially from a petroleum well with known GM, in addition to two 'control' locations. Observed concentration variations ranged over several orders of magnitude at all depths, with generally lower concentrations and more variation observed at shallower depths. Varying concentrations were correlated to meteorological factors, primarily including wind speed and shallow groundwater table elevation. The gas concentration patterns were affected by a 3.5 mm rainfall event, suggesting soil moisture changes affected preferential gas migration pathways. Results indicate potential variability in repeated snapshot GM test results. Although currently recommended GM detection methods would have effectively identified the presence/absence of GM, they would not have quantified order of magnitude

changes in concentration. GM detection success at this site was increased with measurement at more than one location spatially within 30 cm of the well casing, lower concentration detection limits, and greater measurement depth. These findings indicate that meteorological factors should be considered when conducting gas migration surveys (particularly for improving at-grade test reliability). The low-cost approach for long-term concentration measurement facilitates insight into variable gas concentrations and may be advantageous in comparison to snapshot measurements in some circumstances.

3.2 Introduction

Well integrity failures, including Surface Casing Vent Flow (SCVF) and Gas Migration (GM) outside the outermost (or surface) casing, represent safety, environmental, and financial liabilities to the upstream oil and gas industry and negatively affect the oil and gas industry's social license (Dusseault et al., 2014; Cahill et al., 2017; Alboiu and Walker, 2019). Wells with SCVF or GM detected cannot be legally decommissioned in Canada, and therefore appropriate GM detection informs operational decision making on remedial cementing, with important environmental and social consequences, and financial implications (Trudel et al., 2019; Alberta Energy Regulator (AER) 2021; Schiffner et al., 2021). Decommissioning and reclamation costs for wells with SCVF or GM typically cost between $140K to $370K, with 5-10% of wells costing considerably more (e.g., up to millions of dollars) due to SCVF/GM repair challenges (Trudel et al., 2019). These costs further increase if re-entry is required when SCVF/GM is discovered after a well has already been decommissioned (Dusseault et al., 2014; Trudel et al., 2019). Acute GM risk is primarily related to explosive hazard (between the lower and upper explosive limits of 5-15% methane v/v in a mixture with air) (Engelder, T. and Zevenbergen

2018; Molofsky et al., 2021). Therefore, accurately determining the potential for explosive combustible gas-air mixtures is central to classifying the risk of these wells (AER 2014; Molofsky et al., 2021). Importance thus needs to be placed on the detection and measurement approaches for SCVF and GM.

The most common detection method for SCVF is a simple 'bubble test', which determines if the vent flow will generate sufficient pressure to push a bubble through a 6-12 mm diameter tubing directed through a maximum backpressure of 2.5 cm water, within a ten-minute period (AER 2021). Alternate methods to the bubble test, including higher resolution and long-term remote monitoring, are applied commercially in situations benefiting from more definitive or continuous measurement, such as for accurate rate determination, tracking temporal trends, and observing SCVF response to remedial work (Dusseault and Jackson 2014).

Unlike SCVF measurement and monitoring, to our knowledge there are no commercially available approaches for continuous GM testing or monitoring. Commercial detection of the presence of GM outside the casing of energy wells is typically conducted through 'snapshot' GM detection surveys by sequentially measuring methane gas concentrations at numerous specified (and provider-dependent) soil depths and spacings around well-center. The test is comprised of multiple snapshot measurements over a short time period (i.e., less than one hour). Detection of above-background concentrations of 'combustible soil gas' (predominantly methane, along with trace amounts of other natural gas alkanes) indicates the presence of GM (Szatkowski et al., 2002). This approach was developed in the 1990's by an ad hoc industry group to assess presence or absence of GM and remains the recommended approach in Alberta (Abboud et al.,

2020). In this approach, methane gas (hereafter referred to as ‘gas’) concentration is measured at a total of 14 test points: two within 30 cm of the well and then at 2, 4, and 6 m away (radially) orientated in a cross pattern (AER 2021). While not necessarily applied by practitioners, the regulators recommended equipment lower detection limit for this test is 1% of the methane Lower Explosive Limit (LEL, i.e., 500 ppm CH_4). Alternate testing spacings and depths, including at-grade measurement (as opposed to the AER-recommended 50 cm depth; Fleming et al., 2019), are applied by industry practitioners to minimize the added expense of auguring access holes, or sampling depths less than 30 cm to avoid requirements for ground disturbance permitting (e.g., Province of Alberta 2020; BC Oil and Gas Activities Act 2020; Statutes of Saskatchewan 1998). These at-grade and relatively shallow sampling depths are permitted in regulation to encourage innovation and use of newly available technology (Natural Resources Canada, 2019; AER 2021).

The Alberta-recommended GM detection approach is largely duplicated or directly referenced in regulation across Canada (e.g., Government of Saskatchewan, 2015; OROGO, 2017; Pretch and Dempster, 2017; BCOGC, 2019). However, to our knowledge, there are no public reports demonstrating the advantage of subsurface detection strategies (e.g., up to 50 cm depth) or validating this approach in variable field conditions (Abboud et al., 2020). In addition, though it is anecdotally evident that these recommendations are not applied by all practitioners, there is little published information on the GM sampling and detection approach in GM testing reports (e.g., the AER ‘s Well Vent Flow/Gas Migration Report). Negative test results are also unavailable, leading to uncertainty in the total number of wells tested (Abboud et al., 2020; Sandl et al., 2021).

Temporally varying SCVF rates have been reported, indicating that long-term monitoring may be required to fully characterize emission rates and to ensure more reliable detection compared to short-term 'snapshot' measurements (Dusseault et al., 2014; Riddick et al., 2020). Previous researchers have also found soil-surface GM concentrations and effluxes to vary over hourly, daily, and seasonal scales (Forde et al., 2019b; Lyman et al., 2020). Spatiotemporal variation of CH_4 emissions and at-grade concentrations over time scales ranging from < 1 hour to daily scales has been further demonstrated by a two-week efflux experiments at six test points around a GM energy well in Eastern Alberta (Fleming et al., 2021). Historic GM survey test results at this well indicates variation between tests conducted by different parties, and by the same party on different occasions. This suggests a variation in measured concentrations due to both method-dependent mechanisms (e.g., testing depth and location), and method-independent temporal variations in the physical presence of combustible soil gases (Fleming et al., 2021, their Figure 2).

Temporal variation in gas concentrations and effluxes may be driven by episodic and pulsed movement of gas in the saturated zone (Cahill et al., 2017; Van de Ven et al., 2020) and due to changing atmospheric conditions (Kuang et al., 2013; Oliveira et al., 2018). Barometric pressure changes are also known to induce variable effluxes, and may cause atmospheric gases to flow into the soil during rising barometric pressures due to a pressure imbalance between atmospheric and soil gases (Abbas et al., 2010; Forde et al., 2019b). High wind speed has been shown to decrease measured at and above-grade methane concentrations from subsurface sources (Chamindu Deepagoda et al., 2016; Ulrich et al., 2019), and induce subsurface gas pressure variations that may drive higher effluxes and flush soil gases in the soil (Poulsen et al., 2017).

Higher air temperatures may drive higher gas diffusion rates, while convective and buoyant gas movement may be caused by differences in density due to temperature and the relative density of methane compared to air (Nachshon et al., 2011; Chamindu Deepagoda et al., 2016).

While these recoded variations in gas migration effluxes and concentrations may indicate relevant variations in measurable combustible gas concentrations, prior experiments have not explicitly demonstrated whether concentration variations, potentially driven by meteorological factors such as wind speed and atmospheric pressures and temperatures, occur in the subsurface in addition to the measured at-grade concentrations and effluxes. In addition, time series measurements simultaneously at multiple depths were not possible using a single high-resolution gas analyzer connected to multiplexed flux chambers in previous studies (e.g., Forde et al., 2019a; Fleming et al., 2021). While previous studies of gas migration efflux are relevant from a methane emissions measurement perspective (Forde et al., 2019a; Lyman et al., 2020; Fleming et al., 2021) and effluxes may be used to detect GM (Forde et al., 2019a; Schout et al., 2019), most practitioners currently rely on concentration measurement. Thus, understanding methane concentration variability is more applicable to the current practice in GM detection. To the authors knowledge, previously published work has not recorded temporal variation of in-soil fugitive gas concentrations at a high resolution over multiple days, nor analyzed how this variation may affect the successful detection of wells with GM.

Here we use inexpensive chemoresistive sensors to record a high-frequency combustible gas concentration time series at multiple depths around a case study well with GM. With the aim

of improving GM testing and monitoring practices, this field experiment specifically sought to evaluate whether:

- Measurable methane concentrations are higher at greater depths in the soil.
- Measurable methane concentrations are temporally variable both at-grade and at depth into the soil.
- If present, these variations in measurable methane concentration coincide with varying meteorological conditions such as precipitation, wind speed and barometric pressure changes.

3.3 Materials and Methods

3.3.1 Study well description.

Field access to a suspended petroleum production well with GM was provided by an anonymous industry partner. Previous site investigations confirmed the presence of detectable GM focused outside the well casing, with estimated average emissions within a 25 cm radius around the well-center of 0.3 m^3 CH_4 d^{-1} (130 g d^{-1}) and no detectable SCVF (Fleming et al., 2021). Gas concentrations in 14 different detection surveys conducted over > 10 years document a consistently detectable presence of GM focused near the well casing, though the maximum measured concentrations during commercial GM testing have varied from <100 to 110,000 ppm. In each survey, the highest methane gas concentrations were observed near the well casing (i.e., the two measurements spatially located “within 30 cm of wellbore on opposite sides”: AER 2021). This spatial distribution is common in most GM surveys (Erno and Schmitz 1996; Lyman et al., 2020) with some exceptions (Forde et al., 2019a).

Soil gas sampled immediately against the outer casing at 30 cm depth yielded thermogenic methane concentrations as high as 87% gas by volume with minor concentrations of higher alkanes, consistent with common GM composition (Fleming et al., 2021). Compositional analyses of the 61 soil gas samples (sampled by the authors at depths from 0 to 30 cm within 1.5 m of the well) include a mean and maximum concentration of C2+ gas concentrations (including ethane [C2], propane [C3], nC4, iC4, neopentane, iC5, nC5, and nC6) of 0.069 % v/v and 0.378 % v/v, respectively. The mean methane [C1] concentration for the same sample set was 18.4 % v/v, indicating that the combustible soil gases were predominantly (i.e., > 97 % v/v) methane. The balance of average soil gas compositions (in order of decreasing mean abundance) were N_2 (64.5%), O_2 (14.4%), CO_2 (1.4 %), and Ar (0.74%). Atmospheric methane concentrations sampled five meters South of the well in October 2019 averaged 2.5 ppm (max 5.5 ppm) (Fleming et al., 2021). The shallow lithology, as observed by hand auger samples, is fine silty sand down at least 2 meters, with a water table ~ 0.5 m below ground surface. The prevailing wind direction in the region is westerly (Alberta Agriculture and Forestry, 2020).

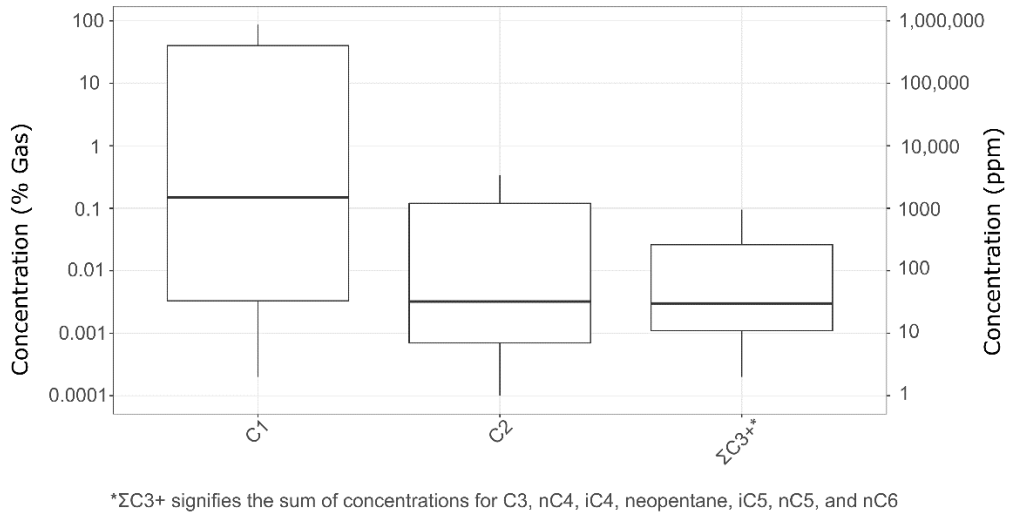

Figure 3.1 Boxplot showing the relative occurrence of C1 (methane), C2 (ethane), and C3+ in combustible soil gas compositions. The boxplots include analyses from 61 samples collected at 0-30 cm depth and < 1.5 meters radius from the study well. The logarithmic vertical axes show percent composition (left axis) and ppm (right axis). The boxplot graphically illustrates the minimum, 1st quartile, median, 3rd quartile, and maximum measured concentrations.

3.3.2 Sensor measurement of methane concentration.

Sensors were installed at four locations to monitor methane gas concentrations at one-minute frequency over 19 days (October 3-22, 2020). Chemoresistive MQ-4 combustible gas sensors with high sensitivity to methane (Henan Hanwei Electronics Co. Ltd.) were inserted into water-resistant housings (Fig C.1.1). Sensor loop resistances were recorded at one-minute frequency on a datalogger (CR1000, Campbell Scientific). Since the dominant form (> 97%) of combustible gas in GM at this site is methane (Figure 3.1), the term gas concentrations is used to represent methane concentration herein. Two vertical sensor nests, which included sensors at depths of 0 (i.e., at-grade), 0.05, and 0.30 meters below ground surface, were located five centimeters radially from the East and West sides of the surface casing (Figure 3.2; Figure D.1.1). Two distal (i.e., 'control' to the GM around the well casing) sensors located 5 m to the

East of the surface casing, were installed at 0.05 m depth to document sensor noise and any response that could be caused by variable temperature and humidity factors. Of the two distal sensors, one was installed in native soil at 0.05 m depth (referred to as the distal 'soil baseline' sensor). The second was isolated from subsurface methane gas efflux by installation at 0.05 m depth in moist filter sand inside an open-topped polyethylene container (0.3 m diameter by 0.3 m depth) that was buried in the soil, with the sand filled to grade (referred to as the distal 'isolated' sensor).

The location of the sensor nests near the well was chosen to represent typical testing practices for measurements nearest the well, with two measurements within 30 cm of the well on opposite sides (e.g., AER 2021). The chosen depths were based on anecdotal information around the common measurement depths employed by service companies that conduct gas migration testing around energy wells. As previously mentioned, the 30 cm threshold is commonly used because depths less than this do not typically require ground disturbance permitting (e.g., Province of Alberta 2020; BC Oil and Gas Activities Act 2020; Statutes of Saskatchewan 1998).

The MQ-4 sensors use a tin dioxide (SnO_2) chemoresistive semiconductor which is responsive to combustible gases, including methane (CH_4) and other light hydrocarbon gases present from gas migration (Honeycutt et al., 2019). The sensor resistance is constant in the presence of clean air (i.e., mostly N_2 and O_2, with negligible CH_4 concentrations; Henan Hanwei Electronics Co. Ltd.). A passive diffusive sampling method is used to deliver target gases to the sensor, where hydrocarbon gases react with available oxygen causing a non-linear decrease in sensing loop resistance with increasing hydrocarbon gas concentration (Honeycutt et al., 2019).

These sensors are reactive in the presence of any light hydrocarbon gas, including other alkanes (C2+), but are most sensitive to CH_4 (Henan Hanwei Electronics Co. Ltd.). Previous experiments on sensors using a similar principle of measurement indicate limited interference by CO_2 (Sekhar et al. 2016). The sensors are also slightly impacted by variable humidity and temperature (Henan Hanwei Electronics Co. Ltd.). These inexpensive sensors (~CAN $5 per unit) have been previously suggested or used for similar applications, including natural gas leak detection (Mitton, 2018), and continuous efflux measurements around wellheads (Riddick et al., 2020). Sensor-specific exponential calibration curves between methane concentration and raw voltage response were developed in the laboratory. While these sensors are responsive to a range of combustible hydrocarbon gases, calibration and reporting as ppm methane is justified by the relatively minor presence (< 3%) of C2+ gases in comparison to methane (Figure 3.1). Manufacturer response curves indicate that low C2+ gas concentrations would induce a similar response to an equivalent concentration where CH_4 is the only alkane present (Henan Hanwei Electronics Co. Ltd.). Previous gas composition data (Figure 3.1) indicate that methane concentrations over the measurement period may have infrequently exceeded the manufacturer recommended 5% methane by volume, potentially leading to an underestimate of true methane concentrations above this 5% threshold. Detailed sensor validation and calibration methods, in addition to details on the solar power supply and field installation, are described in Appendices A through C.

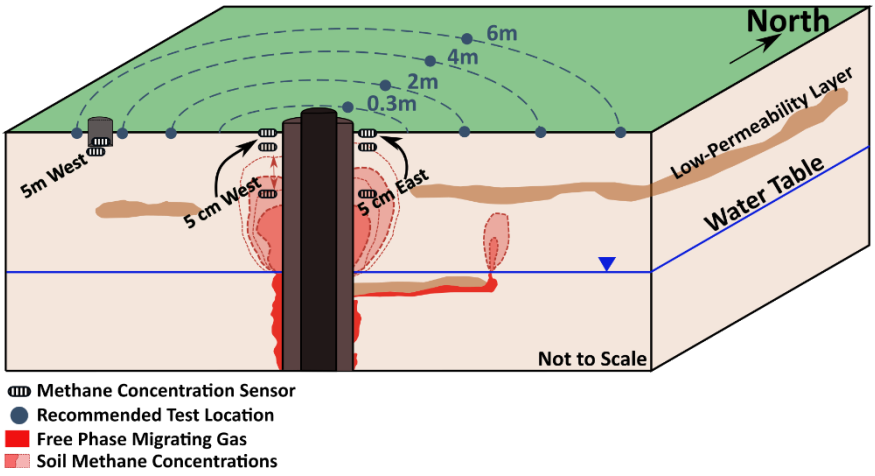

Figure 3.2 Case study site cross section conceptual diagram showing the methane migration along the wellbore and underneath a low-permeability layer (After Forde et al., 2019a). Methane concentration sensors are 5 cm from the well casing on the East and West sides, at depths of 30, 5, and 0 cm. Two additional sensors are 5 m West in-soil and in an isolated enclosure. Recommended test locations for Western Canadian gas migration detection are shown as points.

3.3.3 Meteorological data collection during monitoring period.

Precipitation and wind speed data were retrieved from the nearest public weather station (10-20 km away) (Alberta Agriculture and Forestry, 2020) for the monitoring period. Water levels from a hand-installed piezometer (screen centered 1.0 m depth below ground surface, 1.25 m South of well-center) and on-site atmospheric temperature and pressure were recorded hourly (Levelogger®). The water levels were barometrically compensated with a Barologger®. Water level and barometric pressure change rates were approximated as a five-hour central difference, which was the shortest time interval that returned a visually smooth change rate.

3.3.4 Data processing.

Sensor response data were processed in R (R Core Team 2020), where the calibration curves were used to convert raw voltage to methane gas concentrations before being compared to

meteorological and site conditions. Data analyses included Pearson correlation analyses between gas concentrations and meteorological factors (including wind speed, temperature, barometric pressure and pressure change), and groundwater level and water level change. Short-term (i.e., hourly and daily) and full-period (19 day) variation in concentrations by depth and location were assessed visually and by comparing the coefficient of variation (normalized standard deviation) of different sensors (Appendix C). As a proxy for industry-performed snapshot measurement, the single and dual-point detection success rate was assessed over working hours (07:00 – 18:00). The calculated success rate was the percentage of one-minute frequency measurements that were detected above a range of concentration thresholds (2, 25, 50, 100, 500, 1000, 5000, and 10 000 ppm) at each depth. Dual-point analyses considered both sensors at a given depth (at-grade, 5, or 30 cm) to represent typical testing practices with two measurements within 30 cm of the well, while the single-point analysis presents the results from only one sensor. The detection success rate indicates the percentage of measurement occasions where individual snapshot concentration measurements, or the combination of two snapshot measurements at the same depth, would correctly indicate the presence of GM or potential concentration exceedances. Different concentration thresholds represent different portable measurement equipment with a range of detection limits, and variations in operator decision making (e.g., attributing any concentration below a certain limit to be a non-definitive GM signal).

3.4 Results and Discussion

3.4.1 Meteorological conditions over the monitoring period.

The equipment was deployed, and monitoring data collected over a 19-day period (3-22 October 2020). Diurnally varying on-site air temperature was superimposed on a steadily

temperature decline over the monitoring period, with freezing temperatures overnight first observed on the fifth night (October 7th) that were sustained after October 12th (Figure 3.3). Air temperatures ranged from 10 ℃ to below -14.5 ℃, leading to soil frost (observed to two cm depth by the end of monitoring). Barometrically compensated groundwater levels were moderately variable on daily time scales and showed a sharp response (> 30 cm rise) to a cumulative 3.5 mm precipitation event on October 11th (Figure 3.3). More moderate precipitation events that occurred several days did not show marked water level changes. Wind speeds also demonstrated a quasi-diurnal fluctuation with generally higher wind speeds in the daytime.

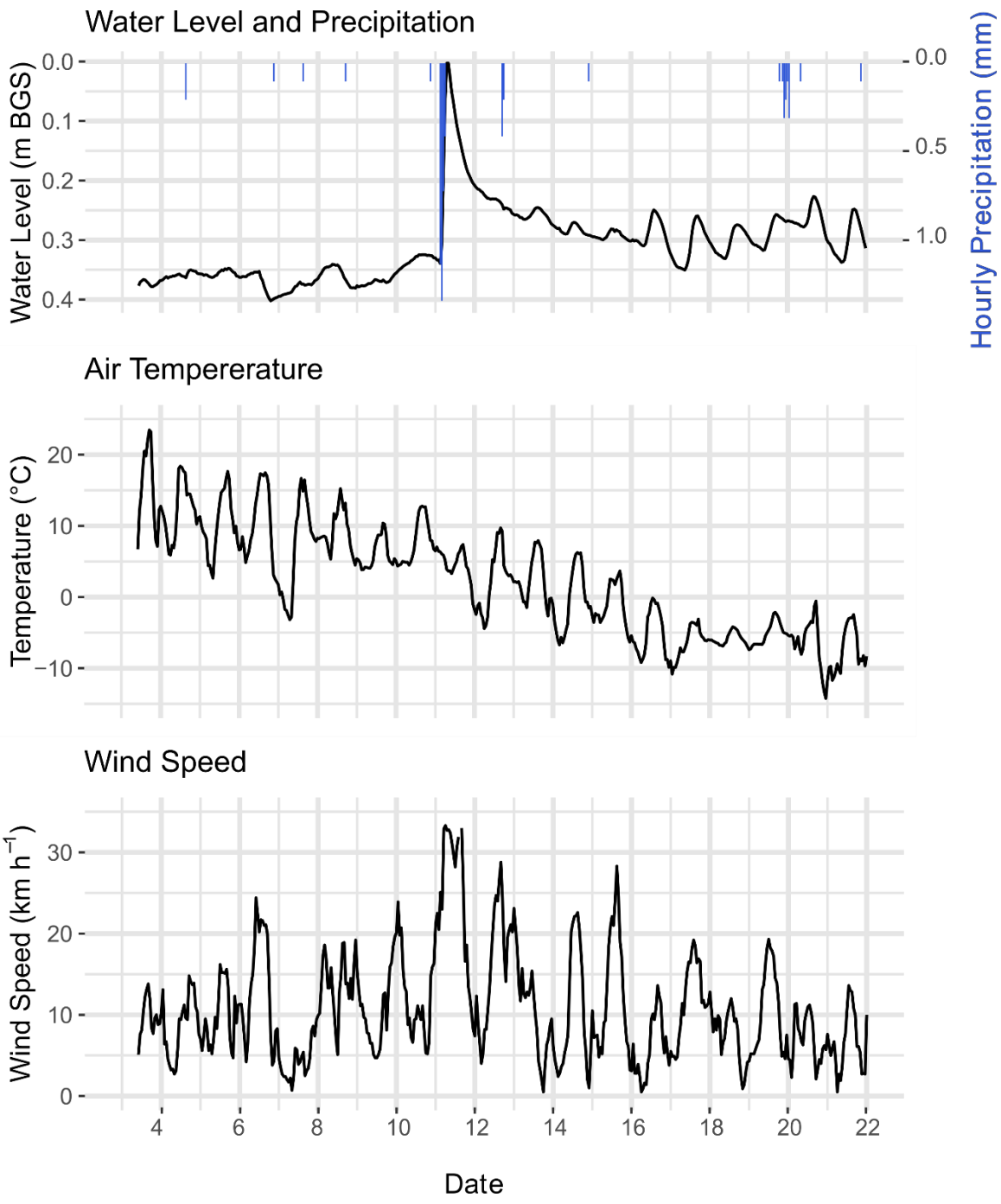

Figure 3.3 Water level in meters below ground surface (m below ground surface), and selected meteorological data from the nearest public weather station, including hourly precipitation (mm), air temperature (°C), and wind speed (km h-1) over the monitoring period. The vertical bars indicate midnight of the October 2020 calendar date indicated.

3.4.2 Time series methane concentrations response.

The sensors in the two sensor nests near the well recorded temporally variable methane concentrations in the soil and at-grade with the soil surface. Methane concentrations tended to be higher at greater depth (Figure 3.4), with mean hourly concentrations combined from both (East and West) nests of 8,500, 11,500, and 25,200 ppm at the 0, 5 and 30 cm depths, respectively. Methane concentrations ranged from <2 ppm to ≥ 50 000 ppm (i.e., 5% of gas composition). Ten mean hourly methane concentration values measured at the West 30 cm depth sensor exceeded the 5% gas manufacturer recommended detection range. Less than 0.1% of one-minute measured concentrations were below 2 ppm (Table 3.2).

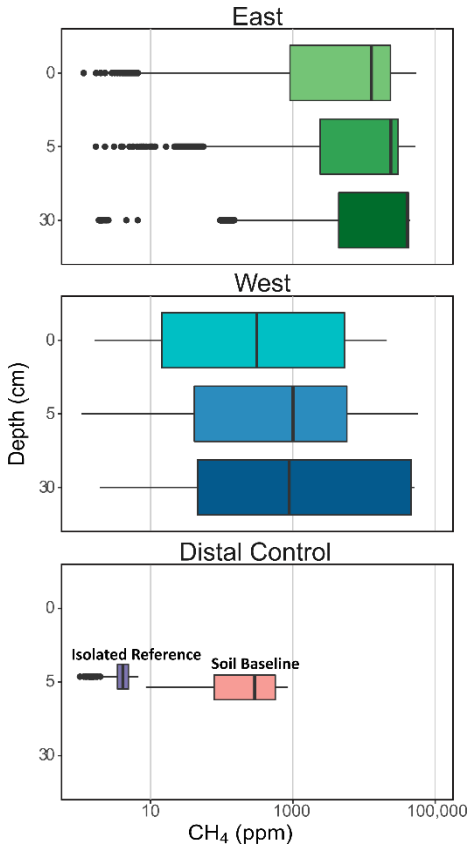

Figure 3.4 One-minute frequency soil methane concentration boxplots (log ppm CH_4) plotted with depth and separated by sensor array location (East, West and Distal Control) over the full 19-day measurement series. Box and whiskers indicate minimum, 1st quartile, median (vertical line), 3rd quartile, and maximum concentrations, with 'outliers' exceeding 1.5 times the interquartile range below the 1st quartile represented as points.

The distal sensors recorded relatively low methane concentrations with moderate variability over the monitoring period (Figure 3.4), and generally lower amounts of variation in comparison to the sensors in the nests near the well (Table D.3.1). Both distal sensors had limited diurnal fluctuations with slightly higher concentrations observed during the daytime. Diurnal variation may be partly explained by the influence of temperature and humidity on the sensors. In future studies, the influence of temperature and humidity should be more robustly

assessed. The distal ‘soil baseline’ sensor recorded a steadily declining concentration over the time series between a maximum of 840 ppm at the start of the testing period to a minimum of 40 ppm, while the ‘isolated reference’ sensor steadily fluctuated between 0-10 ppm over the full measurement period (Figure 3.5). The higher methane concentrations recorded by the ‘soil baseline’ sensor may indicate a moderate subsurface GM signature at a 5 m distance from the well. The modest fluctuation between expected atmospheric concentrations for the ‘isolated reference’ sensor, with no apparent impact from precipitation or freezing air temperatures, indicates that the sensor performance was not significantly affected by these factors. The calibrated concentrations are largely within expected methane concentrations for all sensors based on expected atmospheric concentrations (~2 ppm) and previously measured soil gas concentrations, though the calibration method and sensor detection limits may have led to an underestimate of true methane concentrations which exceeded 5% gas.

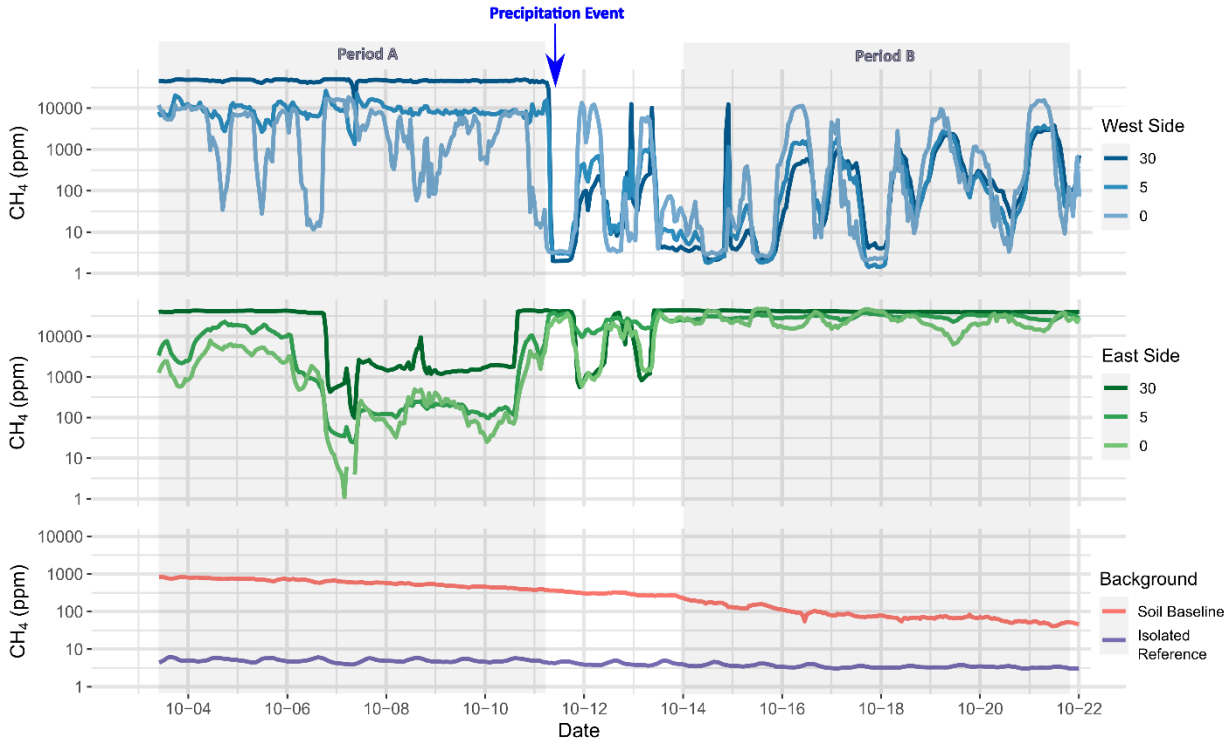

Figure 3.5 Time series of hourly averaged methane concentrations (ppm) around an energy well with gas migration observed between October 3-22, 2020. Sensors were deployed in two arrays (located at 5 cm distance of the energy well casing on each of the East and West sides) at three depths (0, 5, and 30 cm). Additional 'control' sensors were located 5 m distance from the energy well on the east side as a 'baseline' 5 cm in-soil methane concentration (Orange), and an 'isolated reference' sensor placed at 5 cm depth and protected from soil gases in an enclosure (Purple). Period A and B (shaded) correspond to analysis periods with visually regular concentration variations prior to (Period A), and following a three-day lag after a 3.5 mm precipitation event (Period B). The vertical log scale and decreasing sensitivity approaching the sensor detection limit (5% gas; 50 000 ppm) may contribute to the apparently lower variability at high concentrations.

3.4.3 Change in observed distribution of methane concentrations and implications in gas movement behavior associated with a precipitation event.

An observed change in methane concentrations, and concentration variation behavior, coinciding with a minor 3.5 mm precipitation event on October 11th (Figure 3.3) prompted separation of the analysis into two periods preceding and following a three-day lag after the 3.5

mm precipitation event (Figure 3.4. D.4.2). There are relatively distinct methane concentration profile time series in each period (Figure 3.5). Methane concentrations in the Western array sensors were higher and more consistent prior to the October 11th precipitation event, and showed a more pronounced daily-scale variation over several orders of magnitude after the precipitation event. Conversely, the Eastern array sensors had higher concentrations beginning on October 13th, with a lower amount of daily variation. Differences between the two arrays before and after the precipitation event (Period A and B in Figure 3.5) was also evident in different correlations with meteorological factors for the two analysis periods (Table 3.1). The 5 m distal 'soil baseline' and 'isolated reference' sensors concentrations were not visually different following the precipitation event. There were also no substantially different correlations with meteorological factors between the two periods for the reference and baseline sensors, indicating that the precipitation event may not have impacted these measurements.

The precipitation event caused a significant water table rise (~0.33 m; Figure 3.3), with associated changes in the soil moisture content distribution, both of which would have altered the effective gas permeability of the soil around the well. Previous observations of soil gas concentrations and effluxes at this well (Fleming et al., 2021), and by researchers in other settings (Chamindo Deepagoda et al., 2018) suggest that gas movement from the water table to ground surface occurs through preferential flow pathways. The precipitation event and associated change in water level and soil moisture content may have induced a change in the advective movement of gas in the soil around the well casing by occupying pore spaces with water. This would have thereby changed the preferential movement pathway of gas within the saturated and unsaturated zone and lead to a shift in the gas concentration distribution.

3.4.4 Temporal variability patterns as a function of depth and location.

While measured concentrations at all depths varied by several orders of magnitude over the 19-day time series, concentrations were generally higher at greater depths in the soil (Figure 3.4). This concentration distribution is expected given the tendency of saturated zone gas migration to occur in relatively narrow, discrete zones focused around the well casing (Erno and Schmitz, 1996; Dusseault et al., 2014; Lyman et al., 2020; Van de Ven et al., 2020) combined with the shallow water table at the site. The methane gas exits the water table at discrete locations, and once in the unsaturated zone it will disperse radially and vertically by soil gas advection and diffusion (Figure 3.2; Chamindu Deepagoda et al., 2016; Forde et al., 2018). Given the shallow water table, there is relatively little opportunity for radial dispersion.

Temporal variability in measured concentrations were substantially greater in sensors near the energy well (compared to the distal sensors) at short-term (e.g., several minutes), hourly and daily scales. The coefficient of variation (i.e., the measurement variation as a percentage of the mean) was generally higher for sensors closer to the surface (Table D.3.1), and the increasingly pronounced variation at shallower depths is visible in the short-term time series showing one-minute frequency measurements (Figure 3.6). For comparison to variability at other sensors, see the laboratory baseline noise test (Figure D.3.2) and field observations of one-minute frequency variability at the five-meter distal location (Figure D.4.1).

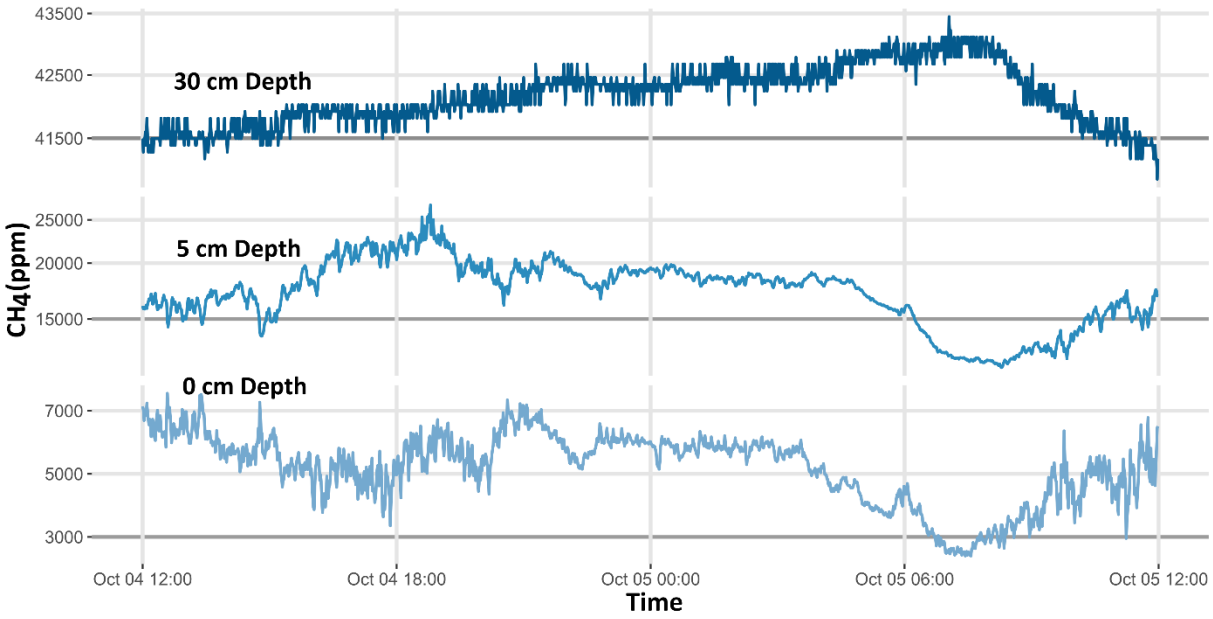

Figure 3.6 Methane concentration (ppm) time series plotted with one-minute measurement frequency over 24 hours for three depths 5 cm from the East side of the casing of an energy well with gas migration. Note the different y axes scales for methane concentration at the three depths.

Temporal variability at all depths may be explained by a combination of i) variations in methane transport and arrival at the water table; and ii) changing rates of advective gas movement in the soil zone causing varied gas exchange and mixing with the atmosphere across the ground surface interface. In the first instance, the complex interaction between buoyancy and capillary forces in a heterogeneous porous media are expected to result in temporally variable and continuous or discontinuous changes in gas movement pathways and transport rates through the saturated zone (Gorody 2012; Van de Ven et al., 2020). Episodic arrivals of migrating gases driven by ebullition events in the saturated zone will induce short-term changes in soil gas concentrations (Forde et al., 2019a). In the second instance, variable soil gas movement pathways, efflux rates, and mixing with atmospheric gases may be caused by varying

meteorological conditions (e.g., barometric pressure, wind, temperature) in addition to soil moisture and groundwater levels (Nachshon et al., 2011; Chamindu Deepagoda et al., 2016). Short-term air pressure fluctuations induced by wind may have caused the observed depth-dependent variation in concentrations at the minute-scale (Figure 3.6; Table D.3.1) (Poulsen et al., 2017).

3.4.5 Methane concentration correlation to meteorological factors.

Simple regression analyses assessed the correlation between hourly averaged soil gas concentrations and meteorological and site factors including atmospheric pressures, temperature, and wind speed, and water level in a shallow piezometer (Figure D.4.2, Figure D.4.3). Given the inherent autocorrelation between meteorological factors (for example, both atmospheric temperatures and wind speeds typically fluctuate diurnally), some of these observed correlations may be spurious.

Table 3.1 Pearson correlation coefficients (r) between methane concentrations at each sensor (where the proximal arrays labelled as West or East of energy well, and depth in cm) and relevant meteorological factors for data periods before and after the rainfall period event (Periods A and B, Figure 3.5). Meteorological factors include wind speed (U_wind), barometric pressure (P_{ATM}), atmospheric temperature (T_air), piezometer water level (WL), and barometric pressure change (dP_{ATM}/dt). Pearson coefficients greater than 0.45 are italicized, while those greater than 0.6 are bolded.

	Before Precipitation Event (Period A)					After Precipitation Event (Period B)				
Sensor Depth (cm)	U_wind	P_{ATM}	T_air	WL	dP_{ATM}/dt	U_wind	P_{ATM}	T_air	WL	dP_{ATM}/dt
West Sensors (windward side)										
0	**-0.68**	0.31	-0.32	0.39	0.03	-0.33	-0.14	-0.29	0.11	-0.26
5	-0.32	0.25	0.08	0.34	0.06	-0.15	0.30	-0.30	0.39	0.05
30	-0.29	0.01	-0.02	0.10	0.03	-0.11	0.31	-0.25	0.36	0.10
East Sensors (leeward side)										
0	0.02	-0.04	0.35	-0.25	0.23	0.24	*0.45*	0.11	0.15	0.19
5	-0.05	-0.02	0.30	-0.25	0.17	0.04	0.41	-0.06	0.12	-0.08
30	0.11	-0.10	*0.45*	-0.26	0.14	-0.23	*0.53*	-0.28	*0.49*	-0.01
Isolated Reference Sensor (5m distance from well)										
5	0.27	-0.19	**0.90**	-0.26	-0.14	*0.55*	**-0.72**	**0.94**	**-0.64**	-0.07
Soil Baseline Sensor (5m distance from well)										
5	-0.27	0.58	0.30	0.34	0.13	0.39	**-0.82**	**0.75**	**-0.66**	0.07

A negative correlation was observed with wind speed in the array on the upwind (West) side of the well (e.g., Pearson r = -0.68 and -0.33 in Period's A and B, respectively in the at-grade sensor), with higher soil gas concentrations are observed during times of lower wind speeds. This negative correlation was absent for the leeward (East) side sensors (Table 3.1). Decreasing correlation strength with depth suggests the wind effect decreases with depth. The impact of wind on soil gas movement is well supported, since wind causes moderate pressure variations at ground surface, leading to pressure pumping and an increased gas exchange

between the soil and atmosphere (Redeker et al., 2015; Poulsen et al., 2017). Near the soil surface, wind may also cause methane transport laterally downwind from preferential efflux pathways (Chamindu Deepagoda et al., 2018). This may potentially explain the negative correlation with wind on the West sensors (upwind of the inferred preferential gas movement pathway along the casing for the predominant wind direction) and a slight positive correlation to the East (generally downwind).

Barometric pressure change has previously been shown to induce exchange between soil and atmospheric gases due to a pressure differential between the atmosphere and soil gases (Börjesson and Svensson 1997; Forde et al., 2019b). This study showed an inconsistent and low correlation (up to -0.26 at the at-grade West sensor; Table 3.1) for the atmospheric pressure change rate, dP_{ATM}/dt. Rising barometric pressure is expected to cause atmospheric gases to be pushed into the upper soil zone and therefore a decrease methane concentration (Abbas et al., 2010). This effect may be stronger in regions with thicker unsaturated zones (Forde et al., 2019b).

Changes in water level can affect soil gas transport pathways and effective gas conductivity as moisture contents change (Chamindu Deepagoda et al., 2018) and/or induce advective gas movement (Fuki, 1987; Abbas 2011), or due to changes in preferential methane transport pathways in the saturated zone. Low correlation coefficients were seen with water level that were variably positive (West sensors; Table 3.1) or negative (East Sensors in Period A; Table 3.1).

A moderate correlation with atmospheric temperature, particularly for the sensors in the Eastern array, may be explained by changes in buoyancy-driven flow and higher diffusion rates at higher temperatures (Nachshon et al., 2011; Chamindu Deepagoda et al., 2016). Increased soil temperature is also related to higher microbial methane oxidation rates (Stein and Hettiaratchi 2001). However, the magnitude of expected daily temperature variation was previously found to be too small to produce daily-scale changes in methane efflux attributable to methane oxidation variation at this site (Fleming et al., 2021). The distal reference sensors 5 m to the West (typically upwind from the well) were used to compare sensor output concentrations that may be attributed to changes in soil temperatures and relative humidity, and atmospheric methane concentrations. The isolated reference sensor showed a very strong positive correlation between atmospheric temperature and concentration, resulting in a daily cycle between 3 and 6 ppm with daily maxima occurring in early afternoon. This indicates the magnitude of variation that might be expected at the 5 cm depth due to changes in soil temperature and humidity (thereby impacting sensor response in ways not related to soil gas concentrations). This variation may also be caused by daily cycles in atmospheric methane mixing ratios (Simpson et al., 1999). Concentrations in the soil baseline sensor also exhibited a moderate daily cycle superimposed on a progressive decline between 840 to <100 ppm CH_4, the cause of which is not clear. Visual comparison and the correlation coefficients both suggest that the soil baseline sensor response was most strongly related to atmospheric temperature, with weaker (and potentially spurious) relationships to wind speed and water levels.

In summary, the measured soil gas concentrations near the well casing are correlated to several meteorological factors that may partially explain some of the observed concentration

variation. The distal reference sensors fluctuate regularly and indicate a small amount of variation, contrasting the pronounced variations observed on the minute, hourly, and daily time scales near the zones of highest methane migration efflux. While several factors were strongly correlated to measured concentrations at particular sensors (most notably wind speed at the Western (windward) array during the pre-precipitation analysis period), no clear patterns were observed for all sensors, or prior to vs. after the precipitation event.

Revisiting the objectives posed in the introduction, it is observed that gas concentrations were generally higher at greater depths, though all sensors varied temporally over multiple orders of magnitude, and occasionally reversals of the methane concentration gradient were observed. The methane concentrations were highly temporally variable and sometimes correlated to wind speed, temperature, and barometric pressure. The complex interaction between these multiple factors and the spatially variable soil migration zone clearly precludes generalization of these effects based on this short time series at a single field site. Confidence in these findings will be increased through additional studies at other field settings with different surface conditions (such as soil type, and vadose zone thickness), and well-specific factors such as gas migration rates, well configuration, and local geology. Commercial and scientific viability of long-term methane concentration measurements will be affected by repeated site access constraints to deploy and collect the equipment, and equipment constraints such as power supply and data logging.

3.4.6 Implications for gas migration detection and risk assessment.

This high frequency methane gas concentrations time series around an energy well with GM has important implications for the GM detection and risk assessment using concentration-based measurements. Variations in methane concentrations within proximity of the well casing at all measured depths indicate the potential variability in repeated snapshot GM tests. Considering the magnitude of potential temporal variability at hourly and daily scales, snapshot, or even repeated snapshot, methane concentrations measurements may falsely indicate trends in measured concentration or underestimate potential concentration-based risk exceedances (e.g., explosive limits).

Methane gas concentrations changed spatially between the two arrays and with depth over several time scales. Surface concentrations at the two arrays, both within 5 cm of the well casing, varied over multiple orders of magnitude between > 10 000 ppm (1 % gas v/v) to < 100 ppm over the 19-day measurement period (Figure 3.5). The magnitude of relative variability and correlation between meteorological factors such as wind speed was generally greater at shallower depths. Results support previous findings that at-grade measurements are particularly susceptible to impacts from variable meteorological factors (Chamindu Deepagoda et al., 2016; Fleming et al., 2021).

Table 3.2 Detection success rate (% of measurements that would have been above a given detection limit lower cut-off), for one-minute-frequency daytime measurements during working hours (07:00 to 18:00) over 19 days. Two-sensor success indicates the success rate where either or both sensors at each depth exceed the concentration cut-off. The recommended detection limit, 500 ppm (i.e., 1% of the Lower Explosive Limit, LEL) is bolded (AER 2021). The 10 000 ppm (i.e., 20% LEL, 1% methane v/v) limit requiring immediate action and restricted worksite access is italicized (Occupational Health and Safety Code; Molofsky et al., 2021).

	Methane Analysis Detection Limit (ppm)							
	2	25	50	100	**500**	1000	5000	*10 000*
Sensor Depth (cm)	Detection Success rate (%) for Individual Sensors							
	West Sensors (Upwind)							
0	99.8	60.6	55.5	50.3	39.7	35.4	20.1	6.1
5	95.6	74.6	69.0	66.1	57.3	51.0	23.9	12.4
30	98.3	77.7	73.2	69.6	56.3	51.1	43.0	42.9
	East Sensors (Leeward)							
0	98.8	98.0	97.9	92.1	79.4	76.1	60.2	52.3
5	99.9	98.7	97.9	97.7	79.6	76.2	71.5	69.2
30	99.8	99.6	99.6	99.2	98.0	97.9	77.5	76.7
	Detection Success (%) for Two Sensors (East and West) at the Same Depth							
0	99.9	99.7	99.7	99.6	97.3	93.4	75.5	55.7
5	99.9	99.7	99.6	99.6	99.6	97.7	87.5	79.0
30	99.9	99.6	99.6	99.6	99.6	99.6	96.3	96.0

One-minute frequency measurements were below the expected atmospheric concentration (~2 ppm) in 4.4 to 0.1% of measurements, indicating the frequency of potential range issues with these sensors and the calibration method used (Table 3.2). The chances of detecting GM at a 500 ppm cut-off during working hours using at-grade single-point measurement was 39.7% and 79.4 % for the West and East 0 cm sensors, respectively. Both single-point and dual-point measurement detection success rates were generally higher at greater depths and declined with

higher concentration cut-offs (Table 3.2). Dual-sensor detection success was greater than single-point detector success, though 2.7% of at-grade dual-sensor measurements did not exceed 500 ppm.

At-grade concentrations were only marginally detectable for single-point measurements during some periods of the 19-day monitoring record, indicating lower detection success for at-grade measurements when using a single point (Table 3.2; Schout et al., 2019). When both measurement points were considered at each depth (i.e., two measurement points within 30 cm of the wellbore, as currently recommended in Alberta; AER 2021), the detection success rate was substantially higher (i.e., > 97.3 % when the recommended detection limits (500 pm) is used; Table 3.2). This indicates the tendency for increasing testing success with higher spatial measurement density, especially near the well. When detection limits were < 500 ppm, greater measurement depth did not substantially improve two-sensor detection success. These results indicate that shallower measurements using lower sensitivity detectors (e.g., 500 ppm, or 1% LEL, detection limit) have a lower chance of detecting above-background gas concentrations indicative of GM in comparison to deeper measurements or measurements made with more sensitive instruments.

Gas concentrations were generally higher at greater depths; however, their temporal fluctuations indicates that even subsurface measurements may need to consider temporal variability and meteorological influences. The advantages of higher subsurface methane concentration measurements were obtained without exceeding the 30 cm depth ground disturbance threshold, and greater detection success was obtained through two at-grade test

points instead of a single test point at greater depth. The use of lower detection limits (< 100 ppm) with two at-grade measurements, obviated the advantage to subsurface measurement at this site. Increased confidence in GM test results may be obtained by using higher sensitivity detectors, measuring at greater depths in soil or at higher spatial density, and by withholding GM testing during periods of inappropriate meteorological conditions such as high wind speeds, barometric pressure increases, or following precipitation events.

This study has demonstrated the feasibility of installing inexpensive long-term sensors at-grade with the soil-surface, or in the shallow soil zone, as an alternative method to detecting and monitoring the presence of GM, in a manner that is resilient to temporal variability. Considering the financial, social, and environmental liability implications, accurate GM testing may be particularly relevant in higher risk areas such as where urbanization is encroaching on legacy oil/gas infrastructure (Gurevich et al., 1993; AER 2014; Abboud et al., 2020).

Variable concentrations observed at-grade can potentially introducing error into risk assessments based on snapshot concentration measurements. In comparison to the relatively reliable GM detection using two-sensor snapshot measurements during this case-study, 44% of at-grade measurements (and 4% of 30 cm depth measurements) would have failed to recognize the capacity for gas concentrations around this case-study well to occasionally exceed 10 000 ppm (Table 3.2). In outdoor spaces, elevated methane concentrations at-grade or within the soil are expected to rapidly decrease to low (non-explosive) concentrations upon mixing in the atmosphere above the well (Ulrich et al., 2019). However, these data show that testing conducted at certain times may underestimate the maximum potential concentrations. Improved confidence

in these GM risk assessments will be obtained with long-term measurement, especially over periods that might be expected to result in higher at-grade gas concentrations (such as lower wind speeds). Accurate long-term concentration data can also be used to guide site-specific mitigation and management options.

Decreasing detection limits in gas measurement equipment (e.g., high-precision optical absorption gas sensors) and refinements to GM testing techniques inevitably leads to increased detectability of lower methane concentrations. This makes it increasingly difficult to meet the requirement to repair wells to a state of non-detectable gas migration in Alberta (AER 2021). Existing and historically available technologies and methods already detect the higher concentrations which are associated with higher rates of leakage (Erno and Schmitz 1996; Forde et al., 2018; Fleming et al., 2021). In essence, improved GM detection will increase the total number of wells classified with GM, with most of them in the 'low-rate' GM category (e.g., efflux of < 1 m^3 CH_4 day^{-1}).

The challenge and expense in well repair has led to a disproportionate number of wells that are idle (i.e., with suspended status in Alberta) (Muehlenbachs, 2017; Schiffner et al., 2021). Incorporating the 'social cost' of methane emissions may economically incentivize the repair and decommissioning of wells with higher emissions (e.g., 43 m^3 day^{-1} considering both GM and SCVF; Schiffner et al., 2021). However, the 'low-leaker' wells (like the well presented here; Fleming et al., 2021) are anecdotally the most difficult to repair. They are consequently the largest fraction of idle wells, which contribute to insolvency in the energy industry (Schiffner et al., 2021). Emission distributions suggest that the average GM and SCVF rates are heavily

influenced by a small number of ‘super-emitter’ wells which contribute disproportionately to the overall leakage volumes (Erno and Schmitz 1996; Brandt et al., 2014; Kang et al., 2014; Zavala-Araiza et al., 2015; Saint-Vincent et al., 2020). From a methane emissions perspective, the detection and repair of these ‘super emitter’ wells will contribute the most to decreasing total emissions from GM sources. In contrast, at many well pads the contribution of methane emissions through low-rate GM may be insubstantial in the larger perspective of all emissions at the well pad scale, and more broadly within the upstream oil and gas industry (Lyman et al., 2020). Given the conundrum presented by improved GM detection and investigation, with decreasing returns on emissions reduction through the repair of ‘low-leaker’ wells, it may be prudent for regulators to consider adopting a non-zero permissible GM rate (Natural Resources Canada, 2019). In this case, regulators could permit well decommissioning with low, but acceptable, methane emissions or risk classification (Dusseault et al., 2014; Natural Resources Canada 2019).

We have shown that point measurements may be insufficient to assess methane concentration-based risk, and it is known that emission rates of both GM and SCVF can be variable over time, requiring long-term measurement for accurate assessment (Lyman et al., 2020; Riddick et al., 2020; Fleming et al., 2021). Longer term high-frequency measurement may thus present a viable alternative GM monitoring method, providing higher confidence in GM investigation. In turn, this may provide sufficient confidence for regulators to permit well decommissioning with a low rate of methane leakage. Given the potential for methane biofiltration to further reduce atmospheric emissions (Stein and Hettiaratchi 2001; Reddy et al., 2014; Gunasekera et al., 2018), this could reduce the total number of idle wells and industry

insolvency (Muehlenbachs, 2017). Financial and technical resources could also then be devoted to other more cost-effective emission reduction initiatives (Natural Resources Canada, 2019).

3.5 Conclusion

Inexpensive combustible gas concentration sensors were installed at several depths near to a case-study energy well with gas migration to collect a high-frequency time series of methane concentrations over a 19-day period. Results indicate several findings with potential application to enhance the understanding of GM detection and risk assessment practices:

1. Methane gas concentrations are generally higher at greater soil depths. A depth of only five cm below ground surface yielded order-of magnitude increases in measured concentrations compared to sensors at-grade with ground-surface.

2. Changes in methane concentrations observed after a moderate rain event indicate changes to the free phase gas migration pathways in the saturated or unsaturated zone.

3. Pronounced temporal variability in measured concentrations occurred over time scales of minutes to hours and days, with concentration changing by as much as four orders of magnitude over a few hours. More variation was observed at shallower depths and at-grade measurements (which are common practice) were most susceptible to temporal variation. Changing repeated snapshot gas migration test results are expected when considering potential temporal variability at all depths.

4. Temporal variation in measured concentrations were correlated to wind speed, changing groundwater level, and barometric pressure.

5. GM detection success was generally high at this well. GM detection success was improved by using two measurement locations (in alignment with currently recommended practices), a lower detection limit, and greater measurement depth.
6. Repeated or long-term measurement may be necessary to observe concentration exceedances relevant for risk assessment.

These data will be useful to support policy development for GM detection, risk evaluation, and the end-of-life management of low-leaking energy wells that are not easily repaired.

Chapter 4: **Conclusion**

4.1 Summary

This thesis presents results from investigations into the factors affecting the measurement and detection of gas migration outside the surface casing of energy wells. Previous authors have reported that migrating gases are unevenly spatially distributed at the well pad scale, and will vary temporally due to combined effects of subsurface and meteorological factors (e.g., Forde et al., 2018b; Lyman et al., 2020). Current practices in the GM detection industry also include a range of testing methodologies including differing measurement spacings, depths, and equipment, with unknown resiliency to these spatial and temporal variations. The combined effects of varying testing methodology and spatiotemporal variability of migrating gases may result in poorly quantified impacts to measured concentrations and other indications of the presence and associated risk and impact of GM at a wellsite.

A comparison of GM testing using standard industry practices (Appendix A) demonstrates that measured combustible gas concentrations, widely used to indicate the presence or absence of GM around an energy well, vary over orders of magnitude in historic and recent GM records, with some dependence on both service provider (i.e., testing party), testing approach, and likely other factors (as demonstrated in Chapter 3 and 4). Both the maximum recorded concentrations and the pass/fail test result had a statistically significant dependence on the testing party. The examined dataset was relatively small (93 GM tests conducted across six wells), and greater confidence in these findings would be obtained with a larger and more geographically representative sample of GM tests across Alberta.

Method dependence on measured methane concentrations were further investigated through more intensive GM testing at two sub-selected wells, which showed that methane concentrations were generally higher at greater depths below ground surface. Elevated concentrations were limited to several spatially discrete areas within ~five meters of the 14 m x 14 m testing area centred around the well casing. Substantial variation in GM test maximum concentrations, even within the same testing party at the same well, indicate method-independent causes of GM test result variability such as the spatiotemporal variation in migrating gases.

Spatiotemporal variation of migrating gases was studied using gas efflux and subsurface gas compositional analyses, presented in Chapter 3. Two spatial surveys of gas flux across the soil-atmosphere boundary showed that both CH_4 and CO_2 effluxes were spatially concentrated nearby the energy well. A two-week high-resolution sampling time series at six locations showed that both methane concentrations and effluxes varied temporally, with correlation to several meteorological factors, including wind speed and atmospheric temperatures. Despite this temporal variation, effluxes and concentrations within the chamber at well-centre remained consistently above background values. Observed behavior of migrating gases around the well were consistent with published conceptual understandings developed through previous field and laboratory work, where steady and advection-dominated gas transport near the well casing transitioned to more intermittently detectable episodic release and diffusion-driven efflux further away (Chamindu Deepagoda et al., 2016; Van de Ven et al., 2020). Estimated total GM-related methane emissions at the well pad scale were 350 g CH_4 d^{-1} (or 0.5 m^3 d^{-1}), although the uncertainty ($p = 0.05$) ranged from non-detectable to 1750 g d^{-1}, and with some dependence on the full-site emission estimation method used.

In Chapter 4, a quasi-continuous time series of methane gas concentrations at multiple locations around the GM study well indicated temporal variability with some apparent correlation to meteorological factors. This investigation documented that temporal variability in migrating gas concentrations occurs at depths up to at least 30 cm, with generally higher concentrations and lower amounts of temporal variation recorded at greater depth. While GM testing using at least two spatial measurement points would have indicated the presence of GM at this well across a high percentage of the time series examined (e.g., > 99% of daytime dual-sensor measurements at detection limits of at most 100 ppm, at all depths examined), the results demonstrate potential for errors in the concentration-based risk assessment around this well.

4.2 Methane emissions and other risks resulting from gas migration

Reliable detection of fugitive gas migration outside the surface casing has important economic, environmental, and safety implications. GM methane emissions contribute to greenhouse gas emissions from the upstream petroleum sector, and interaction between migrating gases and groundwater may result in deteriorating groundwater quality (Riddick et al., 2020; Cahill et al., 2017; McMahon et al., 2018). Concern for the environmental and safety impacts of fugitive methane also results in negative public perception of active, suspended, and decommissioned energy wells, and necessitates safety precautions around these sites. GM testing is currently only mandated in certain regions or circumstances (e.g., within the required testing area or for specific well construction types in Alberta, and where its presence is already suggested in British Colombia), potentially leading to an underestimate in the total number of cases (AER 2018a; BCOGC 2020; Abboud et al., 2020). GM at any detectable rate prevents legal decommissioning until the well is successfully repaired, with a relatively high financial

burden for well repair ($CAN 150,000 up to millions of dollars in extreme cases; Dusseault et al., 2014; Trudel et al., 2019). Liability for the well owner persists when wells cannot be legally abandoned due to GM (Abboud et al., 2020).

Emission estimates from the case-study well presented in this thesis indicate that a relatively low GM emission rate (in this case averaging less than 1 m^3 d^{-1}) is required for reliable GM detection using a variety of techniques in this field circumstance. On a per-well basis, this 1 m^3 d^{-1} emission rate is relatively small compared current estimations for other sources, both as a proportion of upstream petroleum activities and in comparison to other anthropogenic activities. Uncertainty in the absolute number of wells with GM impacts estimated industry-wide methane emission contributions from this source (Abboud et al., 2020). However, previous studies have shown that methane emissions from leaks typically follow a heavy-tailed distribution, where a small minority of wells contribute a disproportionately large volume of the total emissions (Figure 1.1; Lan et al., 2015; Lavoie et al., 2015; Kang et al., 2016). Based on limited previous data on GM and the understanding of the distribution of SCVF rates and other gas emission sources, it can be expected that GM emission rates follow a similar distribution (Erno & Schmidt, 1996; Kang et al., 2014; AER 2018; Lyman et al., 2020). Following this logic, the findings of this thesis indicate that in similar field settings the GM emission sources that are most important from a greenhouse gas emission standpoint will be readily detected using common measurement techniques. The presence of GM at this well was reliably detected using concentration-based sensors with at least two measurement points spatially near the well (at depths from 30 cm BGS to at-grade), and with efflux measurements. Rapid detection and repair of the most significant ‘super-emitters’ will have the largest impact on decreasing total methane

emissions from GM, and therefore the largest positive impact in decreasing greenhouse emissions from this source. Detection techniques for lower emission rate GM may be enhanced through improvements in equipment, testing methodology, and testing timing in relation to expected temporal variation. However, the expected impact on total emissions from the detection and repair of these marginally detectable wells will be comparatively smaller.

Assessment of other risks from GM, including potential for accumulation of explosive gases even at low surface emission rates, may be more susceptible to spatiotemporal variability in test results. The measured spatial distribution of GM, and the surface concentrations and emission rates, all varied temporally during the studies presented in this thesis. The maximum surface concentrations (and potential for concentration-based exceedances relevant from a safety standpoint) were observed to vary over orders of magnitude between measurements collected a few hours apart. Despite reliable detection of the presence of GM, single 'snapshot' measurements at one moment in time demonstrated a poor capacity for assessing the average (or maximum) potential concentration at that location. From this standpoint, desired GM detection methods and testing sensitivity, and resilience to temporal variability, will need to consider testing objectives, be it those of potential explosive atmosphere development, methane emissions above a certain rate, or simply the presence of a well integrity issue producing GM. While discussed only to a limited extent in this thesis, GM testing standards may also need to consider the potential for free-phase methane gas migration to impact groundwater quality.

4.3 Implications for detection and quantification of gas migration outside the surface casing

The work presented in this thesis shows that GM surface emissions at the well, while variable in magnitude, were reliably detected with either conventional concentration-based measurement methods or efflux-based detection. For example, case study results indicate consistently detectable efflux at the wellhead and a >99% detection success rate considering all working hour measurements using two concentration-based detectors with at most a 100-ppm lower detection limit. However, documented temporal variability may affect the detection of lower-emission rate GM instances when using lower sensitivity methods.

Analysis of historical GM tests results indicate that testing party was related to maximum detected concentration and indicates a potential for false negatives using some currently practiced GM detection methods within Alberta. However, common accepted measurement techniques were found to be reliable for GM detection when compared by the University of Calgary research team. It is recommended that the regulator works with service providers and operators to update the recommended AER Directive 20 gas migration detection method to reflect currently available sensor technology and the improved scientific understanding of GM since these recommendations were originally developed in the 1990's. This update should also include a minimum required standard of detection that will provide improved transparency and confidence in all test results. Clearer guidance on standard practice could be implemented while still allowing space for competitive advancement between service providers.

GM detection reliability is shown to be higher (through higher measured methane concentrations or effluxes), when performing GM testing at a higher spatial resolution, at greater

soil depths, with more sensitive detectors, and when conducting long-term monitoring instead of instantaneous measurement. At all depths, GM detection and measurement may be impacted by temporal variability, potentially driven by meteorological factors and short-term ebullition. Higher measured methane concentrations and effluxes were correlated with lower wind speeds. There was also a weaker relationship to higher concentrations or effluxes at steady or decreasing barometric pressures and lower atmospheric temperatures. Higher concentrations and lower temporal variabilities were observed at greater soil depths. A depth of five or 30 cm was sufficient to observe this benefit at the locations studied.

Detection and measurement will also be impacted by local geology (e.g., low permeability surficial sediments; Forde et al., 2019a), specific details of the well construction, and spatial and temporal variability of the wellsite soils. Improved emission estimates and more accurate determination of potential maximum methane concentrations (for the purposes of risk assessment) will be improved by repeated or long-term measurement, especially during the meteorological conditions described above. Future commercial and scientific GM evaluation will benefit from considering the influence of spatial and temporal variability on the detection and measurement methodology.

References

Abbas, T. R., Abdul-Majeed, M. A., Ghazi, I. N. 2010. Flow zones in unsaturated soil due to barometric pumping. *Eng. and Tech. J.* 28(10): 1900-1909.

Abbas, T. R. 2011. Effect of Water Table Fluctuation on Barometric Pumping in Soil Unsaturated Zone. *Jordan J. Civil Eng.* 5 (4): 504-509. Jordan University of Science and Technology.

Abboud, J. M., Watson, T. L., Ryan, M. C. 2020. Fugitive methane gas migration around Alberta's petroleum wells. Greenh. Gases: Sci. Technol. https://doi.org/10.1002/ghg.2029

Abichou, T., Powelson, D., Chanton, J., Escoriaza, S., Stern, J., 2006. Characterization of methane flux and oxidation at a solid waste landfill. *J. Environ. Eng.* 132(2), 220-228. https://doi.org/10.1061/(ASCE)0733-9372(2006)132:2(220)

Ahlfeld, D. P., Dahmani, A., & Ji, W., 1994. A conceptual model of field behavior of air sparging and its implications for application. *Groundw. Monit. Remediat.* 14(4), 132-139. https://doi.org/10.1111/j.1745-6592.1994.tb00491.x

Akaike, H., 1974. A new look at the statistical model identification. IEEE transactions on automatic control, 19(6), 716-723.

Alberta Agriculture and Forestry, Alberta Climate Information Service (ACIS). Retrieved from https://agriculture.alberta.ca/acis

Alberta Government. 2006. Agri-facts: Methane gas in well water. Retrieved from https://open.alberta.ca/publications/3538631

Alberta Energy Regulator. 2003. Interim Directive 2003-01: Surface Casing Venting Flow/Gas Migration Testing, Reporting, and Repair Requirements. Retrieved from https://www.aer.ca/regulating-development/rules-and-directives/interim-directives/id-2003-01

Alberta Energy Regulator (AER). 2014. Directive 079: Surface Development in Proximity to Abandoned Wells. Retrieved from https://www.aer.ca/documents/directives/Directive079.pdf

Alberta Energy Regulator (AER). 2020. Directive 009: Casing Cementing Minimum Requirements. Alberta, Canada. Retrieved from https://static.aer.ca/prd/2020-10/Directive009.pdf

Alberta Energy Regulator (AER). 2018. Vent Flow/ Gas Migration Report. Alberta, Canada. Retrieved from http://www1.aer.ca/ProductCatalogue/365.html

Alberta Energy Regulator (AER). 2021. Directive 20: Well Abandonment. Alberta, Canada. Retrieved from https://static.aer.ca/prd/documents/directives/Directive020.pdf

Alboiu, V., Walker, T. R., 2019. Pollution, management, and mitigation of idle and orphaned oil and gas wells in Alberta. Canada. *Environ. Monit. Assess,* 191(10), 611. https://doi.org/10.1007/s10661-019-7780-x

Almon, E., Magaritz, M, 1990. Dissolved common gases in groundwaters of the Appalachian region. *J. Hydrol.* 121(1-4), 21-32. https://doi.org/10.1016/0022-1694(90)90222-J

Anenberg, S. C., Schwartz, J., Shindell, D., Amann, M., Faluvegi, G., Klimont, Z., ...Emberson, L. 2012. Global air quality and health co-benefits of mitigating near-term climate change through methane and black carbon emission controls. *Environ. Health Persp.* 120(6), 831-839. https://doi.org/10.1289/ehp.1104301

Annunziatellis, A., Beaubien, S. E., Bigi, S., Ciotoli, G., Coltella, M., Lombardi, S., 2008. Gas migration along fault systems and through the vadose zone in the Latera caldera (central Italy): Implications for CO2 geological storage. *Int. J. Greenh. Gas Con.* 2(3), 353-372. https://doi.org/10.1016/j.ijggc.2008.02.003

Bachu, S., 2017. Analysis of gas leakage occurrence along wells in Alberta, Canada, from a GHG perspective – Gas migration outside well casing. *Int. J. Greenh. Gas Con.* 61, 146-154. https://doi.org/10.1016/j.ijggc.2017.04.003

Barth-Naftilan, E., Sohng, J., Saiers, J. E. 2018. Methane in groundwater before, during, and after hydraulic fracturing of the Marcellus Shale. *Proc. Nat. Acad. Sci.* 115(27), 6970-6975.

BC Oil and Gas Activities Act. 2020. Pipeline Crossing Regulation. Accessed October 2020 from: https://www.bclaws.ca/civix/document/id/complete/statreg/147_2012

BC Oil and Gas Commission (BCOGC). 2020. Oil & Gas Operations Manual Version 1.30. Chapter 9 Well Activity: Completion, Maintenance and Abandonment. Accessed September 2020 from: https://www.bcogc.ca/files/operations-documentation/Oil-and-Gas-Operations-Manual/ogaom-chapter-9.pdf

Bol, G., Grant, H., Keller, S., Marcassa, F., De Rozieres, J. 1991. Putting a stop to gas channeling. *Oilfield Rev.* 3(2), 35-43.

Boothroyd, I, M, Almond, S, Qassim, S, M, Worrall, F, Davies, R, J, 2015. Fugitive emissions of methane from abandoned, decommissioned oil and gas wells. *Sci. Tot. Environ.* 547, 461–469. https://doi.org/10.1016/j.scitotenv.2015.12.096.

Börjesson, G., Danielsson, Å., Svensson, B. H., 2000. Methane fluxes from a Swedish landfill determined by geostatistical treatment of static chamber measurements. *Environ. Sci. Technol.* 34(18), 4044-4050. https://doi.org/10.1021/es991350s

Börjesson, G., Svensson, B., 1997. Seasonal and diurnal methane emissions from a landfill and their regulation by methane oxidation. *Waste Manag. Res.* 15(1) 33-54 https://doi.org/10.1177/0734242X9701500104

Brady, N. C., & Weil, R. R. 2002. *The nature and properties of soils, 13th ed.* Pearson Prentice Hall.

Brandt, A.R., Heath, G.A., Kort, E.A., O'sullivan, F., Pétron, G., Jordaan, S.M., Tans, P.,Wilcox, J., Gopstein, A.M., Arent, D., Wofsy, S., Brown, N.J., Bradley, R., Stucky, G.D., Eardley, D., Harris, R., 2014. Energy and environment methane leaks from North American natural gas systems. *Sci.* 343(6172), 733–735. https://doi.org/10.1126/science.1247045

Cahill, A. G., Parker, B. L., Mayer, B., Mayer, K. U., Cherry, J. A. 2018. High resolution spatial and temporal evolution of dissolved gases in groundwater during a controlled natural gas release experiment. *Sci. Tot. Environ.* 622, 1178-1192. https://doi.org/10.1016/j.scitotenv.2017.12.049

Cahill, A., Steelman, C., Forde, O., Kuloyo, O., Ruff, S., Mayer, B., Mayer, K.U., Strous, M., Ryan, M.C., Cherry, J.A., Parker, B.L., 2017. Mobility and persistence of methane in groundwater in a controlled-release field experiment. *Nat. Geosci*. 10, 289.

Cardellini, C., Chiodini, G., Frondini, F., Granieri, D., Lewicki, J., Peruzzi, L., 2003. Accumulation chamber measurements of methane fluxes: application to volcanic-geothermal areas and landfills. *Appl. Geochem*. 18(1), 45-54. https://doi.org/10.1016/S0883-2927(02)00091-4

Chamindu Deepagoda, T.K.K., Smits, K. Oldenburg, C. 2016. Effect of subsurface soil moisture variability and atmospheric conditions on methane gas migration in shallow subsurface. *Int. J. Greenh. Gas Con*. 55:105–117. doi:10.1016/j.ijggc.2016.10.016

Chao, J., Cahill, A., Lauer, R., Van De Ven, C., Beckie, R. D. 2020. Propensity for fugitive gas migration in glaciofluvial deposits: An assessment of near-surface hydrofacies in the Peace Region, Northeastern British Columbia. *Sci. Tot. Environ.* 749, 141459.

Deepagoda TKK, C., Mitton, M., Smits, K. 2018. Effect of varying atmospheric conditions on methane boundary-layer development in a free flow domain interfaced with a porous media domain. *Greenh. Gas*: *Sci. and Tech.* 8(2), 335-348. https://doi.org/10.1002/ghg.1743

Chan, E, Worthy, D.E., Chan, D., Misa Ishizawa, M., Moran, M.D., Delcloo, A., Vogel, F. 2020. Eight-year estimates of methane emissions from oil and gas operations in Western Canada are nearly twice those reported in inventories. *Environ. Sci. Technol.* 54(23), 14899-14909. https://doi.org/10.1021/acs.est.0c04117

Chao, J. T. H., Cahill, A. G., Lauer, R. M., Van De Ven, C. J., Beckie, R. D. 2020. Propensity for fugitive gas migration in glaciofluvial deposits: An assessment of near-surface hydrofacies in the Peace Region, Northeastern British Columbia. *Sci. Tot. Environ.* 749, 141459. https://doi.org/10.1016/j.scitotenv.2020.141459

Chen, K., O'Leary, R. A., Evans, F. H., 2019. A simple and parsimonious generalised additive model for predicting wheat yield in a decision support tool. *Agric. Syst*. 173, 140-150. https://doi.org/10.1016/j.agsy.2019.02.009

Cheung, T. T. M. 2019. Establishing High-Resolution Hydrogeological, Geochemical and Isotopic Baseline Conditions of the Fresh Water Zone at a Field Research Site Near Brooks, Alberta, Canada [MSc. Thesis]. University of Calgary. https://prism.ucalgary.ca/handle/1880/111381

Christiansen, J. R., Outhwaite, J., Smukler, S. M. 2015. Comparison of CO2, CH4 and N2O soil-atmosphere exchange measured in static chambers with cavity ring-down spectroscopy and gas chromatography. *Agric. Forest Meteorol.* 211, 48-57. https://doi.org/10.1016/j.agrformet.2015.06.004

D'Aniello, A., Fabbricino, M., Ducci, D., Pianese, D. 2020. Numerical Investigation of a Methane Leakage from a Geothermal Well into a Shallow Aquifer. *Groundwater.* 58(4), 598-610. doi:10.1111/gwat.12943

Drilling and Completions Committee. D.A.C.C. 1993. Surface Casing Vent Flow Subcommittee Report.

Dusseault, M., Jackson, R. 2014. Seepage pathway assessment for natural gas to shallow groundwater during well stimulation, in production, and after abandonment. *Environ. Geosci.* 21(3), 107-126. https://doi.org/10.1306/eg.04231414004

Dusseault, M.B., Gray, M.N. Nawrocki, P.A. 2000. Why oilwells leak: cement behavior and long-term consequences. Presented at the SPE International Oil and Gas Conference and Exhibition. Beijing, China. https://doi.org/10.2118/64733-MS

Dusseault, M., Jackson., R., MacDonald, D. 2014., Towards a Road Map for Mitigating the Rates and Occurrences of Long-Term Wellbore Leakage. University of Waterloo & Geofirma Engineering Ltd. (2014). Retrieved from http://geofirma.com/wp-content/uploads/2015/05/lwp-final-report_compressed.pdf.

Energy Resources Conservation Board (ERCB). Bulletin 2011-35: Surface casing vent requirements for wells. 2011. Retrieved from https://static.aer.ca/prd/2020-07/Bulletin-2011-35.pdf

Engelder, T., Zevenbergen, J. 2018. Analysis of a gas explosion in Dimock PA (USA) during fracking operations in the Marcellus gas shale. *Process Safe. Environ. Protec.* 117, 61-66. https://doi.org/10.1016/j.psep.2018.04.004

Environment and Climate Change Canada. 2020. National inventory report: greenhouse gas sources and sinks in Canada: executive summary. Retrieved from http://publications.gc.ca/pub?id=9.816345&sl=0

Engineering ToolBox, 2003. Thermal Conductivity of selected Materials and Gases. Retrieved from https://www.engineeringtoolbox.com/thermal-conductivity-d_429.html

Environment and Climate Change Canada. 2018. Canada's methane regulations for the upstream oil and gas sector. Retrieved from https://www.canada.ca/en/environment-climate-change/services/canadian-environmental-protection-act-registry/proposed-methane-regulations-additional-information.html

Erno, B., & Schmitz, R. 1996. Measurements of soil gas migration around oil and gas wells in the Lloydminster area. *J Canad. Petrol. Tech.* 35(07).

Fleming, N., Morais, T., Kennedy, C. Ryan, M.C. 2019. Evaluation of SCVF and GM measurement approaches to detect fugitive gas migration around energy wells. Presented at Geoconvention 2019. Calgary, Canada. 13-17 May 2019.

Fleming, N. Morais, T. Mayer, K.U. Ryan, M.C. 2021. Spatiotemporal variability of fugitive gas migration emissions around a petroleum well. *Atmos. Poll. Res.* 12(06). https://doi.org/10.1016/j.apr.2021.101094

Forde, O., Mayer, K., Cahill, A., Mayer, B., Cherry, J., Parker, B. 2018. Vadose zone gas migration and surface effluxes after a controlled natural gas release into an unconfined shallow aquifer. *Vadose Zone J.* 17, 1-16

Forde, O. N., Mayer, K. U., Hunkeler, D. 2019a. Identification, spatial extent and distribution of fugitive gas migration on the well pad scale. *Sci. Tot. Environ*. 652, 356-366. https://doi.org/10.1016/j.scitotenv.2018.10.217

Forde, O. N., Cahill, A. G., Beckie, R. D., Mayer, K. U., 2019b. Barometric-pumping controls fugitive gas emissions from a vadose zone natural gas release. *Sci. Rep.* 9(1), 1-9.

Fox, T. A., Barchyn, T. E., Risk, D., Ravikumar, A. P., Hugenholtz, C. H. 2019. A review of close-range and screening technologies for mitigating fugitive methane emissions in upstream oil and gas. *Environ. Res. Lett.* 14(5), 053002.

Frederick, G., Wolfram, K., Eric, P., Gaëtan, B., Pierrick, D., Bernhard, M., Eric, C. G. 2017. Natural CH4 gas seeps in the French Alps: characteristics, typology and contribution to CH4 natural emissions to the atmosphere. *Energy Procedia*. 114, 3020-3032. https://doi.org/10.1016/j.egypro.2017.03.1430

Fukui, M. 1987. Soil water effects on concentration profiles and variations of 222Rn in a vadose zone. *Health Physics* 53(2): 181-186.

Gas Measurement Instruments Ltd. 2016. GT series user handbook. Retrieved from https://www.manualslib.com/manual/1680676/Gmi-Gt-Series.html?page=2#manual

Gorody, A. W. 2012. Factors affecting the variability of stray gas concentration and composition in groundwater. *Environ. Geosci*. 19(1), 17-31. https://doi.org/10.1306/eg.12081111013

Government of Alberta. Reducing methane emissions. Retrieved from https://www.alberta.ca/climate-methane-emissions.aspx.

Government of Saskatchewan. 2015. Gas Migration, Guideline PNG026. The Oil and Gas Conservation Regulations, 2012. https://pubsaskdev.blob.core.windows.net/pubsask-prod/84462/84462-Guideline_PNG026_Gas_Migration.pdf

Gunasekera, S. S., Hettiaratchi, J. P., Bartholameuz, E. M., Farrokhzadeh, H., Irvine, E. 2018. A comparative evaluation of the performance of full-scale high-rate methane biofilter (HMBF) systems and flow-through laboratory columns. *Environ. Sci. Pollut. Res*. 25, 35845-35854. https://doi.org/10.1007/s11356-018-3100-1

Gurevich, A. E., Endres, B. L., Robertson Jr, J. O., Chilingar, G. V. 1993. Gas migration from oil and gas fields and associated hazards. *J. Petrol. Sci. Eng.* 9(3), 223-238. https://doi.org/10.1016/0920-4105(93)90016-8

Hammond, P. A. 2016. The relationship between methane migration and shale-gas well operations near Dimock, Pennsylvania, USA. *Hydrogeo. J.* 24(2), 503-519.

Hastie, T., 2019. gam: Generalized Additive Models. R package version 1.16.1.

Hastie, T. J., Tibshirani, R. J., 1990. Generalized additive models, Vol. 43. CRC press.

He, J., Naik, V., Horowitz, L. W., Dlugokencky, E., Thoning, K. (2020). Investigation of the global methane budget over 1980–2017 using GFDL-AM4. 1. *Atmos. Chem. Phys.* 20(2), 805-827. https://doi.org/10.5194/acp-20-805-2020

Health Canada. 2019. Guidelines for Canadian Drinking Water Quality—Summary Table. Water and Air Quality Bureau, Healthy Environments and Consumer Safety Branch, Health Canada, Ottawa, Ontario. Retrieved from https://www.canada.ca/content/dam/hc-sc/migration/hc-sc/ewh-semt/alt_formats/pdf/pubs/water-eau/sum_guide-res_recom/sum_guide-res_recom-eng.pdf

Henan Hanwei Electronics Co., Ltd. MQ-4 Semiconductor Sensor for Natural Gas. Retrieved from https://www.pololu.com/file/0J311/MQ4.pdf

Hendry, M. J., Schmeling, E. E., Barbour, S. L., Huang, M., Mundle, S. O., 2017. Fate and transport of shale-derived, biogenic methane. *Sci. Rep.* 7(1), 1-9. https://doi.org/10.1038/s41598-017-05103-8

Hoch, O. F. The dry coal anomaly-the Horseshoe Canyon Formation of Alberta, Canada. SPE Annual Technical Conference and Exhibition, October 9-12, 2005, Dallas, TX, Society of Petroleum Engineers (2005). https://doi.org/10.2118/95872-MS

Hoeks, J. 1972. Effect of leaking natural gas on soil and vegetation in urban areas. Report published by the Centre for Agricultural Publishing and Documentation, Wageningen, Netherlands,.

Honeycutt, W. T., Ley, M. T., Materer, N. F. 2019. Precision and limits of detection for selected commercially available, low-cost carbon dioxide and methane gas sensors. *Sensors*, 19(14), 3157. https://doi.org/10.3390/s19143157

Humez, P., Mayer, B., Ing, J., Nightingale, M., Becker, V., Kingston, A., ... Taylor, S. 2016. Occurrence and origin of methane in groundwater in Alberta (Canada): Gas geochemical and isotopic approaches. *Sci. Total Environ*. 541, 1253-1268.

IPCC. 2013. Climate Change 2013: The Physical Science Basis. Contribution of Working Group I to the Fifth Assessment Report of the Intergovernmental Panel on Climate Change [Stocker, T.F., D. Qin, G.-K. Plattner, M. Tignor, S.K. Allen, J. Boschung, A. Nauels, Y. Xia, V. Bex and P.M. Midgley (eds.)]. Cambridge University Press, Cambridge, United Kingdom and New York, NY, USA, 1535 pp.

IPCC. 2019. 2019 Refinement to the 2006 IPCC Guidelines for National Greenhouse Gas Inventories. Volume 4, Chapter 10. Accessed August 2020 from https://www.ipcc-nggip.iges.or.jp/public/2019rf/vol4.html.

Jackson, R. B. 2014. The integrity of oil and gas wells. *Proc. Nat. Acad. Sci.* 111(30), 10902-10903. https://doi.org/10.1073/pnas.1410786111

Jackson, M. B., & Attwood, P. A. 1996. Roots of willow (Salix viminalis L.) show marked tolerance to oxygen shortage in flooded soils and in solution culture. *Plant Soil*, 187(1), 37-45.

Jackson, R. E., Gorody, A. W., Mayer, B., Roy, J. W., Ryan, M. C., Van Stempvoort, D. R., 2013. Groundwater protection and unconventional gas extraction: The critical need for field-based hydrogeological research. *Groundwater*. 51 (4), 488–510. https://doi:10.1111/gwat.12074.

Jerrett, M., Burnett, R. T., Pope III, C. A., Ito, K., Thurston, G., Krewski, D., ... Thun, M. 2009. Long-term ozone exposure and mortality. *New England J. Medic*. 360(11), 1085-1095.

Johnson, M. R., Tyner, D. R., Conley, S., Schwietzke, S., Zavala-Araiza, D. 2017. Comparisons of airborne measurements and inventory estimates of methane emissions in the Alberta upstream oil and gas sector. *Environ. Sci. Tech*. 51(21), 13008-13017. https://doi.org/10.1021/acs.est.7b03525

Kang, M., Christian, S., Celia, M.A., Mauzerall, D.L., Bill, M., Miller, A.R., Chen, Y., Conrad, M.E., Darrah, T.H., Jackson, R.B. 2016. Identification and characterization of high methane-emitting abandoned oil and gas wells. Proc. Natl. Acad. Sci. U.S.A. 113, 13636–13641. https://doi.org/10.1073/pnas.1605913113

Kang, M., Kanno, C. M., Reid, M. C., Zhang, X., Mauzerall, D. L., Celia, M. A., Chen, Y., Onstott, T. C., 2014. Direct measurements of methane emissions from abandoned oil and gas wells in Pennsylvania. Proc. Natl. Acad. Sci. 111(51), 18173-18177. https://doi.org/10.1073/pnas.1408315111

Kelly, W. R., Matisoff, G., Fisher, J. B. 1985. The effects of a gas well blow out on groundwater chemistry. *Environ. Geol. Water Sci*. 7(4), 205-213. https://doi.org/10.1007/bf02509921

Kovach, E. M. 1945. Meteorological influences upon the radon-content of soil-gas. Eos, Trans. *Am. Geophys. Union*, 26(2), 241-248. https://doi.org/10.1029/TR026i002p00241

Kuang, X., Jiao, J. J., Li, H. 2013. Review on airflow in unsaturated zones induced by natural forcings. *Wat. Resour. Res.* 49(10): 6137-6165. https://doi.org/10.1002/wrcr.20416.

Lan, X., Talbot, R., Laine, P., Torres, A. 2015. Characterizing fugitive methane emissions in the Barnett Shale area using a mobile laboratory. *Environ. Sci. Technol*. 49(13), 8139-8146. https://doi.org/10.1021/es5063055

Lackey, G., Rajaram, H. 2019. Modeling gas migration, sustained casing pressure, and surface casing vent flow in onshore oil and gas wells. *Water Resour. Res*, 55(1), 298-323. https://doi.org/10.1029/2018WR024066

Lavoie, T. N., Shepson, P. B., Cambaliza, M. O., Stirm, B. H., Karion, A., Sweeney, C., ... Lyon, D. 2015. Aircraft-based measurements of point source methane emissions in the Barnett Shale basin. *Environ.l Sci. Technol.,* 49(13), 7904-7913. https://doi.org/10.1021/acs.est.5b00410

Lebel, E. D., Lu, H. S., Vielstädte, L., Kang, M., Banner, P., Fischer, M. L., Jackson, R. B. 2020. Methane Emissions from abandoned oil and gas wells in California. *Environ. Sci. Technol*. 54(22), 14617-14626. https://doi.org/10.1021/acs.est.0c05279

Lyman, S. N., Tran, H. N., Mansfield, M. L., Bowers, R., Smith, A. 2020. Strong temporal variability in methane effluxes from natural gas well pad soils. *Atmos. Pollut. Res*. 11(8):1386-1395. https://doi.org/10.1016/j.apr.2020.05.011

Maier, M., Mayer, S., Laemmel, T. 2019. Rain and wind affect chamber measurements. *Agric. For. Meteorol*. 279, 107754. https://doi.org/10.1016/j.agrformet.2019.107754

Martin, G. E., Snow, D. D., Kim, E., Spalding, R. F., 1995. Simultaneous determination of argon and nitrogen. *Groundwater*. 33(5), 781-785. https://doi.org/10.1111/j.1745-6584.1995.tb00024.x

McMahon, P. B., Thomas, J. C., Crawford, J. T., Dornblaser, M. M., Hunt, A. G. 2018. Methane in groundwater from a leaking gas well, Piceance Basin, Colorado, USA. *Sci. Total Environ.* 634, 791-801. https://doi.org/10.1016/j.scitotenv.2018.03.371

Mikkelä, C., Sundh, I., Svensson, B. H., Nilsson, M. 1995. Diurnal variation in methane emission in relation to the water table, soil temperature, climate and vegetation cover in a Swedish acid mire. *Biogeochem*. 28(2), 93-114. https://doi.org/10.1007/BF02180679

Milbert, D. 2018. Solid Earth Tide. Accessed 08-2020 from https://geodesyworld.github.io/SOFTS/solid.htm#link2

Mitton, M. 2018. Subsurface methane migration from natural gas distribution pipelines as affected by soil heterogeneity: field scale experimental and numerical study. [MSc Thesis]. Colorado School of Mines. Retrieved from

https://mines.primo.exlibrisgroup.com/permalink/01COLSCHL_INST/1i00sit/alma997582702902341.

Molofsky, L. J., Connor, J. A., Van De Ven, C. J., Hemingway, M. P., Richardson, S. D., Strasert, B. A., ... Paquette, S. M. 2021. A Review of Physical, Chemical, and Hydrogeologic Characteristics of Stray Gas Migration: Implications for Investigation and Remediation. *Sci. Tot. Environ*. 146234. https://doi.org/10.1016/j.scitotenv.2021.146234

Montague, J. A., Pinder, G. F., Watson, T. L. 2018. Predicting gas migration through existing oil and gas wells. *Environ. Geosci*. 25(4), 121-132. https://doi.org/10.1306/eg.01241817008

Muehlenbachs, L. 2017. 80,000 inactive oil wells: A blessing or a curse? The School of Public Policy, University of Calgary, Alberta, Canada. *SPP Briefing Paper* 10(3). https://www.policyschool.ca/wp-content/uploads/2017/03/Inactive-Oil-Wells-Muehlenbachs-1.pdf.

Nachshon, U., Weisbrod, N., Dragila, M. I., Ganot, Y. 2011. The importance of advective fluxes to gas transport across the earth-atmosphere interface: the role of thermal convection. Planet Earth 2011-Global Warming Challenges and Opportunities for Policy and Practice. IntechOpen.

Natural Resources Canada. Greenhouse Gases Equivalencies Calculator- Calculations and References. Accessed from: https://oee.nrcan.gc.ca/corporate/statistics/neud/dpa/calculator/refs.cfm

Natural Resources Canada. 2019. Technology roadmap to improve wellbore integrity: summary report. Accessed from: https://www.nrcan.gc.ca/sites/www.nrcan.gc.ca/files/pdf/NRCan_Wellbore_e_WEB(1)%20(1).pdf

Noomen, M. F., van der Werff, H. M., van der Meer, F. D. 2012. Spectral and spatial indicators of botanical changes caused by long-term hydrocarbon seepage. *Ecolog. Informatic*, 8, 55-64.

Nowamooz, A., Lemieux, J. M., Molson, J., Therrien, R. 2015. Numerical investigation of methane and formation fluid leakage along the casing of a decommissioned shale gas well. *Wat. Resour. Res.* 51(6), 4592-4622. https://doi.org/10.1002/2014WR016146

Occupational Health and Safety Code. 2009. Part 10: Fire and Explosion Hazards. Alberta, Canada. Accessed from: https://open.alberta.ca/dataset/757fed78-8793-40bb-a920-6f000853172b/resource/c8f462b7-e8c3-4c4a-a5b3-c055648c61ee/download/4403880-part-10-fire-and-explosion-hazards.pdf

Office of the Regulator of Oil and Gas Operations (OROGO). 2017. Well Suspension and Abandonment Guidelines. Northwest Territories Oil and Gas Operations Act. Retrieved from https://www.orogo.gov.nt.ca/sites/orogo/files/resources/orogo_well_suspension_and_abandonment_guidelines_and_interpretation_notes.pdf#page=24&zoom=100,92,96

Oliveira, S., Viveiros, F., Silva, C., Pacheco, J. E. 2018. Automatic Filtering of Soil CO2 Flux Data; Different Statistical Approaches Applied to Long Time Series. *Front. Earth Sci.* 6, 208. https://doi.org/10.3389/feart.2018.00208

Osborn, S., Vengosh, A., Warner, N., Jackson, R. 2011. Methane contamination of drinking water accompanying gas-well drilling and hydraulic fracturing. *Proc. Natl. Acad. Sci.* 108(20), 8172-8176. https://doi.org/10.1073/pnas.1100682108

Pinti, D. L., Y. Gelinas, M. Larocque, D. Barnetche, S. Retailleau, A. Moritz, J. F. Helie, and R. Lefebvre. 2013, Concentrations, sources et mécanismes de migration préférentielle des gaz d'origine naturelle (méthane, hélium, radon) dans les eaux souterraines des Basses-Terres du Saint-Laurent, Rep. E3–9, 94 pp., Comité d'évaluation environnementale stratégique pour le gaz de schiste au Québec, Qué., Canada. Accessed from: http://espace.inrs.ca/id/eprint/2111/1/R001503.pdf

Poulsen, T. G., Møldrup, P. 2006. Evaluating effects of wind-induced pressure fluctuations on soil-atmosphere gas exchange at a landfill using stochastic modelling. *Waste Manag. Res.* 24(5), 473-481. https://doi.org/10.1177/0734242X06066363

Poulsen, T. G., Pourber, A., Furman, A., Papadikis, K. 2017. Relating wind-induced gas exchange to near-surface wind speed characteristics in porous media. *Vadose Zone J.* 16(8), 1-13. https://doi.org/10.2136/vzj2017.02.0039

Pretch, P. and Dempster, D. 2017. Newfoundland & Labrador Basis for Development of Guidance Related to Hydraulic Fracturing: Part 3. Accessed from: http://www.nr.gov.nl.ca/nr/energy/pdf/nl_hydraulic_fracturing_pt3_appendix.pdf

Province of Alberta. 2020. Pipeline Act. Retreived from https://www.qp.alberta.ca/documents/Acts/p15.pdf

R Core Team. 2020. R: A language and environment for statistical computing. R Foundation for Statistical Computing, Vienna, Austria. Accessed 10-2020 from https://www.R-project.org/

Reddy, K. R., Yargicoglu, E. N., Yue, D., et al. 2014. Enhanced microbial methane oxidation in landfill cover soil amended with biochar. *J. Geotech.and Geoenviron. Eng.* 140(9): 04014047. https://doi.org/10.1061/(ASCE)GT.1943-5606.0001148

Redeker, K. R., Baird, A. J., Teh, Y. A. 2015. Quantifying wind and pressure effects on trace gas effluxes across the soil-atmosphere interface. Biogeosci. 12(24), 7423-7434. doi:10.5194/bg-12-7423-2015

Riddick, S. N., Mauzerall, D. L., Celia, M. A., Kang, M., Bandilla, K. 2020. Variability observed over time in methane emissions from abandoned oil and gas wells. *Intern.J. Greenh. Gas Control*. 100, 103116. https://doi.org/10.1016/j.ijggc.2020.103116

Riley, W. J., Gadgil, A. J., Bonnefous, Y. C., Nazaroff, W. W. 1996. The effect of steady winds on radon-222 entry from soil into houses. *Atmos. Environ.* 30(7), 1167-1176. https://doi.org/10.1016/1352-2310(95)00248-0

Risk, D., McArthur, G., Nickerson, N., Phillips, C., Hart, C., Egan, J., Lavoie, M., 2013. Bulk and isotopic characterization of biogenic CO2 sources and variability in the Weyburn injection area. *Int. J. Greenh. Gas Control*. 16, S263-S275. https://doi.org/10.1016/j.ijggc.2013.02.024

Romanak, K.D., Wolaver, B., Yang, C., Sherk, G.W., Dale, J., Dobeck, L.M., Spangler, L.H., 2014. Process-based soil gas leakage assessment at the Kerr Farm: comparison of results to leakage proxies at ZERT and Mt. Etna. *Int. J. Greenh. Gas Control*. 30, 42-57. https://doi.org/10.1016/j.ijggc.2014.08.008

Roscioli, J. R., Herndon, S. C., Yacovitch, T. I., Knighton, W. B., Zavala-Araiza, D., Johnson, M. R., Tyner, D. R. 2018. Characterization of methane emissions from five cold heavy oil production with sands (CHOPS) facilities. *J. Air Waste Manag. Assoc*. 68(7), 671-684. https://doi.org/10.1080/10962247.2018.1436096

Rowe, D., Muehlenbachs, K. 1999. Isotopic fingerprints of shallow gases in the Western Canadian sedimentary basin: tools for remediation of leaking heavy oil wells. *Organic Geochem.* 30(8), 861-871. https://doi.org/10.1016/S0146-6380(99)00068-6

Roy, N., Molson, J., Lemieux, J. M., Van Stempvoort, D., Nowamooz, A. 2016. Three-dimensional numerical simulations of methane gas migration from decommissioned hydrocarbon production wells into shallow aquifers. *Water Resour. Res.* 52(7), 5598-5618. https://doi.org/10.1002/2016WR018686

Rumble, Bruno, T. J., Doa, M.J. 2020. *CRC handbook of chemistry and physics 101st Edition.* Online. Taylor and Francis Group. http://hbcponline.com/faces/contents/ContentsSearch.xhtml

Saint-Vincent, P. M., Reeder, M. D., Sams III, J. I., et al. 2020. An analysis of abandoned oil well characteristics affecting methane emissions estimates in the Cherokee Platform in Eastern Oklahoma. *Geophys. Res. Lett.* 47:(23). https://doi.org/10.1029/2020GL089663.

Sandau, C. D., Prokipchuk, M., Dominato, K. R., Mundle, S. O., 2019. Soil gas investigation of an alleged gas migration issue on a residential farm located above the Weyburn-Midale CO2 enhanced oil recovery project. *Int. J. Greenh. Gas Control*. 81, 11-20. https://doi.org/10.1016/j.ijggc.2013.02.024

Sandl, E., Cahill, A. G., Welch, L., et al. 2021. Characterizing oil and gas wells with fugitive gas migration through Bayesian multilevel logistic regression. *Sci. Tot. Environ.*769: 144678. https://doi.org/10.1016/j.scitotenv.2020.144678.

Schiffner, D. 2020. Methane Emissions from Suspended Wells: Can Internalizing the Cost of Methane Leaks Incentivize Plugging and Reclamation of Petroleum Wells in Alberta? Proc. World Geothermal Congress, April 26 – May 2, 2020, Reykjavik, Iceland.

Schiffner, D., Kecinski, M., Mohapatra, S. 2021. An updated look at petroleum well leaks, ineffective policies and the social cost of methane in Canada's largest oil-producing province. *Climatic Change*. 164(3), 1-18.

Schloemer, S., Furche, M., Dumke, I., et al. 2013. A review of continuous soil gas monitoring related to CCS–Technical advances and lessons learned. *Applied Geochemistry* **30:** 148-160. https://doi.org/10.1016/j.apgeochem.2012.08.002.

Schmitz, R., Carlson, P. B., Lorenz, G. D., Watson, M. D., & Erno, B. P. 1993. Husky Oil's gas migration research effort: An update (No. CU/FCE--CE04462).

Schout, G., Griffioen, J., Hassanizadeh, S. M., de Lichtbuer, G. C., Hartog, N. 2019. Occurrence and fate of methane leakage from cut and buried abandoned gas wells in the Netherlands. *Sci. Total Environ.* 659, 773-782. https://doi.org/10.1016/j.scitotenv.2018.12.339

Sekhar, P. K., Kysar, J., Brosha, E. L. et al. 2016. Development and testing of an electrochemical methane sensor. *Sensors and Actuators B: Chemical*. 228, 162-167. https://doi.org/10.1016/j.snb.2015.12.100

Seo, D. H., Han, W. S., Park, E., Jeong, J., Oh, Y. Y., Kim, H. J., ...Yun, S. T. 2020. Analyses and numerical evaluation of integrated time-series monitoring datasets including CO2 concentration and fluxes at controlled CO2 release site in South Korea. *J. Hydro.* 590, 125213. https://doi.org/10.1016/j.jhydrol.2020.125213

Sihota, N. J., Mayer, K. U., Toso, M. A., Atwater, J. 2013. Methane emissions and contaminant degradation rates at sites affected by accidental releases of denatured fuel-grade ethanol. *J. Contam. Hydrol*. 151, 1-15. https://doi.org/10.1016/j.jconhyd.2013.03.008

Simpson, I. J., Edwards, G. C., Thurtell, G. W. 1999. Variations in methane and nitrous oxide mixing ratios at the southern boundary of a Canadian boreal forest. *Atmos. Environ.* 33(7): 1141-1150. https://doi.org/10.1016/S1352-2310(98)00235-0.

Smith, Ann P., Bowers, Richard L., Boyd, Victoria H., Lyman, S. 2019. Long-Term Methane Emissions Quantification and Alert System for Natural Gas Storage Wells and Fields. GSI Environmental, Inc., Austin, Texas. doi:10.2172/1526753.

Soares, J. 2019. Characterization of gas migration and surface emissions through a controlled release experiment at the Hudson's Hope Field Research Station, BC, Canada. [MSc Thesis]. University of British Colombia. Accessed from: https://open.library.ubc.ca/cIRcle/collections/ubctheses/24/items/1.0389535

Spokas, K., Graff, C., Morcet, M., Aran, C., 2003. Implications of the spatial variability of landfill emission rates on geospatial analyses. *Waste Manag.* 23(7), 599-607. https://doi.org/10.1016/S0956-053X(03)00102-8

Statistics Canada, 2016. 2016 Census- Boundary Files. Accessed From: https://www12.statcan.gc.ca/census-recensement/2011/geo/bound-limit/bound-limit-2016-eng.cfm

Statutes of Saskatchewan. 1998. The Pipeline Act. Accessed October 2020 from: https://www.canlii.org/en/sk/laws/stat/ss-1998-c-p-12.1/latest/part-1/ss-1998-c-p-12.1-part-1.pdf

Steelman, C. M., Klazinga, D. R., Cahill, A. G., Endres, A. L., Parker, B. L. 2017. Monitoring the evolution and migration of a methane gas plume in an unconfined sandy aquifer using time-lapse GPR and ERT. *J. Contam. Hydrol*. 205, 12-24. https://doi.org/10.1016/j.jconhyd.2017.08.011

Stein, V., Hettiaratchi, J. P. 2001. Methane oxidation in three Alberta soils: influence of soil parameters and methane efflux rates. *Environ. Technol.* 22(1), 101-11. https://doi.org/10.1080/09593332208618315

Szatkowski, B., Whittaker, S., and Johnston, B. 2002. Identifying the source of migrating gases in surface casing vents and soils using stable Carbon Isotopes, Golden Lake Pool, West-central Saskatchewan. Summary of Investigations, vol 1 Saskatchewan Geological Survey, Regina, SK, Canada.

Tang, J., Bao, Z., Xiang, W., Gou, Q. 2008. Geological emission of methane from the Yakela condensed oil/gas field in Talimu Basin, Xinjiang, China. J. Environ. Sci. 20(9), 1055-1062 https://doi.org/10.1016/S1001-0742(08)62149-X

Tilley, B., Muehlenbachs, K. 2011. Fingerprinting of gas contaminating groundwater and soil in a petroliferous region, Alberta, Canada. Presented at Proceedings from International Network of Environmental Forensics Conference, 2011, Cambridge (UK) (2011) pp. 115-125.

Tokida, T. Miyazaki, T., Mizoguchi, M., Nagata, O., Takakai, F., Kagemoto, A., Hatano, R., 2007. Falling atmospheric pressure as a trigger for methane ebullition from peatland. *Glob. Biogeochem. Cycles.* 21(2). https://doi.org/10.1029/2006GB002790

Townsend-Small, A., Ferrara, T. W., Lyon, D. R., Fries, A. E., Lamb, B. K. 2016. Emissions of coalbed and natural gas methane from abandoned oil and gas wells in the United States. *Geophys. Res. Lett.* 43(5), 2283-2290. https://doi.org/10.1002/2015GL067623

Trudel, E., Bizhani, M., Zare, M. et al. 2019. Plug and abandonment practices and trends: A British Columbia perspective. *J. Petrol. Sci. Eng.* 183: 106417. https://doi.org/10.1016/j.petrol.2019.106417.

Ulrich, B. A., Mitton, M., Lachenmeyer, E., Hecobian, A., Zimmerle, D., Smits, K. M. 2019. Natural gas emissions from underground pipelines and implications for leak detection. *Environ. Sci. Technol. Lett.* 6(7), 401-406. https://doi.org/10.1021/acs.estlett.9b00291

Van De Ven, C., Abraham, J., Mumford, K. 2020. Laboratory investigation of free-phase stray gas migration in shallow aquifers using modified light transmission. *Adv. Water Resour.* 103543.

Van De Ven, C., Mumford, K. 2020. Intermediate-Scale Laboratory Investigation of Stray Gas Migration Impacts: Methane Source Architecture and Dissolution. *Environ. Sci. Technol.* 54(10), 6299-6307.

Van Stempvoort, D., Maathuis, H., Jaworski, E., Mayer, B., Rich, K. 2005. Oxidation of fugitive methane in ground water linked to bacterial sulfate reduction. *Groundwater*. 43(2): 187-199. https://doi.org/10.1111/j.1745-6584.2005.0005.x

Vidic, R., Brantley, S., Vandenbossche, J., Yoxtheimer, D., Abad, J. 2013. Impact of shale gas development on regional water quality. *Sci.* 340(6134). https://doi.org/10.1126/science.1235009.

Watson, T. L., Bachu, S. 2009. Evaluation of the potential for gas and CO_2 leakage along wellbores. *SPE Drill Complet*. 24(01), 115-126.

Wen, T., Castro, M. C., Nicot, J. P., Hall, C. M., Larson, T., Mickler, P., Darvari, R., 2016. Methane sources and migration mechanisms in shallow groundwaters in Parker and Hood Counties, Texas- A heavy noble gas analysis. *Environ. Sci. Technol*. 50(21), 12012-12021. https://doi.org/10.1021/acs.est.6b01494

West, J. J., Fiore, A. M., Horowitz, L. W., Mauzerall, D. L. 2006. Global health benefits of mitigating ozone pollution with methane emission controls. *Proc. Natl. Acad. Sci.* 103(11), 3988-3993.

Whiticar, M. J., 1999. Carbon and hydrogen isotope systematics of bacterial formation and oxidation of methane. Chem. Geo. 161(1-3), 291-314. https://doi.org/10.1016/S0009-2541(99)00092-3

Wickham, H., 2016. ggplot2: Elegant Graphics for Data Analysis. Springer-Verlag New York.

Williams, G. M., Aitkenhead, N. 1991. Lessons from Loscoe: the uncontrolled migration of landfill gas. Q. J. Eng. Geol. Hydrogeol., 24(2), 191-207. https://doi.org/10.1144/GSL.QJEG.1991.024.02.03

Woods, A. W., Norris, S. 2016. Dispersion and dissolution of a buoyancy driven gas plume in a layered permeable rock. *Water Resour. Res.* 52(4), 2682-2697. https://doi.org/10.1002/2015WR018159

Xu, L., Furtaw, M., Madsen, R., Garcia, R., Anderson, D., McDermitt, D. 2006. On maintaining pressure equilibrium between a soil CO2 efflux chamber and the ambient air. *J. Geophys. Res: Atmos*. 111(D8). https://doi.org/10.1029/2005JD006435

Yin, J, Mayer, K.U., Sihota, N. 2014. Evaluation of gas migration near production wells in Northeastern BC- Results of a preliminary field survey. The University of British Colombia.

Zavala-Araiza, D., Lyon, D. R., Alvarez, R. A., et al. 2015. Reconciling divergent estimates of oil and gas methane emissions. *Proc. Nat.l Acad. S.* 112(51): 15597-15602. https://doi.org/10.1073/pnas.1522126112.

Appendices

A Problem Definition: A Field comparison of gas migration testing methodologies

Abstract

Combustible gas concentrations measurement (often used as equivalent ppm CH_4) around energy wells is the typical approach to detect for the presence or absence of gas migration outside the casing (GM) that may be contributing to fugitive methane emissions, groundwater impacts, and safety concerns. The range in testing methodologies employed by different service companies and operators within the upstream petroleum industry may not have equal efficacy for detecting GM. This study compares historic GM test results performed by multiple different industry partners around six energy wells, supplemented with additional field testing of several of the standard industry test methods at two sub-selected wells. Findings document substantial variability in the maximum recorded concentrations from GM tests around the same well, with the differences attributed to a combined effects of testing party methodology, in addition to method-independent factors such as the spatiotemporal variability in the distribution of migrating gases. Additional field testing at two of the wells shows generally higher measured concentrations at greater soil depth, and the highest measured CH_4 concentrations at each depth consistently restricted to spatially limited zones. At the six locations observed in this study, all tested methods reveal the presence of migrating gases when testing at a high enough spatial density to identify gas migration, but CH_4 concentrations vary considerably.

Introduction

The potential impacts of gas migration outside of the surface casing (GM) include atmospheric methane emissions, groundwater quality impacts, and safety concerns, thereby necessitating the need to identify and repair these wells (Cahill et al., 2017). A test for the presence or absence of GM was developed in the 1990's by the Lloydminster Area Operations Group Gas Migration Team and continues in current regulation in Alberta (and in similar forms elsewhere) as the 'recommended' approach, with the acknowledgement that other testing methodologies are presently used and accepted (Drilling and Completions Committee, 1993; Abboud et al., 2020; BC Oil and Gas Commission, 2020; AER, 2021). The recommended GM testing approach uses a portable field analyzer for combustible hydrocarbon gases at a depth of 50 cm in the soil at two locations within 30 cm of the wellbore, and 2, 4, and 6 m outward from the wellbore every 90 degrees. To the author's knowledge, neither field validation of this testing technique, nor justification of the recommended 50 cm testing depth and test point spacing has been published. Allowance for other accepted testing methodologies causes a range of competitive testing technologies and techniques employed by well operators and service providers, including use of different gas analysers, measurement spacings and depths, and other provider-specific details. In Alberta, economic costs are associated with locating subsurface facilities and ground disturbance permitting for GM tests greater than 30 cm depth, thus incentivising shallow soil and soil-surface GM testing (Pipeline Act, 2020). Different service providers may all employ slightly different GM detection methods, with poorly defined impacts

on the efficacy of detection. The most time efficient testing method – methane concentration measurement at ground surface – was observed to be the most common industry practice.

Differences in GM testing methodology may result in variation in i) measured maximum concentrations and ii) successful detection of the presence of GM, which is defined as the exceedance of the maximum detectable concentration above background values (typically around 2 ppmv CH_4 in atmospheric air; He et al., 2020). The related field of natural gas pipeline leak detection also has a knowledge gap in whether differing detection techniques may be resulting in differences the efficacy of leak detection (Ulrich et al., 2019 and references therein). This comparison of historic GM testing at selected energy wells with gas migration sought to identify if variation in GM test results could be attributed to test service provider (each presumably or explicitly associated with differences in testing methodology). Further field investigations were then conducted by the authors to directly compare common testing methods around two sub-selected case-study wells.

Methodology

Industry partners provided data of historic GM test results from six anonymous energy wells within Alberta, all with known instances of GM. The reports were provided by the licensees on condition of anonymity of the well location and operator, testing company, and specific test details. The geographical and GM characteristics of the wells may not have been representative of all wells across Alberta. The reports, spanning multiple years and different test providers, included the measured concentration at each spatial test point. Most GM reports did not directly contain records of the measurement equipment or testing methodology (e.g., depth), and as such the analyses were restricted to comparison between (anonymized) test providers or

methods instead of test technique directly. It was assumed that test equipment and methodology were potentially different for different providers but did not vary significantly for the same provider over multiple years. Two of the test providers (1 and 4 in Figure A1) performed two types of measurement methods at the same test locations (e.g., above and below ground surface). These dual-method tests were considered in aggregate by the service provider when rating the presence or absence or GM, however both methods are presented separately in this analysis for comparison. In some cases, historic GM reports were supplemented with additional GM tests performed by service providers and observed by the author, however the methods employed are not published here due to agreements of confidentiality.

Analysis of variance tests were conducted on the maximum recorded concentration to determine if testing party had a significant effect on these outcomes. Next, data were grouped from all wells and a Chi-Squared Test of Independence was performed to assess whether there was a relationship between testing party and the detection/non-detection of GM. In this analysis, GM was deemed to have been detected if the maximum concentration recorded methane concentration was > 10 ppm.

The second phase of this study involved detailed spatial characterization of the distribution of soil gases and a direct comparison of GM test techniques around two sub-selected industry wells (#3 in Figure A1, and the well later developed as the case-study well in Chapters 3 and 4). Soil gas concentrations were measured in the field using a portable handheld combustible gas detector (GMI GT-43, Gas Measurement Instruments Ltd.). Surface, barhole, and capped hole measurements (defined below) were completed by sequentially measuring the

concentrations at the 14 test point locations described in the AER Directive 20 (AER 2021). Measurements were performed on the soil surface using a field probe connected to a 72 mm diameter bell-shaped flexible cover held against the soil surface to provide a rough seal. A 30 cm 'barhole' (in-soil) measurement was performed using a slide-hammer gas sampling probe (Retract-A-Tip Gas Vapor Probe, AMS Inc.). Finally, a capped hole measurement was completed by capping the 20 mm diameter 'barhole' created by the slide-hammer probe with a PVC plastic stopper subsequent to probe removal, and allowing a five minute equilibration time until measurement (Figure A4). Soil gas samples were collected with a plastic 60 mL syringe attached to the sampling probe, with appropriate (> three tubing volumes) purging before samples were collected and stored in pre-evacuated glass vials. Subsequent compositional analysis was performed using established methods at the University of Calgary Applied Geochemistry Group gas chromatography laboratory. Gas compositional analysis was conducted with 5 mL aliquot of each gas sample injected into a 4-column gas chromatograph (Scion 450/456) fitted with three thermal conductivity detectors and one flame ionization detector (Cheung, 2019). The lower detection limit was 0.5 ppm for hydrocarbon gases, while the analytical precision and accuracy was typically better than ± 2.5% of the reported concentration.

Results and Discussion

Comparison of GM test results by provider

Historic GM test results were made available for six wells, each tested by between three (test well 6) and six methods (wells 1, 2) across six different commercial parties employing a total of eight different methods (Figure A1). Although test dates are not included for specific

wells or tests to preserve anonymity, all 93 tests were conducted between 2000 and 2018 and results are graphically presented in chronological order. Substantial methane concentration variation (i.e., orders of magnitude) was observed in the data set for each well. Analysis of variance of the maximum recorded methane concentration from each testing occasion, separated by testing method, revealed that there was a statistically significant dependence of testing method on the maximum recorded methane concentration (ANOVA $F(5, N=86) = 8.7$, $p<.001$; Figure A1). Two methods (Parties 2 and 5) were poorly represented across the wells and were removed from this analysis, resulting in only 86 tests analyzed.

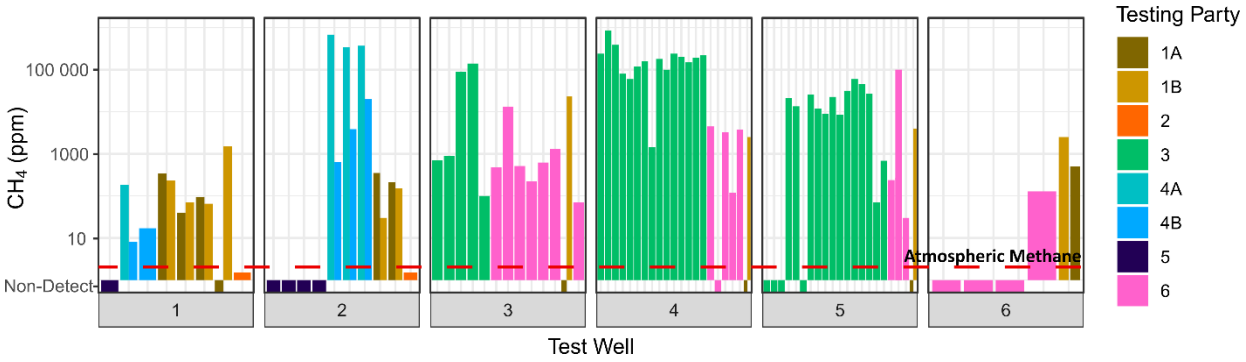

Figure A1 Maximum combustible gas concentrations (reported in ppm as CH_4) from each individual GM test conducted using eight different testing methods across six separate industry parties between 2000 and 2018 for six energy wells with gas migration. The tests are ordered chronologically for each well and colored by industry testing party/method, with grouped tests plotted as a half width representing two methods performed by the same party on the same day. Results show substantial variation (i.e., over multiple orders of magnitude), both in tests conducted by the same testing party on different occasions, and between different testing parties.

The authors considered gas migration to be non-detected (i.e., the test 'fails' to show GM) if the maximum reported methane concentration did not exceed 10 ppm. This detection limit is a conservatively low value which is only marginally higher than the average atmospheric concentration of 2 ppm (He et al., 2020). There were a 19 of the 93 non-detect (failed) tests

unequally distributed across the six wells (Figure A1). A Chi-Squared Test of Independence between GM detection method and the detect/non-detect outcome of the test revealed a statistically significant dependance of testing method on the successful detection of GM (X^2 (7, N=93) =34.5, p<.001). A false negative was reported by five of the eight test methods, and four of the six test parties on at least one occasion. Each of the six wells did not have reported detectable GM for at least one of the GM tests, and only one of the six wells (Well 3) had GM detected by all parties on all reported tests (when considering the aggregate of both methods 1A and 1B, as is the practice for that company). Several GM testing parties recorded tests with maximum methane concentrations > 100 ppm, followed by subsequent tests that are non-detectable. Similarly, one practitioner (Party 6; Figure A1) consistently reported non-detectable methane concentrations for all five tests reported on two separate wells.

There were no apparent temporal trends in the recorded concentrations for the wells that had many repeated tests by the same testing party, although any subtle temporal trends could be obscured by the variability between individual tests. These variable results on tests conducted by the same party indicates method-independent variation in migrating gas concentrations. The presented analyses may have been impacted by limitations in the available data, including the relatively low number of total tests and the unequal distribution of test parties across the six wells. Other assumptions of the analysis (e.g., constant GM rate, similar test methods by the same party across multiple years) have not been met.

While limited, the GM testing results do, however, indicate that currently practiced GM detection and measurement methods within Alberta are not equally reliable for detection and

characterization of GM. This suggests a need for further comparison across a larger sample size (with greater representation of different geographic regions and different operators). As of 2018, a cross-comparison of the GM reports provided for this study with the publicly available GM records indicate that the public records are insufficient for this comparison. The publicly available records did not contain repeated test results or testing method, among other details (AER 2018). This necessitates cooperation with industry partners for further comparisons.

Spatial variation in measured gas composition

Greater depth of measurement reliably led to higher measured concentrations of gases of subsurface origin (CH_4), though at all depths there was substantial lateral spatial variation in measured concentrations across the measurement grid (Figure A2). The distributions in measured concentrations were heavily skewed, where several sample locations showed high concentrations and many other test points were undistinguishable from background locations. This distribution is similar to previous observations of focused migration efflux pathways observed for gas migration around energy wells (Erno & Schmidt, 1996; Forde et al., 2018a; Lyman et al., 2020). The location of these concentration 'hot-spots' generally stayed in the same area for the two concentration surveys spaced one day apart, though the measured methane concentrations changed (Figure A3). The observed spatial and temporal variability in measured methane concentrations can partially explain the differences in historic GM test results since testing parties had completed measurements on different days and are unlikely to use identical locations. Even when using the same testing methodology, the inherent variability in gas migration may complicate any comparison of measured concentrations between different wells or over time at

the same well.

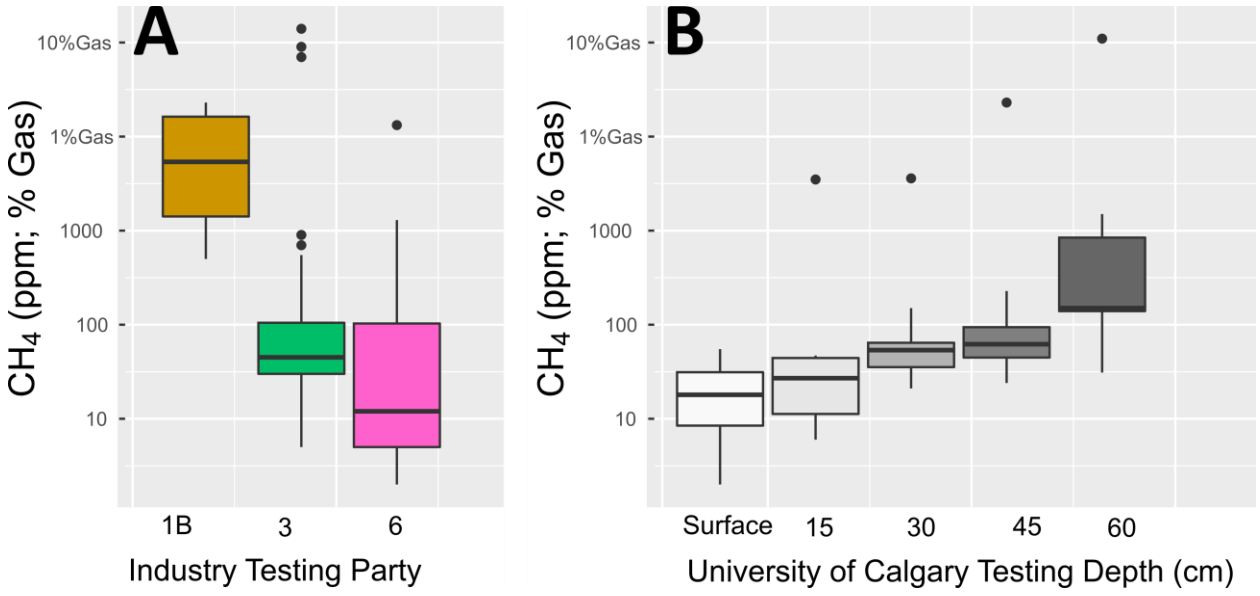

Figure A2 Boxplots showing the minimum, first quartile, median, 3rd quartile, and maximum recorded methane concentration test values (ppm CH_4) for all tests conducted at the same "cut-and-capped" energy well (Test well 3; Figure A1), both for industry partner testing (A), and a vertical profile sampled by the author (B). 'Outliers' greater than 1.5 times the interquartile range above the maximum value are denoted as points. Distributions show the maximum and median recorded concentrations increase with greater sampling depth. Maximum measured concentrations are generally > 1 order of magnitude higher than median concentrations.

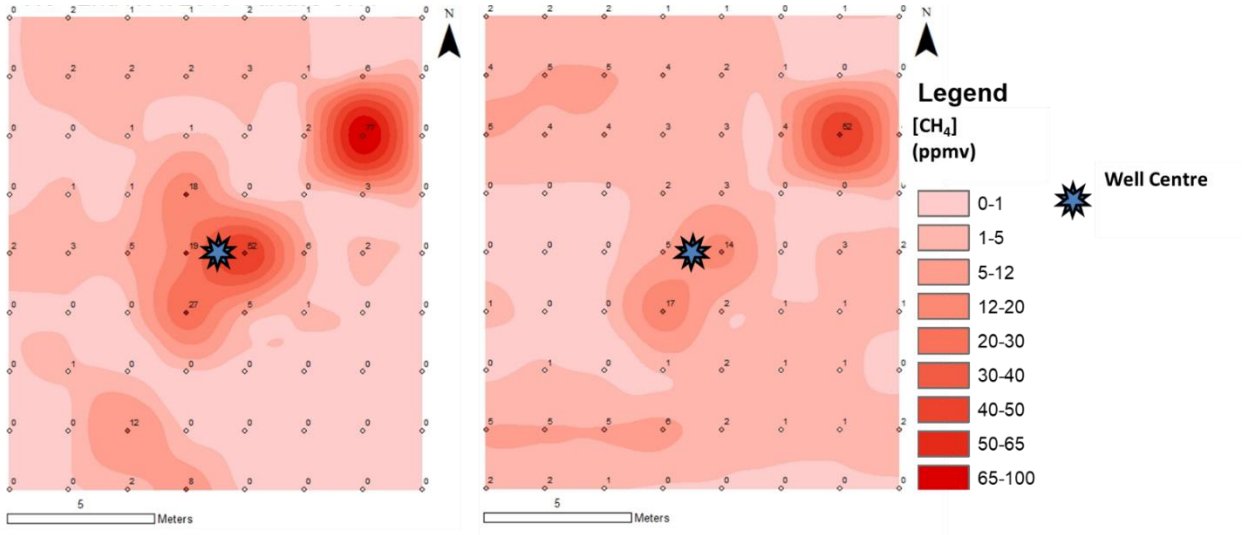

Figure A3 Plan view soil-surface combustible gas concentration as ppmv CH4 above background air concentration around a surface-abandoned industry well with known GM (Test Well 3; Figure A1). Surveys were conducted on a two by two m grid, repeated one day apart (on November 2 and 3, 2019 for the left and right figure, respectively). Inverse Distance Weighting spatial interpolation shows 'hotspot' zones of higher concentration.

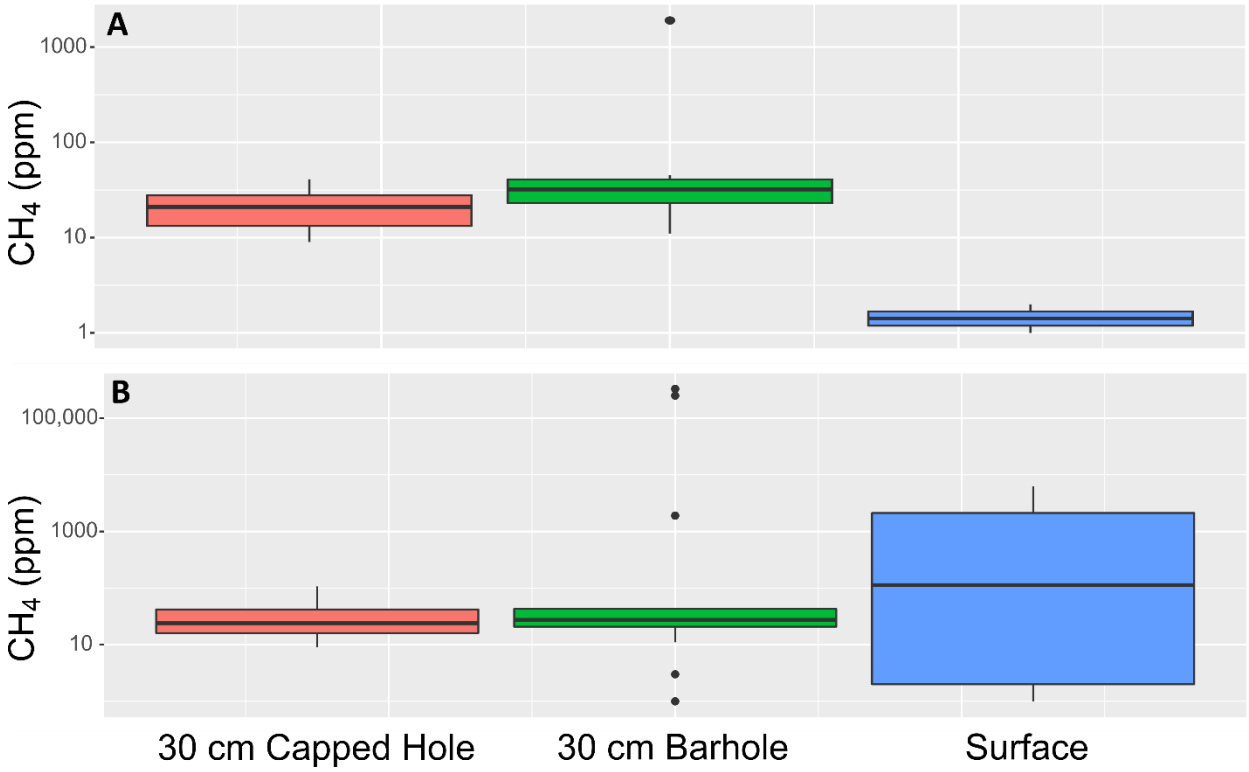

Figure A4 Comparison of CH_4 concentration around a single energy well measured using three different GM measurement methods for two different sample sets, including A) data from 12 measurement locations (each with including four measurements at each of 2, 4, and 6 m distances from the well in a cross pattern), and B) which included four measurements within 30 cm of the well casing (in addition to those at 2, 4 and 6 m distances from the well; AER, 2021).

Further comparison of GM testing methods also revealed lower measured methane concentrations at ground surface compared to the hammer probe and capped hole measurement at a depth of 30 cm in the case of sample locations of 2, 4, and 6 m away from well centre after AER (2021) (Figure A4a), although when samples from within 30 cm of the borehole were added to the sample set these also had measured methane concentrations substantially above background values (Figure A4b). Cross-correlation of the measured concentration with the handheld detector and from 56 soil gas samples analysed with gas chromatography showed that

the detector concentrations were well correlated but slightly underestimated the sample CH_4 concentration (R^2=0.88, m = 1.08).

Conclusions

Gas migration test results from historic surveys performed by multiple different industry testing parties around six energy wells were compared. Results revealed visually evident and statistically significant variability between GM tests conducted by different testing parties, in addition to variation between test results conducted by the same provider on different occasions. While the analysis was limited by a relatively small sample size (i.e., 93 tests) that were unequally distributed between six service companies on six wells, results did indicate a dependence on testing party for both maximum recorded methane concentration and successful GM detection. This indicates that the GM detection methods employed by commercial parties in Alberta may not all be equally effective, and some have a higher chance of under-detecting GM occurrences and maximum methane concentrations. Considering the importance of testing method on the outcomes of the GM tests, it may be important to associate a transparent record of testing method with the pass/fail result.

Independent GM test method comparisons revealed that measured concentrations were spatially variable at all depths and between different sampling methods, although recorded concentrations were generally higher at greater depths and nearer to the well-centre. Considering both historic test comparisons and independent testing performed by the University of Calgary research team, it appears that the lack of standardization of GM test methods may lead, in part, to the observed variation in GM test results. This could impact successful detection of wells with GM.

This potential impact on the successful detection of GM within the range of currently practiced methods suggests that a broader review and validation of GM detection and measurement practices is warranted. This may include comparison of historical GM tests involving a larger dataset with greater geographical representation. Further validation of permitted testing practices is also recommended. At the two case-study test sites examined, direct comparison of certain GM testing methods by the University of Calgary research team indicated several effective GM presence detection methods that were easier to implement (and hence less expensive) than the practice currently recommended by the Alberta Energy Regulator (AER 2021). It is recommended that service companies, operators, and the Regulator work together to update this recommended practice to reflect currently available sensor technology and the understanding of GM behavior. While refinement of GM testing methods will improve reliability, other causes of variation in GM test concentrations may include spatial and temporal variability of migrating gases.

B **Supplementary information for Appendix A:** Field comparison of gas migration testing methodologies

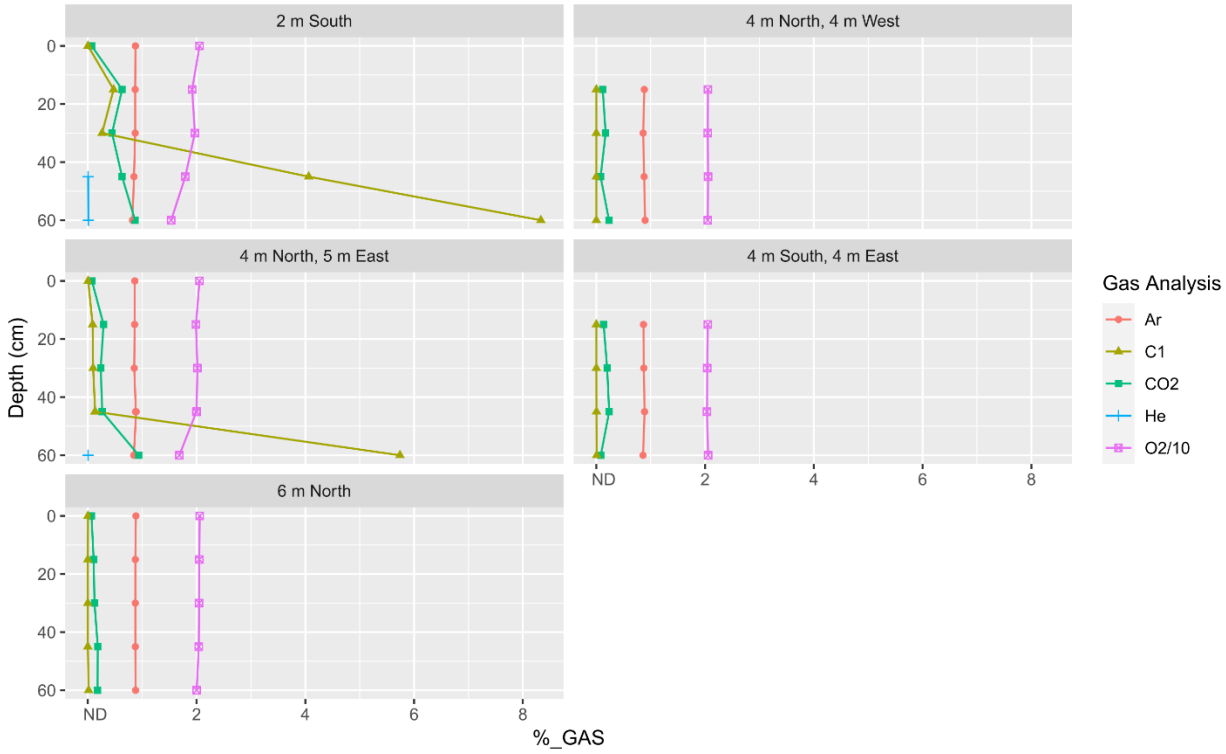

Figure B1 Depth profiles of gas chromatography analysis results of soil gas samples at five locations around a gas migration well with a thick vadose zone (Testing Well #3; Figure A1).

Table B.1 Pearson correlation matrix for field measurement of combustible gas concentrations and soil gas samples analysed with gas chromatography around two wells with GM at sample depths from 0-60 cm and distances up to 6 m radially from the well. Absolute values greater than 0.8 are bolded.

	Field Sensor	He	Ar	O2	N2	CO2	C1	C2
Field Sensor	1.00	**0.92**	**-0.94**	**-0.85**	**-0.94**	0.24	**0.94**	**0.86**
He		1.00	**-0.97**	**-0.90**	**-0.97**	0.23	**0.98**	**0.91**
Ar			1.00	**0.89**	**1.00**	-0.23	**-1.00**	**-0.91**
O2				1.00	**0.88**	-0.62	**-0.92**	-0.72
N2					1.00	-0.22	**-1.00**	**-0.91**
CO2						1.00	0.30	-0.02
C1							1.00	**0.90**
C2								1.00

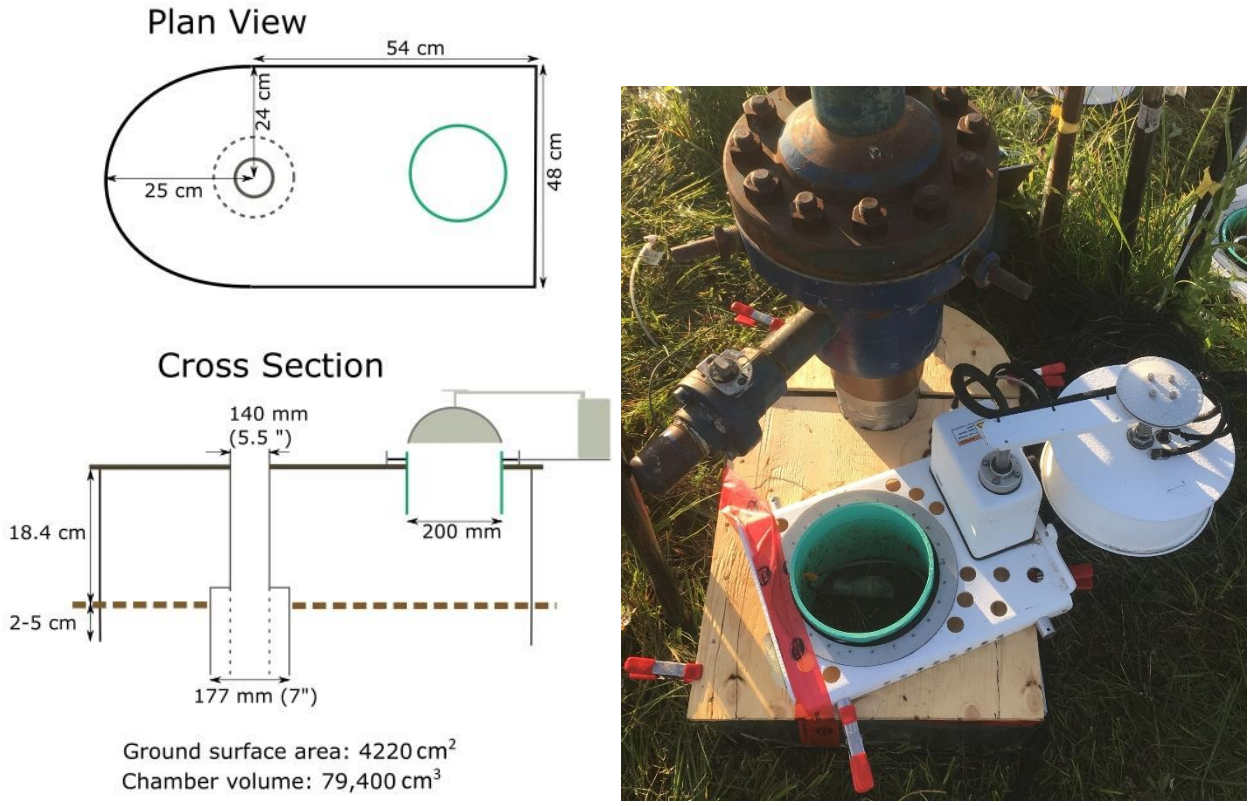

Figure C1 Custom wellhead chamber construction schematic and field photograph showing the coupling of the automated dynamic efflux chamber to the custom chamber. The collar base was constructed with thin sheet metal placed 2-5 cm into the ground surface around the well (the lateral segment of the surface casing preventing deeper installation). Rigid plastic sheeting formed an air-tight seal on the lid-portion of the chamber. A hole in the plastic sheeting accommodated a 200 mm PVC pipe, allowing for coupling with the automated chamber. A plywood external lid to the chamber provided structural support and prevented any pumping/chamber size modifications due to wind acting on the plastic.

Estimation of Minimum Detectable Efflux

The minimum detectable efflux (MDF) was calculated using methods provided in Christiansen et al. (2015):

$$MDF = (\frac{A_a}{t_c})(\frac{VP}{SRT})$$

A_a is the instrument analytical accuracy, t_c is the closure time, V is the total volume (m^3), P is the atmospheric pressure (Pa), S is the chamber surface area (m^2), R is the ideal gas constant (8.314 m^3 Pa^{-1} K^{-1} mol^{-1}), and T is the temperature (K). The analytical accuracy is conservatively taken to be 0.2 ppm for CH_4 and 1 ppm for CO_2 (above reported instrumental accuracies (< 2 ppb CH_4, Los Gatos Research; <1 ppm for CO_2 LI-COR Inc.).

Table C.1 Efflux measurement settings and parameters used for the October 11-26th measurement period, with calculated minimum detectable effluxes considering the average period temperature of 4.8 °C.

Chamber Location Name	Area (cm^2)	Total Volume (cm^3)	Chamber Closure Time (s)	Chamber MDF CO_2 (µmol m^{-2} s^{-1})	Chamber MDF CH_4 (µmol m^{-2} s^{-1})	Surface Area/Volume
Wellhead	4224.7	8 4260	15	0.54	0.11	0.05
1.0 S	317.8	6037	90	0.09	0.02	0.05
0.5 SE	317.8	6124	45	0.17	0.03	0.05
0.5 NE	317.8	5687	90	0.08	0.02	0.06
2.5 N	317.8	5878	90	0.08	0.02	0.05
5.0 S	317.8	6013	90	0.09	0.02	0.05

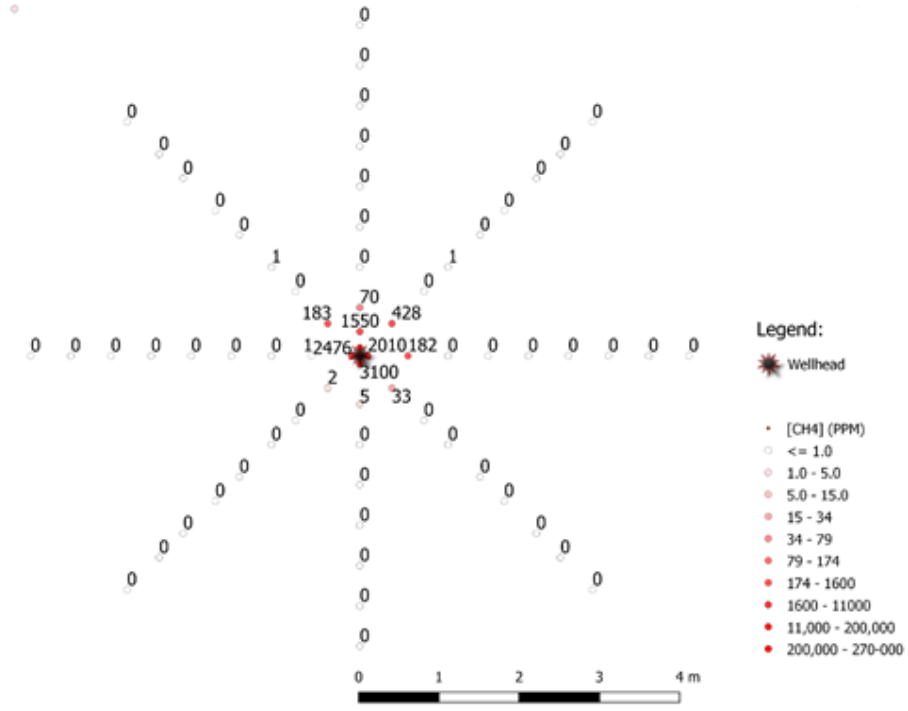

Figure C2 Close view of 2018-11-21 soil-surface methane gas concentrations as ppm CH_4 above background levels centered on the wellhead. Full survey extended to 20 m distance from well center.

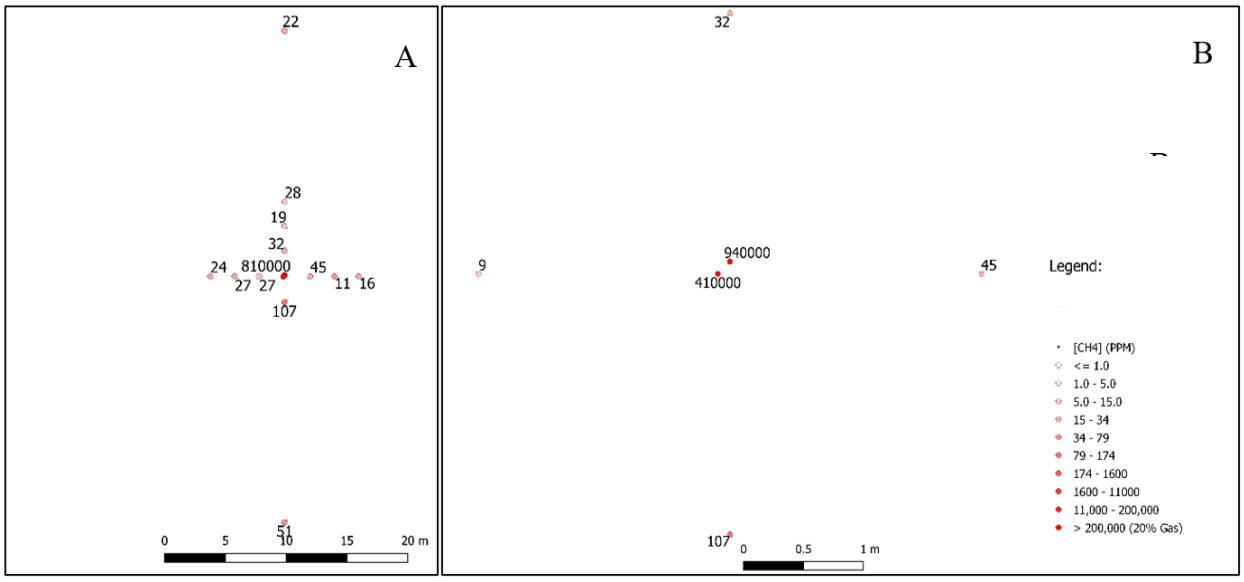

Figure C3 2018-11-21 30 cm depth methane gas concentrations as ppm CH_4 above background levels centered on the wellhead. A) shows full-site measurements, B) shows close-up on well center

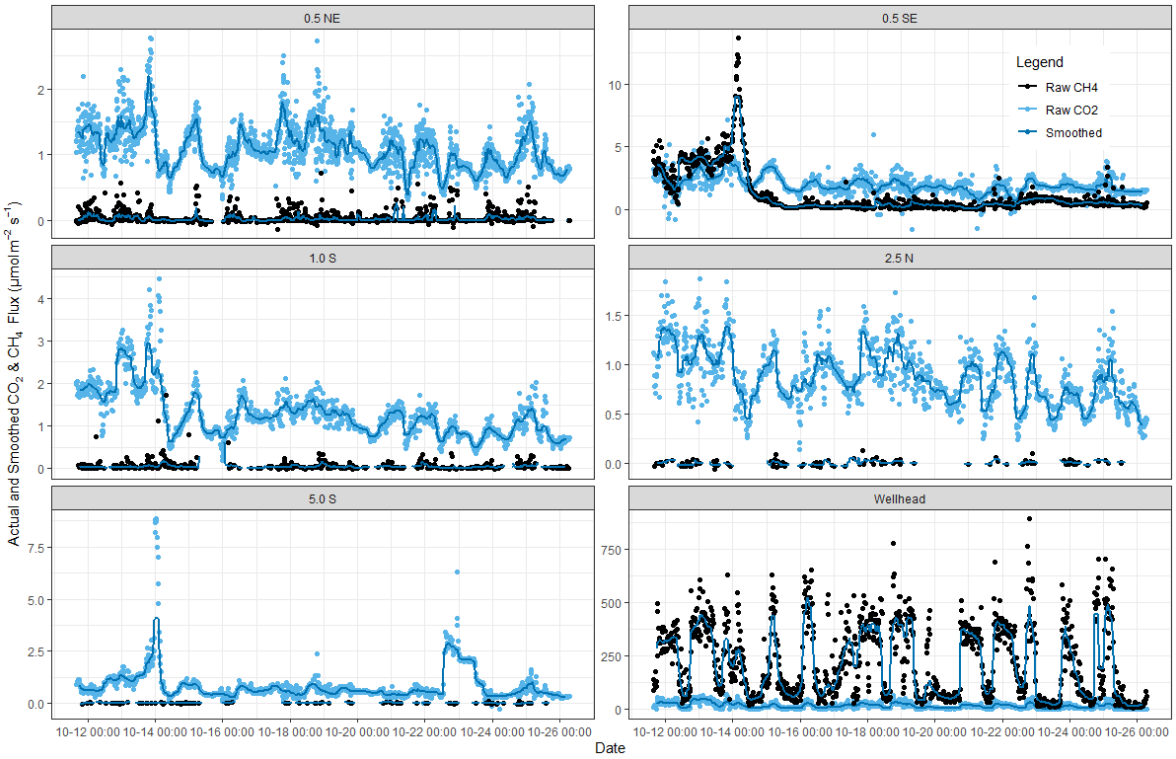

Figure C4 Two-week time series records showing all detectable linear calculated CO_2 and CH_4 effluxes in µmol m^{-2} s^{-1} at six locations. Raw efflux values presented with 20-point (~ 6 hour) moving median smoothing line for clarity in temporal variation.

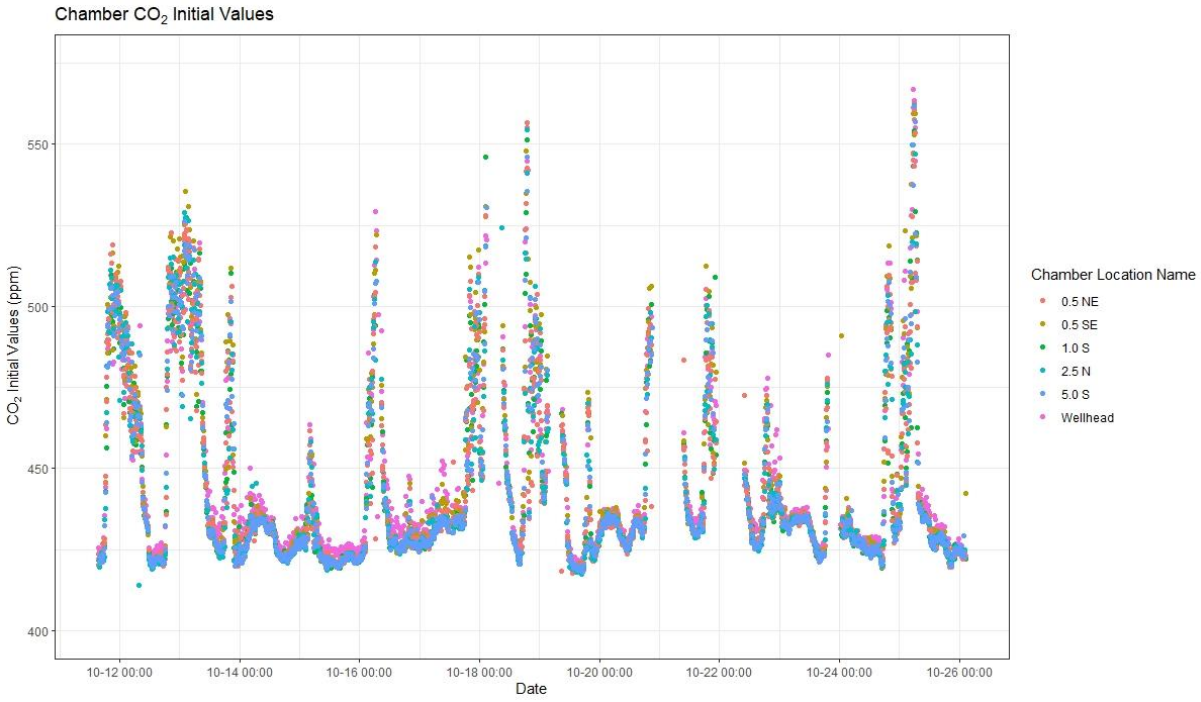

Figure C.5 Initial chamber CO_2 concentrations in ppm for all six long term chambers over the long-term measurement period, showing quasi-diel variation between 420 and > 500 ppm and similarity in measured concentrations for all locations.

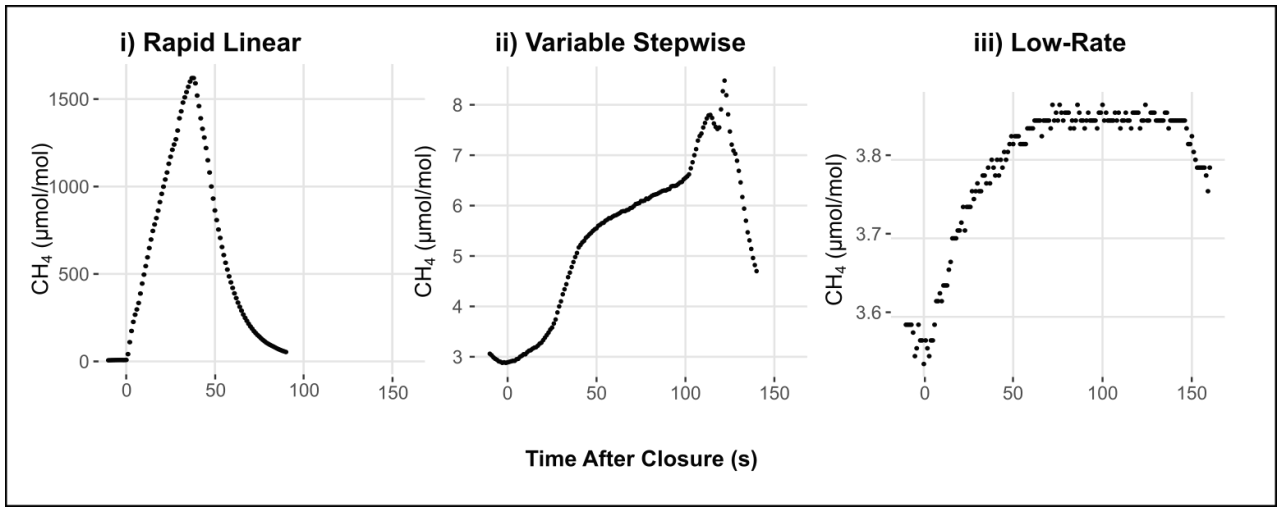

Figure C.6 Representative typologies of methane concentration time series used to calculate efflux, shown as time after the beginning of chamber closure against the measured CH_4 concentration with the greenhouse gas analyzer (note different Y scales). i) Rapid linear increase (Wellhead), ii) Stepwise (0.5 NE), and iii) Low-rate exponential increase (5.0 m S).

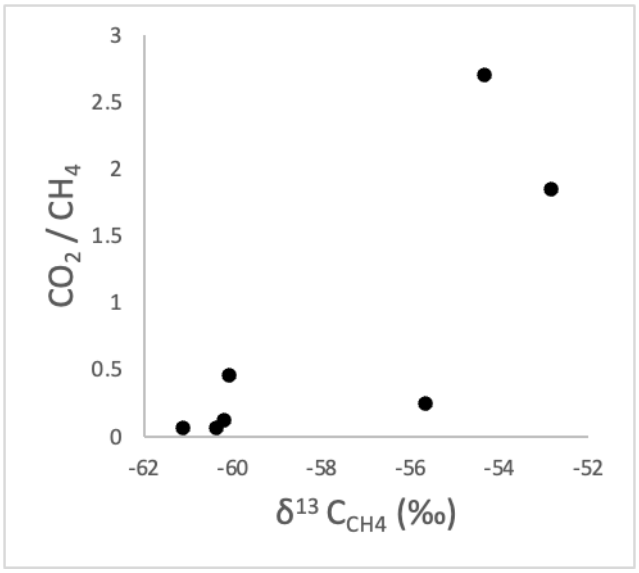

Figure C.7 $\delta^{13}C_{CH4}$ (‰) with respect to the ratio of CO_2/CH_4 for all analysed isotope samples, showing higher values of $\delta^{13}C_{CH4}$ (‰) with greater proportion of CO_2 to CH_4 in the gas samples.

Table C.2 Soil gas and dissolved gas analyses showing distance from wellhead in E-W (X), N-S (Y) and depth from ground surface (Z) in meters, for gas samples collected from soil vapour wells and water samples collected from within shallow groundwater monitoring wells.

X	Y	Z	Sample Date (YY-MM-DD)	Ar	O_2	N_2	CO_2	C1	C2	C3	>C3 *	Total	$\delta\,^{13}C_{CH4}$	$\delta\,^{13}C_{CO2}$	$\delta\,^{2}H_{CH4}$	$\delta\,^{13}C_{C2}$
Samples collected from soil vapour wells																
0.0	0.1	0.3	18-11-21	0.11	0.99	10.90	0.213	85.913	0.331	0.030	0.010	98.5	-60.4	-	-251.8	-
0.0	2.0	0.3	18-11-21	0.89	17.33	78.44	1.404	0.635	0.002	0.000	0.000	98.7	-62.3	-	-213.5	-
0.0	0.1	0.45	19-08-22	0.78	14.39	68.03	1.794	14.790	0.054	0.006	0.002	99.8	-60.2	-63.0	-	-
0.1	0.0	0.1	19-08-22	0.79	18.12	73.70	1.237	5.064	0.020	0.002	0.001	98.9	-55.7	-64.2	-	-
0.5	0.0	0.3	19-08-22	0.36	2.50	28.58	4.350	65.586	0.249	0.023	0.007	101.7	-61.1	-42.2	-	-45.3
0.5	0.0	0.1	19-08-22	0.88	20.13	77.66	0.626	0.340	0.001	0.000	0.000	99.6	-52.8	-54.5	-	-
0.2	0.2	1	19-08-22	0.88	20.25	77.16	0.561	0.208	0.001	0.000	0.000	99.1	-54.3	-53.4	-	-
0.5	0.0	0.3	19-08-23	0.33	1.35	25.14	4.283	70.263	0.270	0.025	0.008	101.7	-60.4	-42.7	-	-44.8
-0.1	0.0	0.5	19-08-23	0.79	20.11	77.09	0.187	0.407	0.002	0.000	0.000	98.6	-60.1	-47.6	-	-
Dissolved concentrations from samples collected from within wellhead chamber																
0.0	-1.3	1	19-08-21	1.15	13.16	63.97	13.983	5.917	0.011	0.001	0.001	98.2	-59.9	-36.5	-	-
1.3	0.0	1	19-08-21	1.13	16.92	73.30	0.274	6.558	0.023	0.001	0.001	98.2	-61.1	-	-	-
0.0	-1.3	1	19-08-23	1.38	13.91	64.67	11.475	7.033	0.014	0.002	0.011	98.5	-59.3	-35.5	-	-
1.3	0.0	1	19-08-23	1.41	11.96	68.07	0.151	16.294	0.065	0.006	0.002	98.0	-62.3	-	-	-
0.0	-0.5	1	19-08-21	1.02	13.65	61.37	0.393	21.529	0.092	0.006	0.001	98.1	-63.7	-	-	-
0.0	-6.0	1	19-08-21	1.76	11.11	75.11	7.521	2.832	0.018	0.001	0.000	98.3	-57.3	-29.3	-	-

*iC4 + nC4 + neopentane +nC5 +iC5. Precision and accuracy of $\delta^{13}C = \pm 0.5$ ‰ and $\delta^{2}H = \pm 2$ ‰

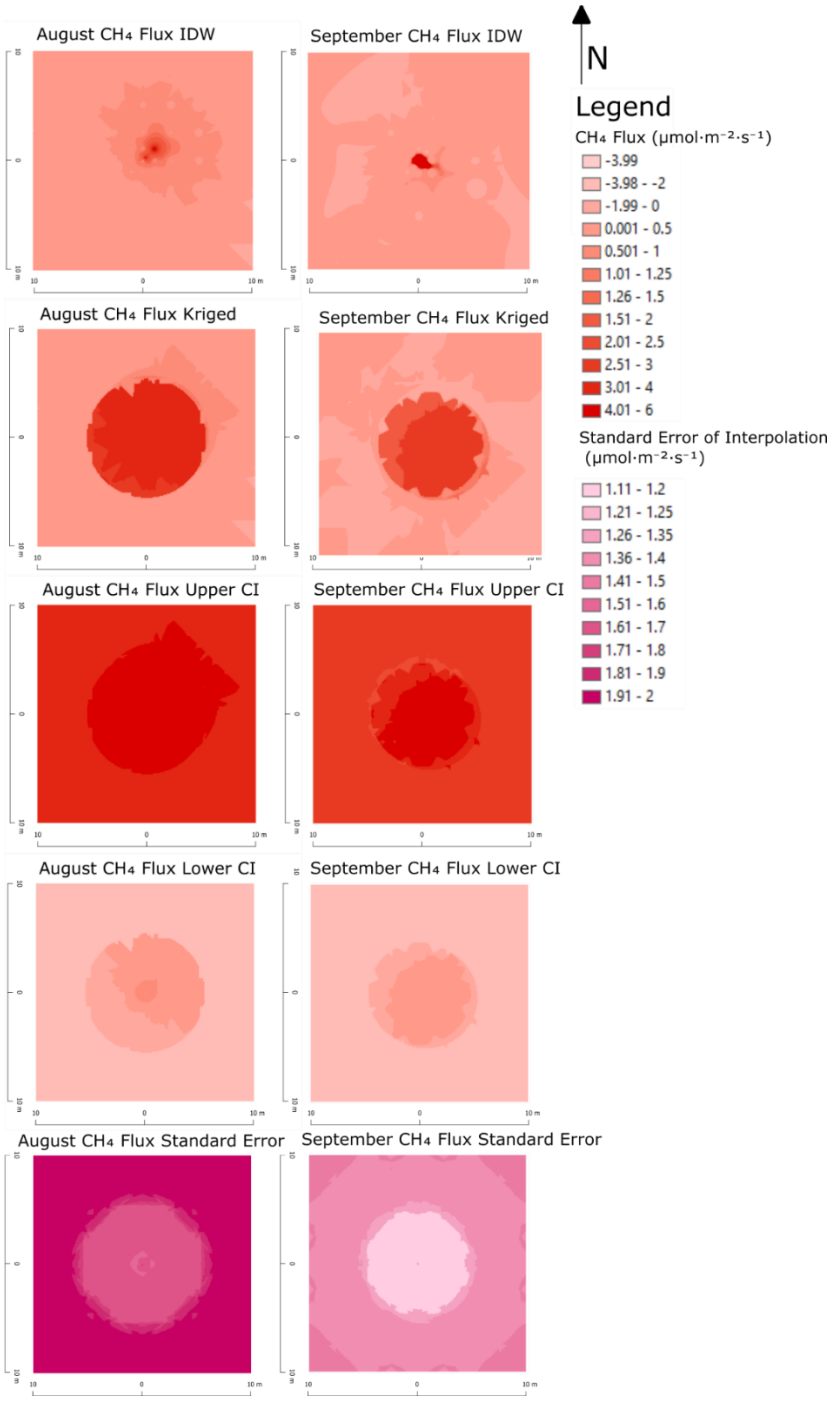

Figure C.8 Spatial interpolation summary plots over the area of the dense well pad measurement grid (20 m X 20 m centered on the energy well).

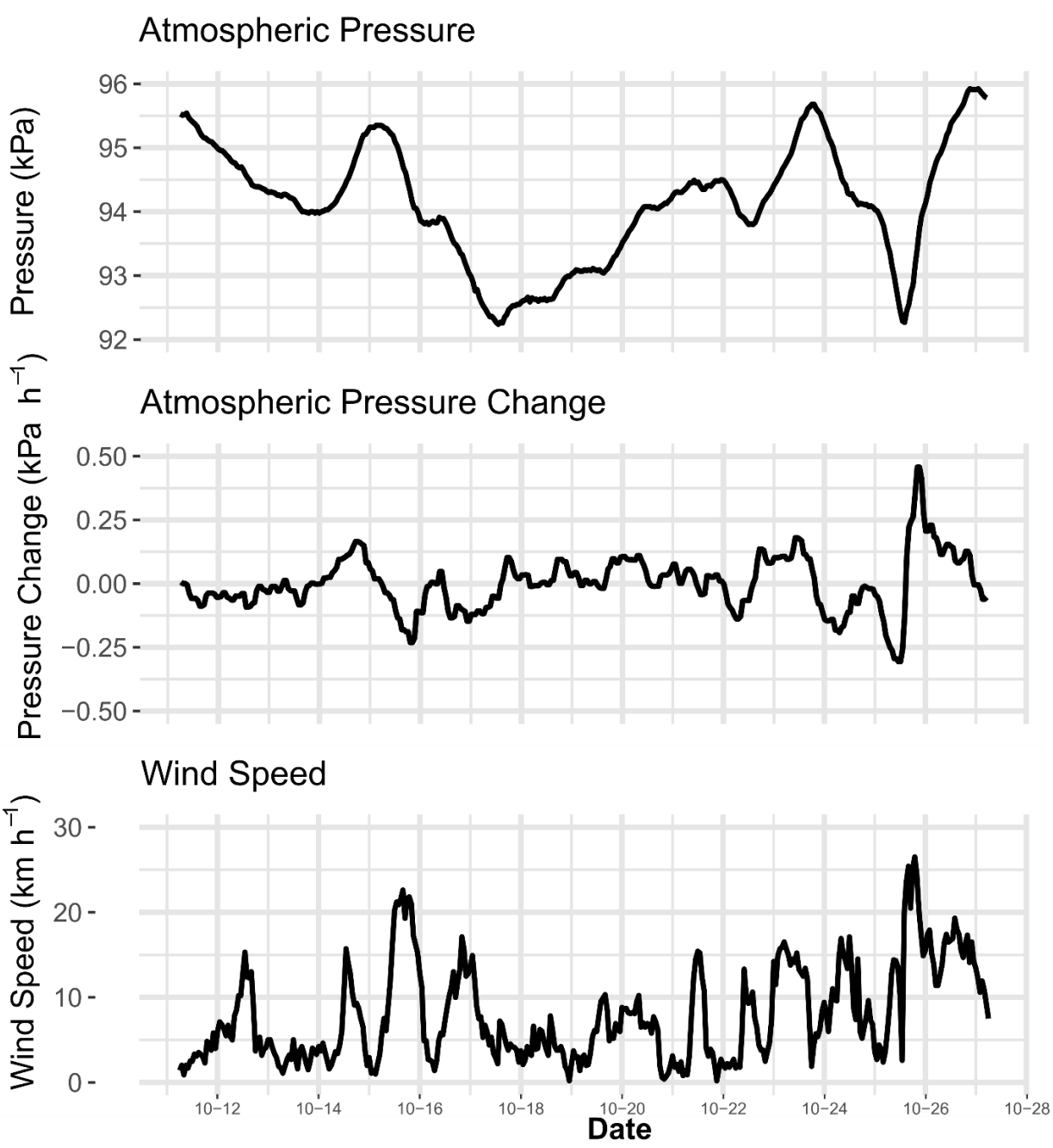

Figure C.9.a Time series records of explanatory environmental factors considered in the stepwise general additive regression model

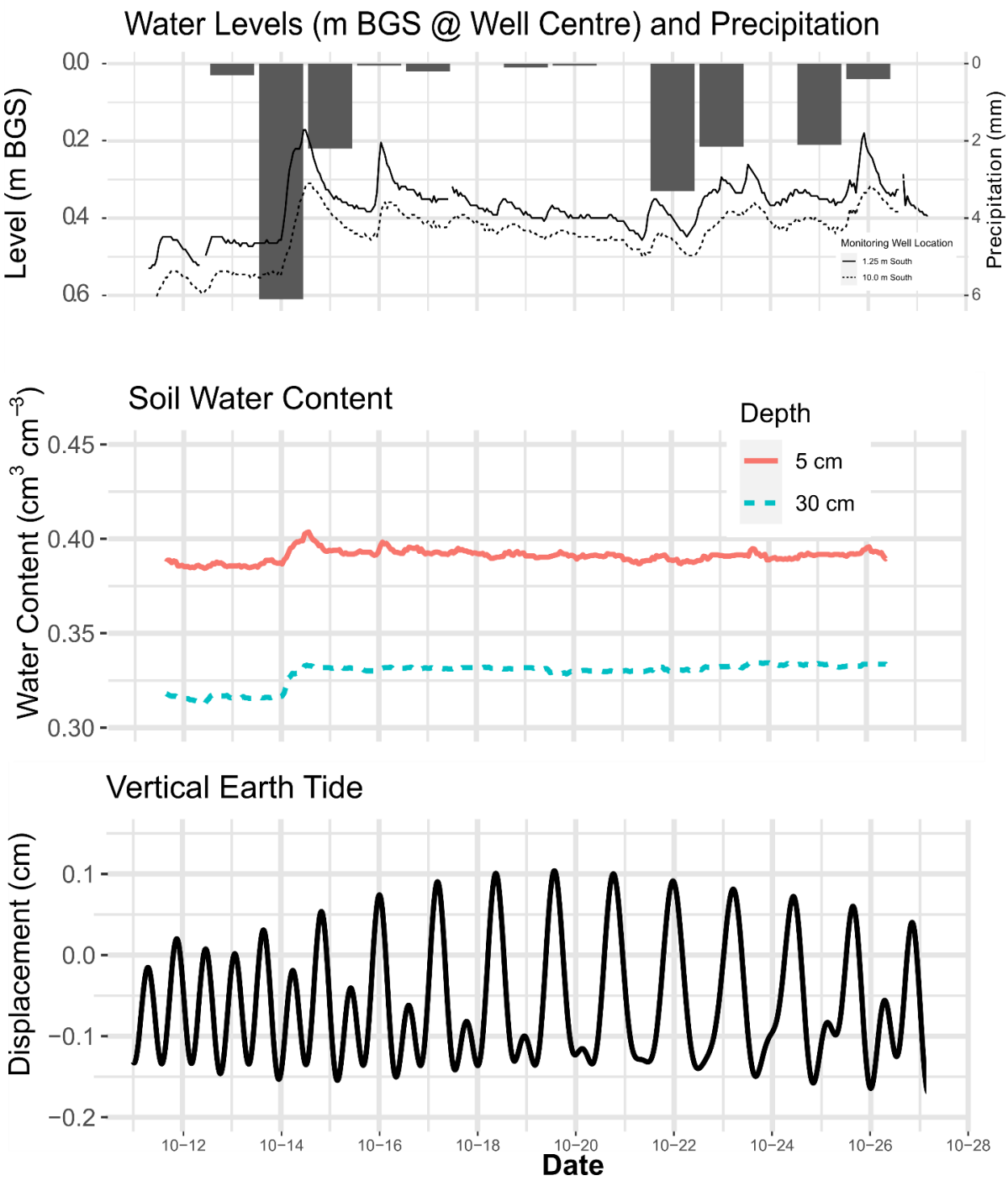

Figure C.9.b Time series records of explanatory environmental factors considered in the stepwise general additive regression model

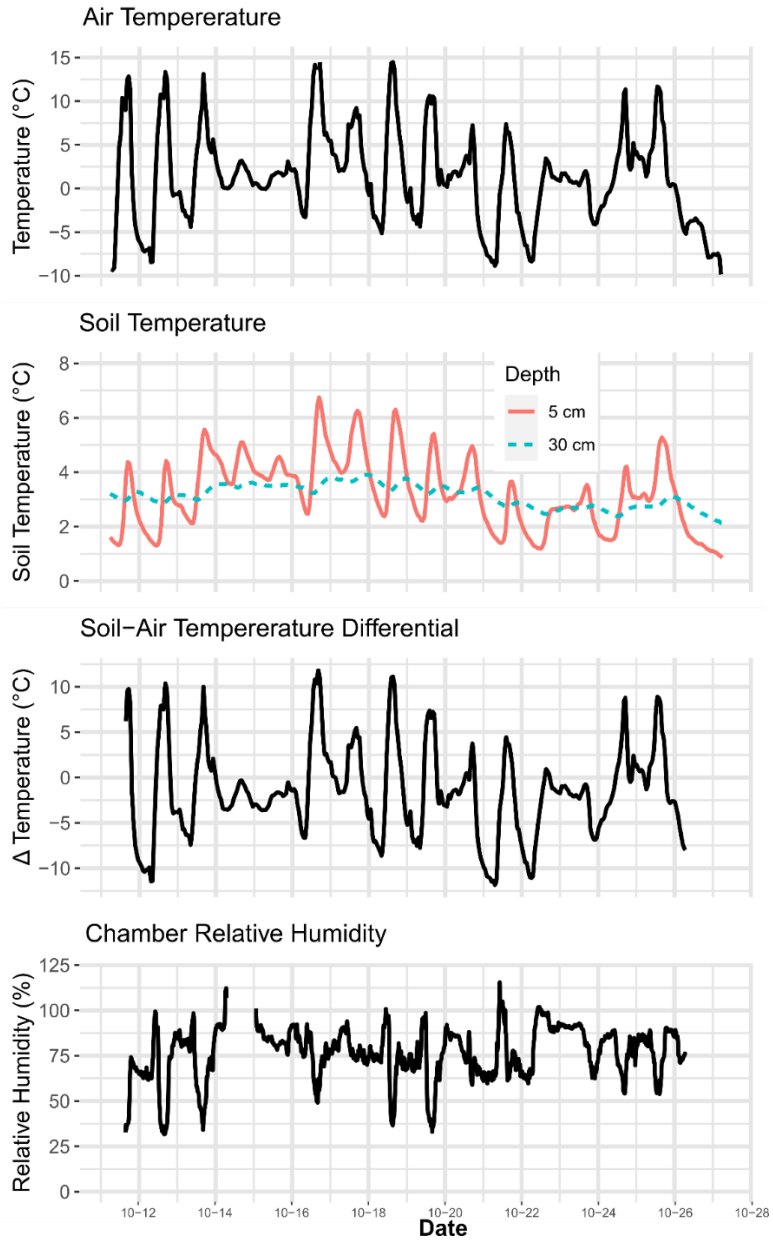

Figure C.9.c Time series records of explanatory environmental factors considered in the stepwise general additive regression model

Table C.3 Summary of stepwise generalized additive modeling of raw CH_4 efflux for each long-term chamber location. ΔR^2 indicates the decrease in full model R^2 fit to raw flux data through removal of each factor. Blank parameters were not included in the full model, at significance of 0.001. Model parameters were Relative Humidity (RH), Absolute barometric pressure (Baro_P), atmospheric temperature (T_atm), approximate barometric pressure change rate (Baro_dP_dt), piezometer water level (Wat.Lev.), approximate change in water level (dWat.Lev_dt), soil temperature at 0.05 m (T_soil_0.05 m) and 0.3 m (T_soil_0.3) below ground surface (BGS), soil water content at 0.05 m (Wat.Cont_0.05) and 0.3 m (WC 0.3) BGS, temperature difference between the atmosphere and 0.3 m soil depth, vertical Earth tide displacement (E_tide), and wind speed (U_wind).

	Wellhead Chamber	**0.5 SE**	**0.5 NE**	**1.0 S**	**2.5 N**	**5.0 S**
	Full Model Fit R^2					
	0.63	0.86	0.15	0.11	0.19	0.19
	Single variable backward removal ΔR^2					
RH	0.02	0.01	0.01			
Baro_P	0.01					
T_atm	0.12		0.04			
Baro_dP_dt	0.02				0.08	
Wat.Lev.		0.01		0.01	0.00	
dWat.Lev.dt	0.01	0.09	0.02	0.02		
T_soil_0.05	0.01					0.04
T_soil_0.3	0.05	0.02	0.02	0.00		
Wat.Cont_0.05	0.01	0.01				
Wat.Cont_0.3	0.02	0.20	0.01		0.03	
Temp_Diff					0.00	0.12
E_tide	0.01		0.01	0.01		
U_wind	0.11	0.01	0.03	0.05		

Table C.4 Parameters most influencing the statistical model for the first three steps of forward stepwise multivariate generalized additive modelling of CH_4 Efflux at each long-term chamber location. Model formulae are in the form: FCH4 ~ $Parameter_1$ + $Parameter_2$ …. The Akaike information criterion (AIC) is listed at each step as an indication of incremental goodness of fit. Factor abbreviations are: U_wind (windspeed), Temp_Diff (temperature differential between 30 cm depth soil and the atmosphere); Wat.Cont_0.3 (30 cm depth soil water content), T_soil_0.05 (soil temperature at 5 cm depth), Baro_dP_dt (approximated barometric pressure change rate), T_atm (atmospheric temperature), Wat.Lev (piezometer water level), dWat.Lev.dt (approximate water level change rate)

Chamber	Step:1	Step:2	Step:3
Wellhead	U_wind ;	T_atm + U_wind ;	T_atm + s(U_wind, df = 2) ;
	15378	15248	15176
0.5 SE	Wat.Cont_0.3 ;	Wat.Lev + Wat.Cont_0.3 ;	Wat.Lev. + s(Wat.Cont_0.3, df = 2) ;
	3876	3575	3423
0.5 NE	T_atm ;	T_atm + U_wind ;	T_atm + dWat.Lev.dt + U_wind ;
	-2339	-2368	-2385
1.0 S	U_wind ;	WL + U_wind ;	Wat.Lev. + dWat.Lev.dt + U_wind ;
	-673	-687	-695
2.5 N	Temp_Diff ;	Baro_dP_dt + Temp_Diff ;	s(Baro_dP_dt, df = 2) + Temp_Diff ;
	-587	-591	-594
5.0 S	Temp_Diff ;	s(Temp_Diff, df = 2) ;	T_0.05 + s(Temp_Diff df = 2) ;
	-462	-465	-468

df refers to the degrees of freedom of the smooth fitting function (1 if not indicated)

Table C.5 Summary of stepwise generalized additive modeling of raw CH_4 pre-closure concentrations for each long-term chamber location. ΔR^2 indicates the decrease in full model R^2 fit to raw flux data through removal of each factor. Blank parameters were not included in the full model, at significance of 0.001. Model parameters were Relative Humidity (RH), Absolute barometric pressure (Baro_P), atmospheric temperature (T_atm), approximate barometric pressure change rate (Baro_dP_dt), piezometer water level (Wat.Lev.), approximate change in water level (dWat.Lev_dt), soil temperature at 0.05 m (T_soil_0.05 m) and 0.3 m (T_soil_0.3) below ground surface (BGS), soil water content at 0.05 m (Wat.Cont_0.05) and 0.3 m (WC 0.3) BGS, temperature difference between the atmosphere and 0.3 m soil depth, vertical Earth tide displacement (E_tide), and wind speed (U_wind).

	Wellhead Chamber	**0.5 SE**	**0.5 NE**	**1.0 S**	**2.5 N**	**5.0 S**
	Full Model Fit R^2					
	0.52	0.37	0.21	0.22	0.33	0.58
	Single variable backward removal ΔR^2					
RH	0.01	0.04	0.01			0.01
Baro_P	0.05	0.01		0.02	0.01	0.08
T_atm	0.03	0.01	0.00	0.02	0.02	0.06
Baro_dP_dt	0.05	0.05	0.02	0.01	0.03	0.03
Wat.Lev.	0.01	0.03	0.00			0.01
dWat.Lev.dt	0.03	0.03	0.02			
T_soil_0.05	0.01	0.08	0.01	0.01	0.01	0.01
T_soil_0.3	0.08		0.00			0.03
Wat.Cont_0.05	0.01		0.00	0.02		0.00
Wat.Cont_0.3		0.00	0.01	0.01	0.03	
Temp_Diff		0.01		0.02		
E_tide				0.00		0.01
U_wind	0.09	0.02	0.05	0.04	0.05	0.04

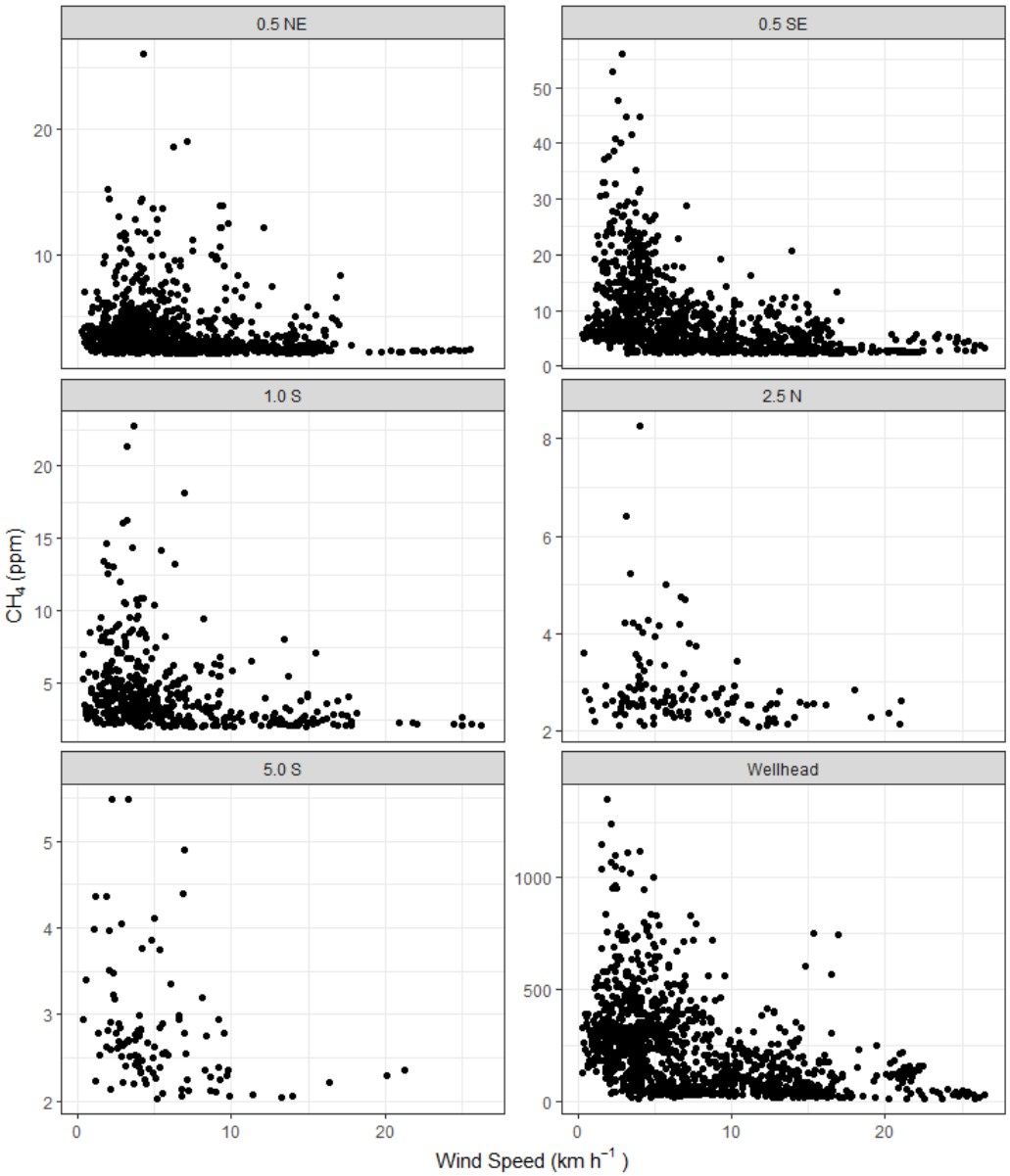

Figure C.10 Wind speed from the nearest weather station (km h^{-1}) with respect to initial CH_4 chamber concentrations in ppm for all detectable efflux measurements over the full two-week long-term measurement period, showing higher measured initial concentrations during periods of lower wind speed.

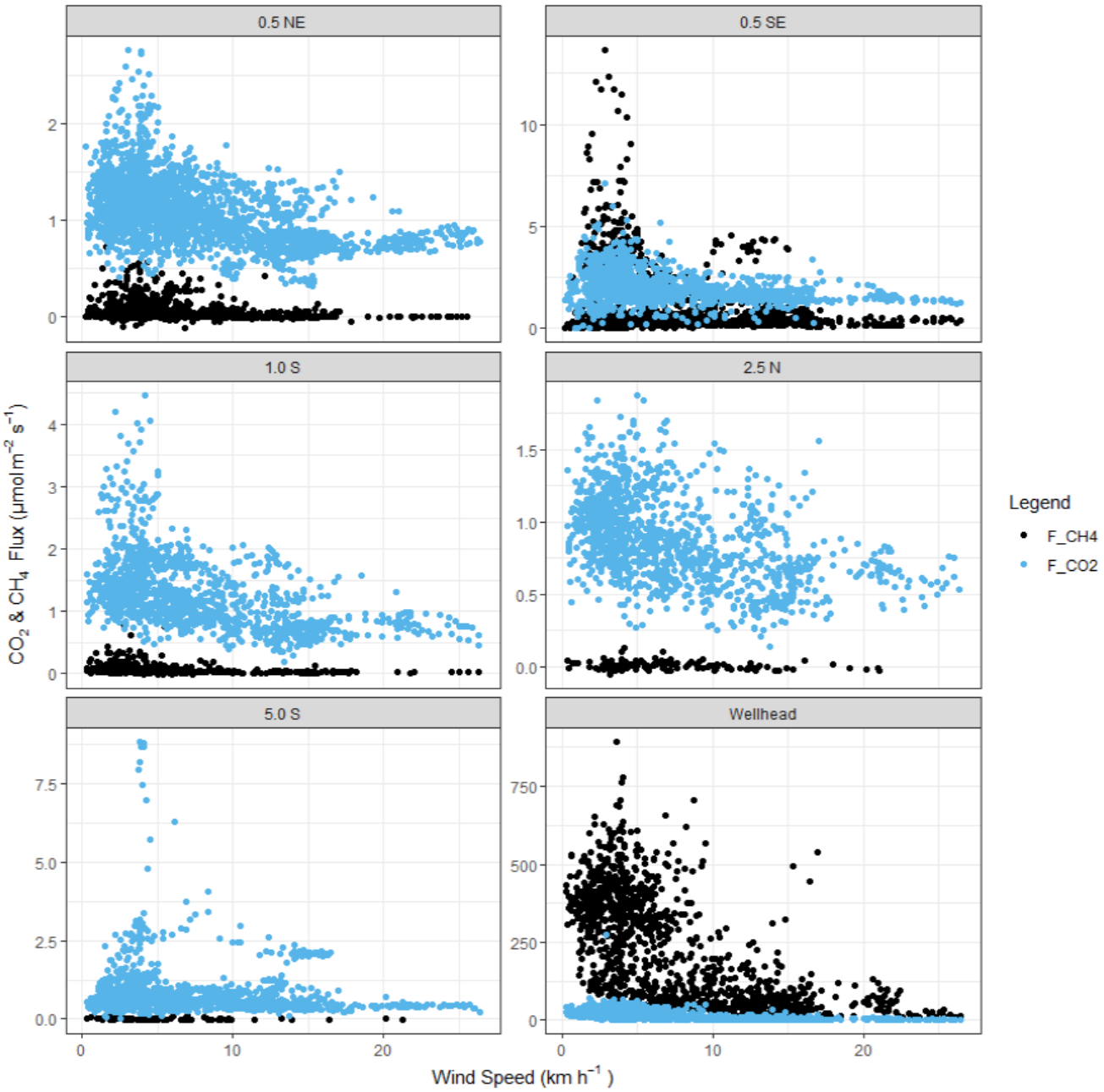

Figure C.11 All detectable linear CH_4 (black) and CO_2 (blue) effluxes in µmol m^{-2} s^{-1} over the full two-week long-term measurement period with respect to wind speed from the nearest weather station (km h^{-1}), showing higher measured effluxes during periods of lower wind speed.

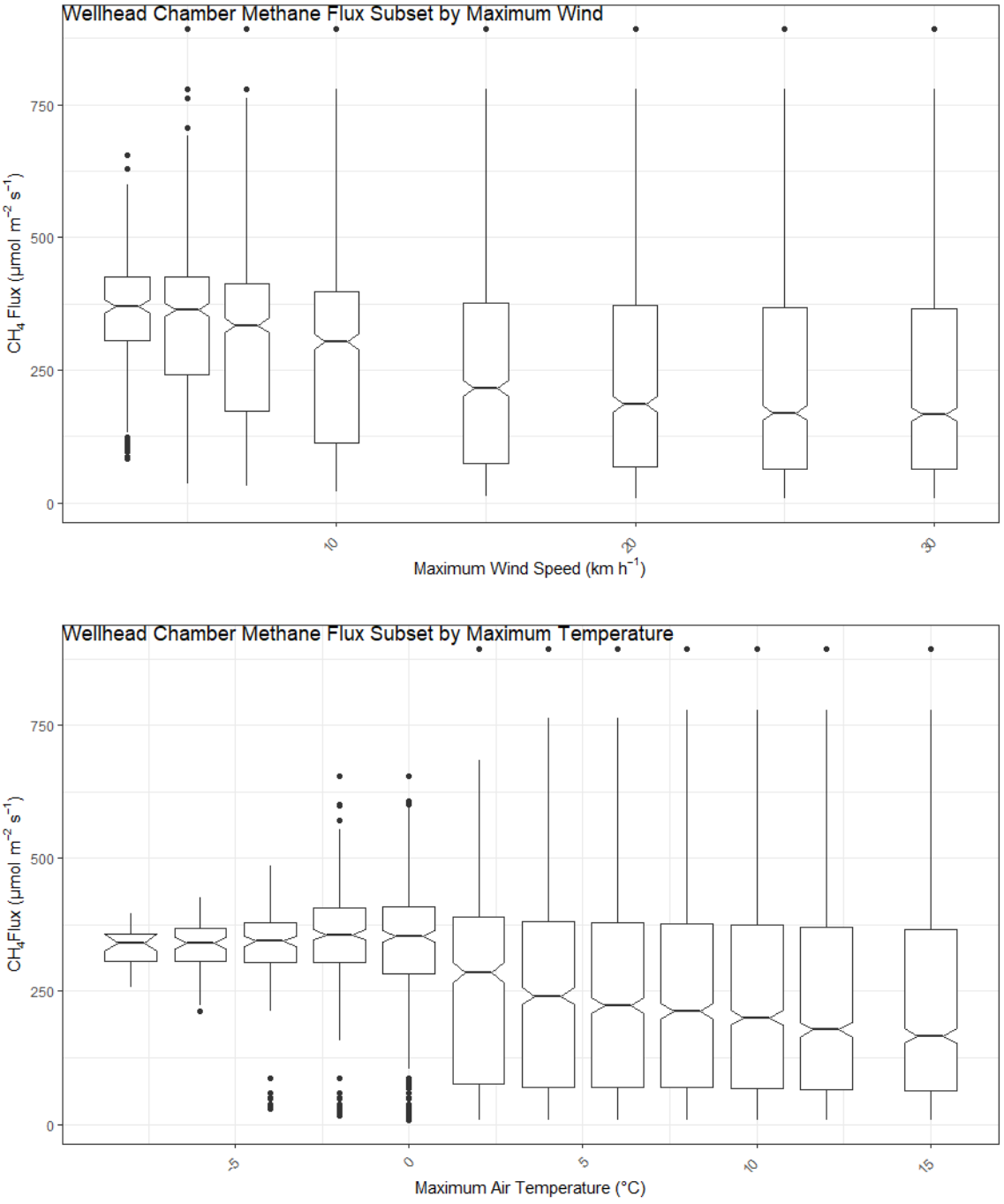

Figure C.12 Boxplots of wellhead chamber methane efflux in µmol m^{-2} s^{-1} subset by maximum wind speeds (top) and maximum temperature (bottom).

D **Supplementary information for Chapter 3:** Low-cost sensors provide insight into temporal variation in fugitive methane gas concentrations around an energy well

Appendix D.1 Sensor description and field installation

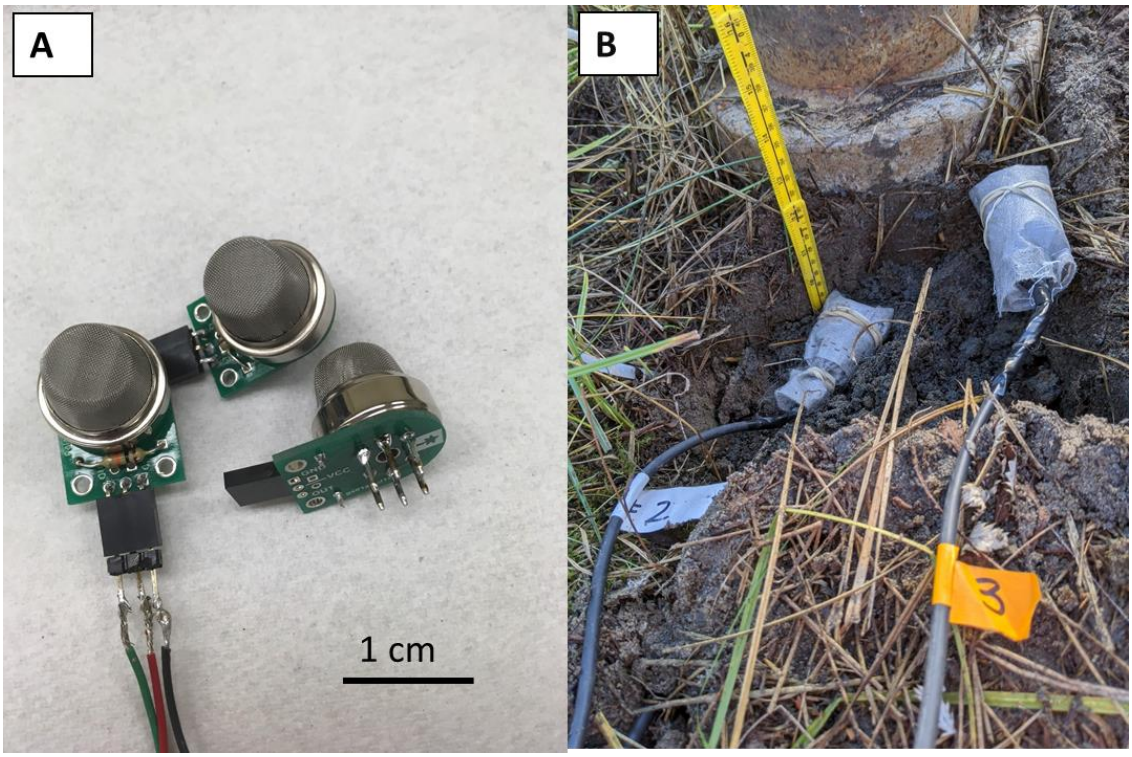

Figure D.1.1 A) Photograph of MQ-4 sensors wired to commercially available circuit board with 10 000 Ω resistor. B) Field-installation of sensors at the 5 cm and 0 cm depth next to outermost well casing. (Soil later backfilled to grade.)

Two nests of MQ4 chemoresistive gas sensors were installed near the well casing, with sensors at 0, 5, and 30 cm depths. The sensors within the nests were horizontally offset to limit vertical preferential gas flow, while maintaining a radial distance from the outermost well casing of approximately five centimeters. The sensor housings were centered on the described depth, such

that ‘0 cm depth’ sensor was partially buried at ground surface. Two additional control sensors were installed five meters west of the wellhead, both at 5 cm below ground surface with one sensor in native soil and one sensor enclosed within a plastic container (0.3 m diameter by 0.3 m depth) filled with moist sand to isolate the sensor from subsurface gases while allowing exchange with atmospheric gases and heat. The sensors were mounted on a commercially available circuit board with a three-wire output, then enclosed within a perforated plastic 40 mL bottle wrapped in geotextile to exclude sediment from direct contact with the sensor and installed in an orientation that would shield the sensors from downward water drainage (Figure D.1.1). A common external five-volt DC power supply ensured adequate current for the sensor heating loops, with estimated continuous per-sensor requirements of ≤900mW (Henan Hanwei Electronics Co. Ltd). The continuous power supply was provided by an overpowered on-site photovoltaic system with 6 X 300 W solar panels charging an 1800 Ah battery bank outputting steady 120V AC power through a 4000 W inverter, which then powered the 12 VDC and 5 VDC power adapters for the datalogger and heating loops, respectively. (Estimated total continuous system power demands for the 8 sensors was less than 30 W).

Single-ended analog circuit voltages (mV) were sampled from the sensor circuit every minute and recorded on a datalogger (CR1000, Campbell Scientific) over a period of 20 days. The first 24 hours of the data series was discarded, following the recommended ‘burn-in’ time for full heating of the sensor (Henan Hanwei Electronics Co. Ltd.; Honeycutt et al. 2019).

Appendix D.2 Sensor calibration

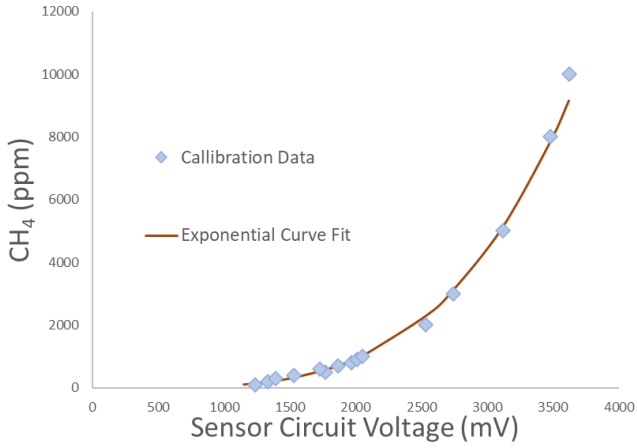

Figure D.2.1 Example exponential curve fit to calibration data for sensor #8.

While the manufacturer provides empirically derived formulae for converting the sensor output to a combustible gas concentration estimates, an independent calibration was preferred to fully account for the non-linear sensor-specific response to increasing voltages across the wide range of encountered methane gas concentrations (Henan Hanwei Electronics Co. Ltd.; Riddick et al. 2020). Sensors were lab calibrated to determine the non-linear response between sensor circuit voltage and methane concentrations (Fig. D.2.1). Calibration procedure involved injecting progressively greater volumes of pure CH_4 gas into an enclosed vessel containing all 8 sensors and registering the sensor response at each step. The vessel was vented between injections, allowing the sensors to stabilize to background values. The sensor circuit response was manually averaged at stable values to exclude the sensor overshoot peak (Honeycutt et al. 2019). These data of sensor circuit voltage and CH_4 concentration (obtained through calculation of injected gas volume in comparison to the vessel volume) were fitted to an exponential-type curve by varying the parameters c, E, and b to optimize the least sum of squared deviations using MS

Excel's 'Solver' function, yielding a calibration curve specific to each sensor (Eq. C.2.1; Table D.2.1).

$$[CH_4]_{pppm.estimated} = c * E^{Raw.Voltage*b} + k \quad \text{..... (C.2.1)}$$

The exponential curves were then adjusted with a constant k value so it output 2 ppm CH_4 as the free-air background concentration for the mean sensor circuit voltage obtained in the field at the end of the measurement period when all sensors were placed exposed to fresh air 50 m upwind from the well. While the sensors response is known to vary slightly depending on relative humidity and temperature, no corrections were made for these parameters (Honeycutt et al. 2014). Previous field measurements by other authors have shown a good agreement between MQ4 measurements and concentrations measured from gas samples analyzed with gas chromatography (Riddick et al. 2020). This gives greater confidence in the capability of the MQ4 sensor to distinguish between the responses closer to the well compared to the lower concentrations further away. No gas sampling or additional concentration measurements were performed during this field experiment. While this did avoid perturbing in-soil gas movement, it was not possible to validate the MQ4 sensor concentrations against another measured value.

Sensor	1	2	3	4	5	6	7	8
Coeff c	0.022	0.776	0.260	0.186	0.421	0.140	25.933	43.956
Coeff b	0.0026	0.0021	0.0026	0.0027	0.0026	0.0027	0.0020	0.0015
Exponent	3.1437	2.9540	2.5257	2.7066	2.4722	2.5604	2.2504	2.6591
Constant (k)	1.7	-4.1	0.2	-219.0	-1.3	0.5	-86.6	-188.3
R^2	0.970	0.971	0.993	0.951	0.989	0.992	0.998	0.994
Field Installation Location (Distance from Well, Depth in Soil Below Ground Surface)	30 cm, West	5 cm, West	0 cm, West	5 m West, 5 cm Native Soil	5 m West, 5 cm Isolated Sand	30 cm, East	5 cm, East	0 cm, East

Table D.2.6 Calibration curve parameters and description of sensor field installation location as depth below ground surface and side of well casing

Appendix D.3 Baseline noise and sensor response tests

Since all sensors were using a common external five-volt source for the sensing and heating loop, independent sensor response was verified by individually subjecting each sensor to a high concentration of combustible gas and ensuring that the voltage output of other sensors were not affected (Figure D.3.1).

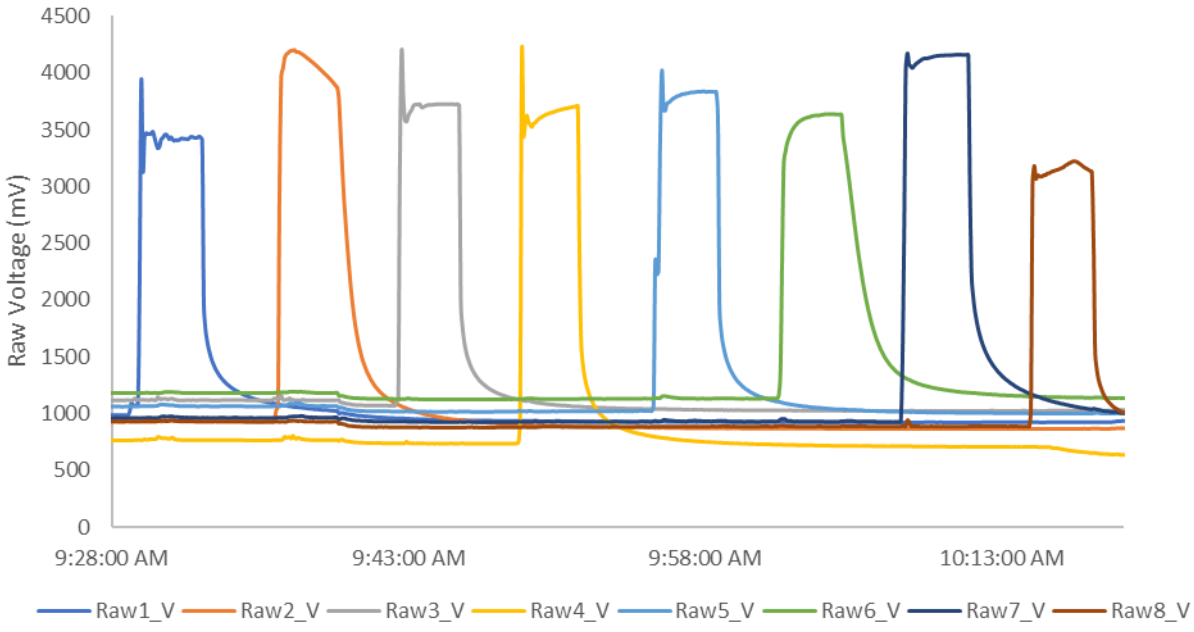

Figure D.3.1—Independent sensor response showing unchanged sensor circuit voltages on other sensors while individually subjecting sensors to elevated methane gas concentrations

A baseline noise test then sought to determine the expected degree of variation in sensor response that might be expected during normal operation in atmospheric air (after Honeycutt et al. 2014). The sensors measured atmospheric concentration responses in an open laboratory setting every 15 seconds for several days, after which the sensing voltage was converted to ppm CH_4 using the field-adjusted calibration parameters (Table D.3.1). Variance is displayed graphically and represented through the coefficient of variation, CV

$$CV = \frac{\sigma}{\mu}$$

Where σ is the standard deviation of measurement, and μ is the mean calibrated sensor response in ppm CH_4.

Table D.3.1 Coefficient of variation (normalised standard deviation of measurement) in % for lab baseline noise tests and field data, demonstrating the variability in measured values as ppm CH_4. Field locations correspond to the direction on the side of the well casing as West (W) or

East (E) and depth in-soil (30 cm, 5 cm, or 0 cm). The “5 (isolated)” sensor was 5 m east of the well at 5 cm depth and isolated from soil gases.

Coefficient of Variation

Sensor #	Field Location	Field Depth	Lab		Field		
			Full Period	Shaded Stable Period	Full Series	Mean of all 12 h periods	Mean of all 1 h periods
		-- cm --	---------- % ----------				
1	West along casing	30	2.0	0.6	113.3	49.9	11.0
2		5	10.4	3.7	169.4	73.7	47.2
3		0	7.7	2.0	148.7	89.7	52.1
6	East along casing	30	8.8	1.3	57.1	15.8	5.9
7		5	12.4	4.3	71.5	12.9	5.1
8		0	79.1	88.6	97.7	31.4	9.4
4	5 m Distal	5 (baseline)	0.1	0.0	77.2	4.8	1.0
5		5 (isolated)	8.9	1.8	20.5	4.0	3.7

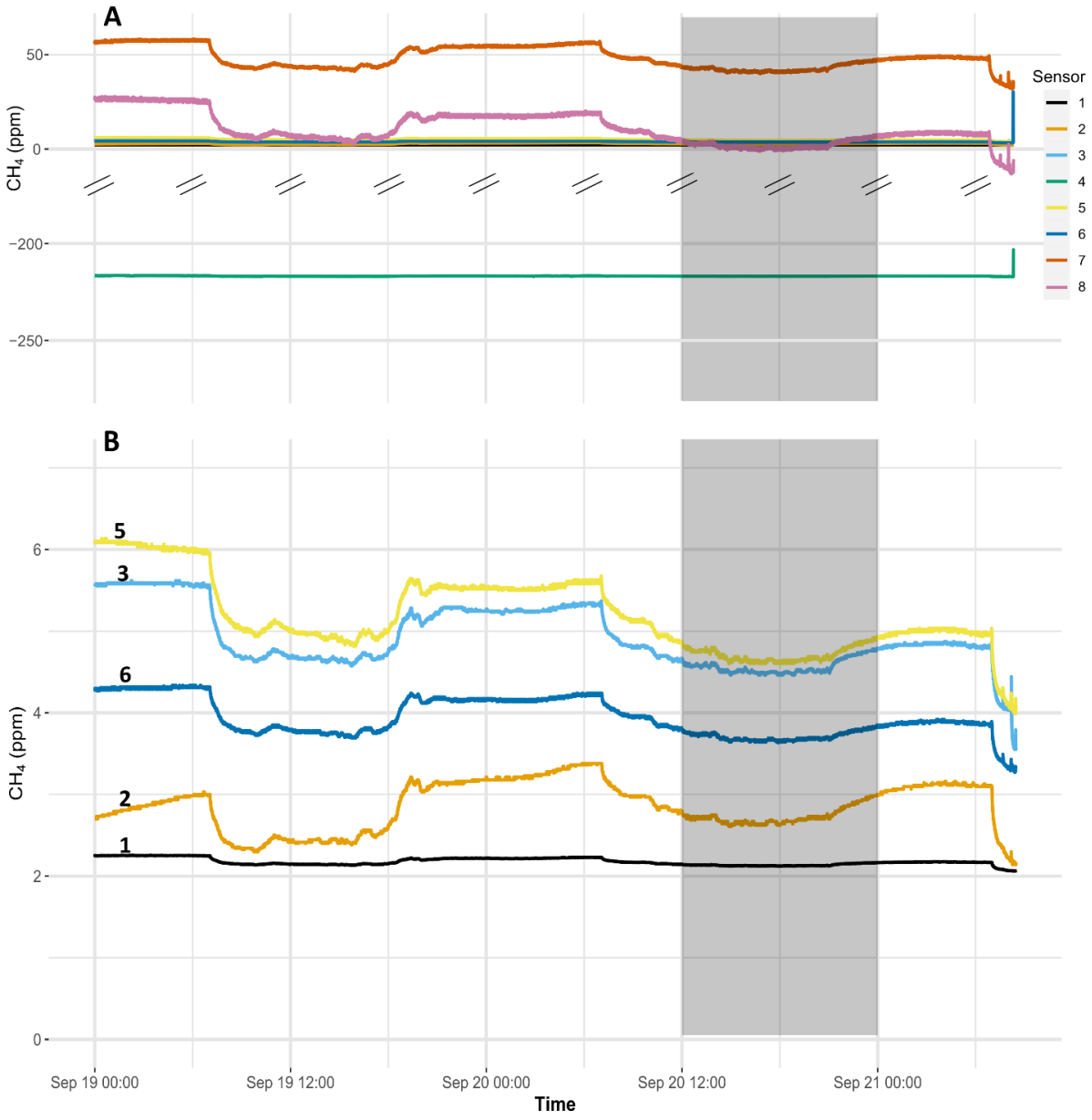

Figure D.3.2 Lab baseline noise test showing sensor response as calibrated ppm CH_4 for 15 second frequency measurements over > two days. A) shows all sensors (note Y scale break at 0 ppm), while B) shows a close-up of 5 selected sensors, with concentrations close to expected atmospheric values, labelled by sensor number. Shaded region corresponds to a 12-hour selected 'Shaded Stable Period' shown in Table D.3.1.

Appendix D.4 Supplementary field data and discussion

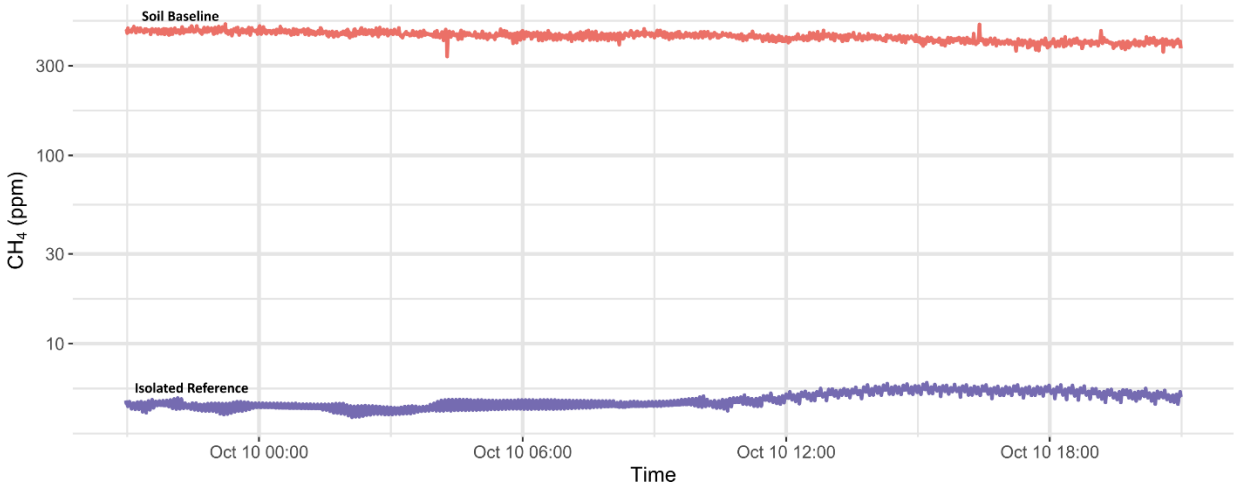

Figure D.4.1 Time series one-minute frequency combustible soil gas concentrations (log ppm CH_4) over 48 hours at 0.05 m depth and 5 m East of the energy well casing. The 'Soil Baseline' sensor is installed in native soil, while the 'Isolated Reference' sensor is excluded from site soil gases.

The 'Isolated Reference' sensor still displays some moderate variability, both on a pronounced daily cycle (Figure 3.5) and as short-term variation (Figure D.4.1). It is expected that all sensors will exhibit some amount of noise and varying sensor response due to changing sensor temperatures and relative humidity. Ideal sensing relative humidity below 65% may have been exceeded in the soil (Henan Hanwei Electronics Co. Ltd.) A lack of gas samples or additional field measurements precluded direct verification of the MQ4 CH_4 concentrations in field temperature and humidity conditions, and there may have been small changes impacting the accuracy of the (laboratory derived) calibration curves in the field conditions. However, the short-term and daily variations for the distal sensors were relatively minor (e.g., resulting in calibrated sensor responses ranging between 0-10 ppm for the 'Isolated Reference' sensor), despite changing weather conditions and temperatures ranging over 30 °C. There was a much larger range in sensor response for the sensors adjacent to the well casing, despite exposure to

similar variations in temperature and humidity. Therefore, the relatively small variation in the two distal sensors, and especially for the 'Isolated Reference', indicates that a large variation in sensor response in the nests around the well casing is best explained by changing soil gas concentrations as opposed to other gas-concentration independent factors such as temperature, humidity, or sensor noise.

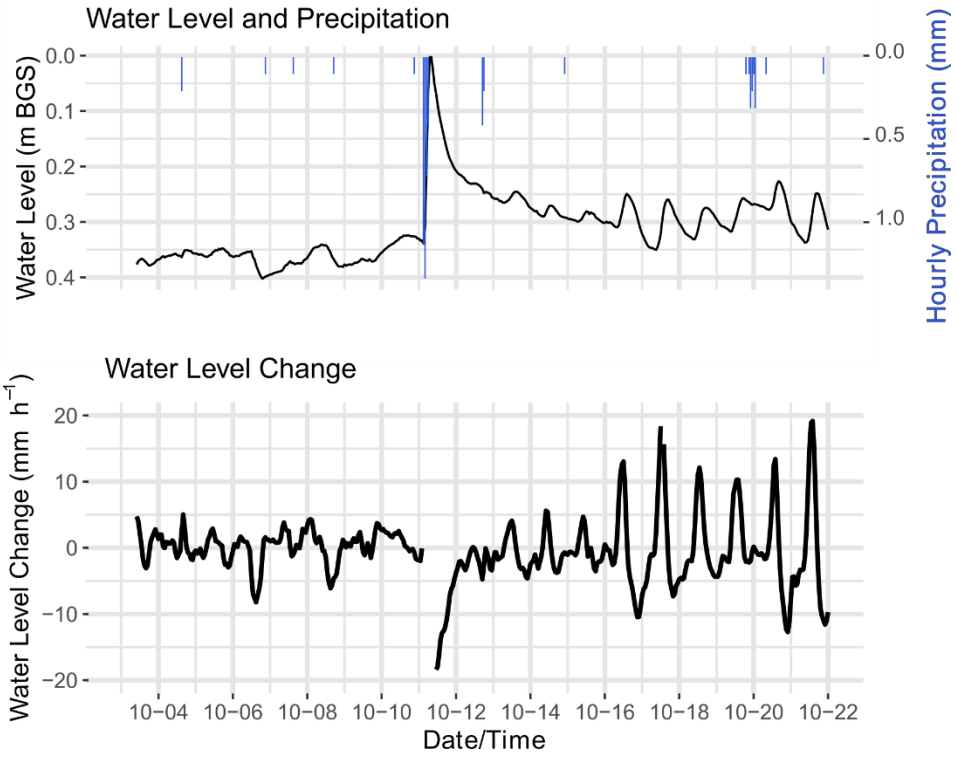

Figure D.4.2—Measured site water level in a piezometer 1.25 m south of well-centre and 1.0 m below ground surface (BGS), and precipitation at the nearest weather station. Water level change rate excludes a large change occurring at the time of the cumulative 3.5 mm precipitation event on Oct. 11, 2020.

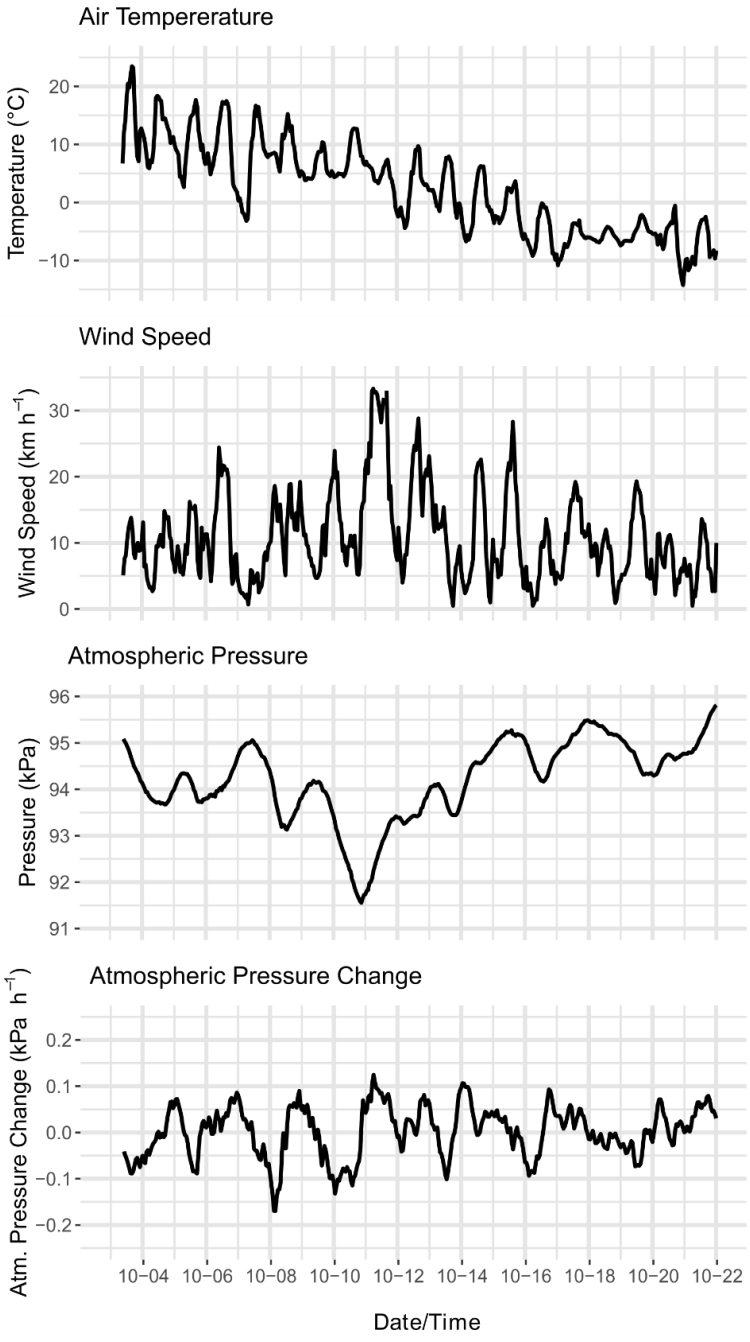

Figure D.4.3—Meteorological factors considered in regression analysis with measured soil gas concentrations.

E Supplementary field site characterization data

The unpublished data in this section is provided for reference to future characterisation efforts of the gas migration case-study site presented in Chapters 3 and 4.

Appendix E.1 Hydraulic Conductivities

Table E.1 Hydraulic conductivity values estimated from slug test data results for piezometers installed on the gas migration field research project case study site.

Piezometer Location	Screen Centre Depth	Test Date/Time	Hvorslov Solution K	Bauwer-Rice Solution K
	m		$m\ s^{-1}$	$m\ s^{-1}$
30 m E	2	10 July 2019	4.8×10^{-6}	3.69×10^{-6}
6 m E	2	10 July 2019	1.36×10^{-6}	9.40×10^{-6}
#7 -1.25 S	1	14 November 2019, 09:16	3.95×10^{-6}	2.45×10^{-6}
#5- 1.25 W	1	14 November 2019, 10:48	3.98×10^{-6}	2.86×10^{-6}
#2 – 10 N	1	14 November 2019, 12:15	2.13×10^{-6}	1.35×10^{-6}
Arithmetic Mean			3.25×10^{-6}	3.95×10^{-6}

Table E.2 Lab permeameter horizontal hydraulic conductivity results on a minimum of 5 replicate lab measurements for soil core obtained at the specified location. Samples were obtained from soil pits using horizontal insertion of a metal 100mm length by 46.5 mm ID metal ring with minimal disturbance. All data are from constant head permeameter measurements, except in the case of the sample from 6 m East at the 0.05 m depth (*) which required use of the falling head method to observe the lower magnitude hydraulic conductivity.

Sample Location East of Well Centre (m)	Sample Depth (m)	Arithmetic Mean Hydraulic Conductivity (m/s)	Standard Deviation of Measurement (m/s)
6	0.3	3.04×10^{-5}	7.38×10^{-7}
6*	0.05	2.99×10^{-11}	$2.89 \times 10^{-}12$
2.5	0.3	1.29×10^{-5}	9.17×10^{-7}
2.5	0.05	1.65×10^{-4}	3.31×10^{-6}
1	0.3	1.31×10^{-5}	2.68×10^{-6}
1	0.05	4.01×10^{-5}	3.78×10^{-6}

Appendix E.2 Soil gas concentration surveys

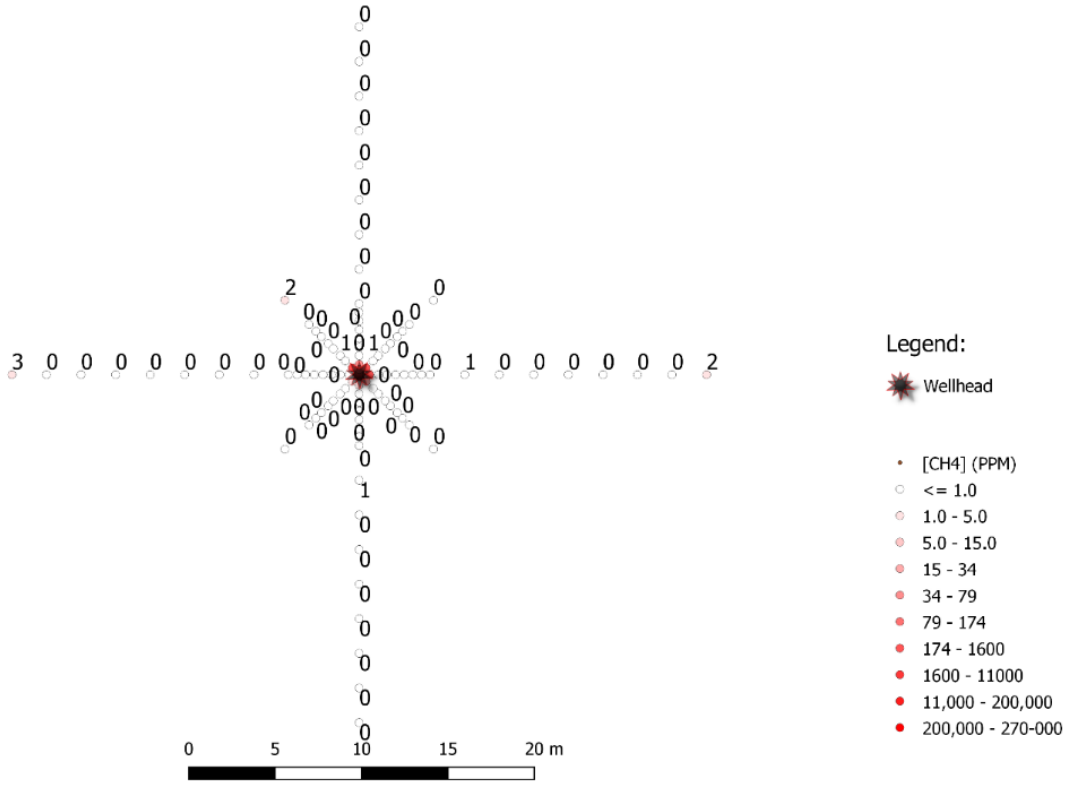

Figure E.2.1 2018-11-21 Soil-surface methane gas concentrations as ppm CH_4 above background levels.

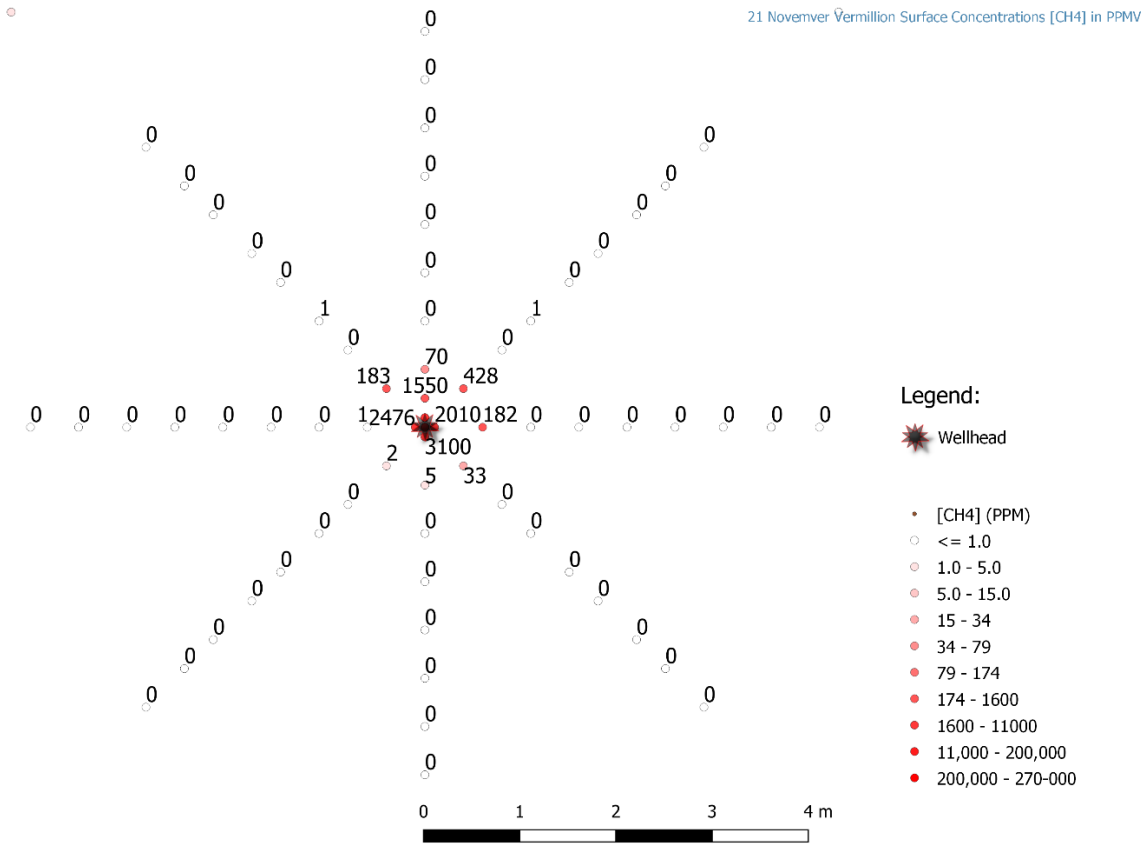

Figure E. 2.2 Zoomed view of 2018-11-21 soil-surface methane gas concentrations as ppm CH_4 above background levels.

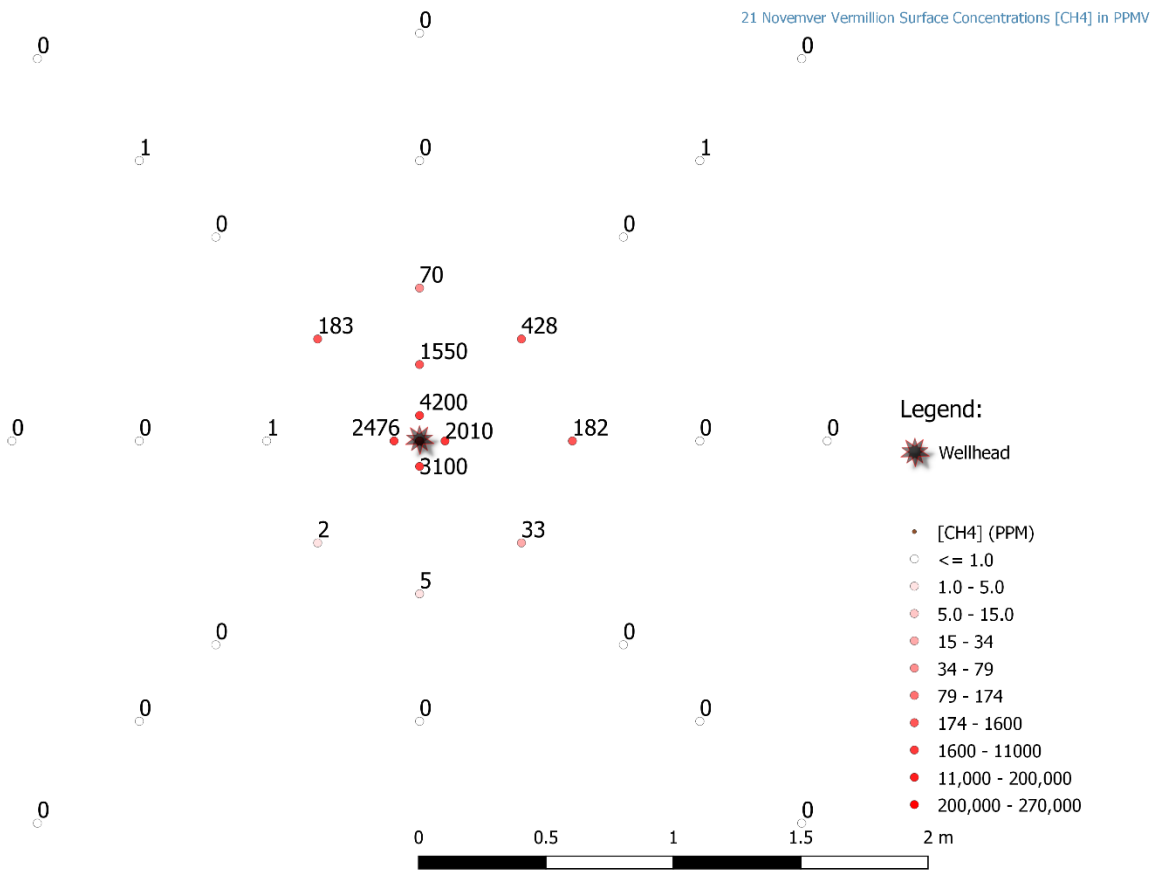

Figure E. 2.3 Close-up 2018-11-21 soil-surface methane gas concentrations as ppm CH_4 above background levels.

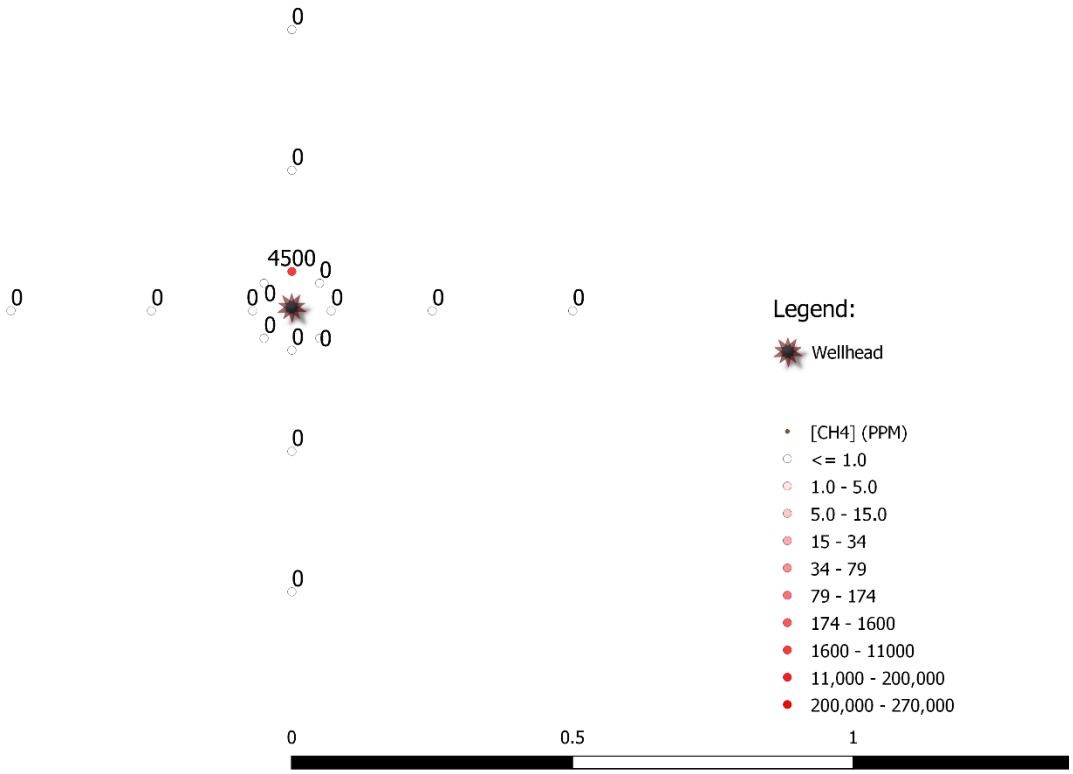

Figure E. 2.4 2019-01-09 soil-surface methane gas concentrations as ppm CH_4 above background levels.

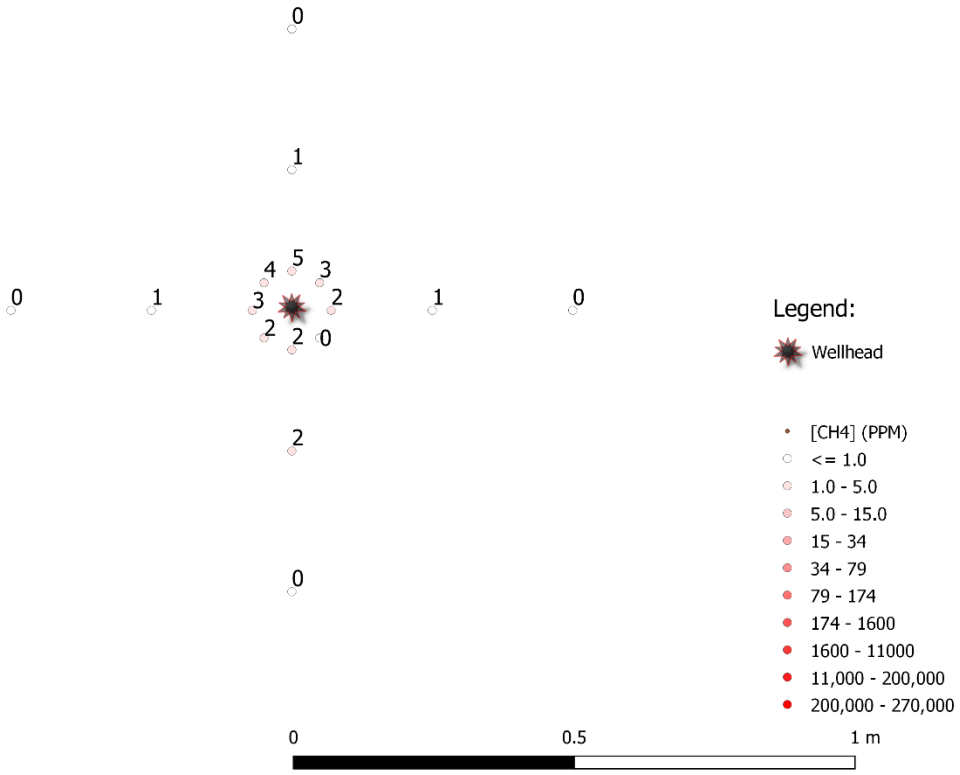

Figure E. 2.5 2019-02-22 soil-surface methane gas concentrations as ppm CH_4 above background levels.

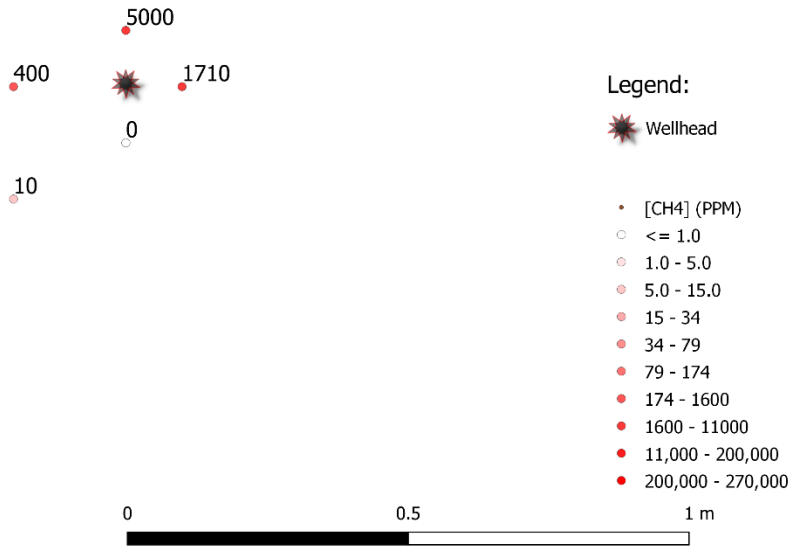

Figure E. 2.6 2019-04-24 soil-surface methane gas concentrations as ppm CH_4 above background levels.

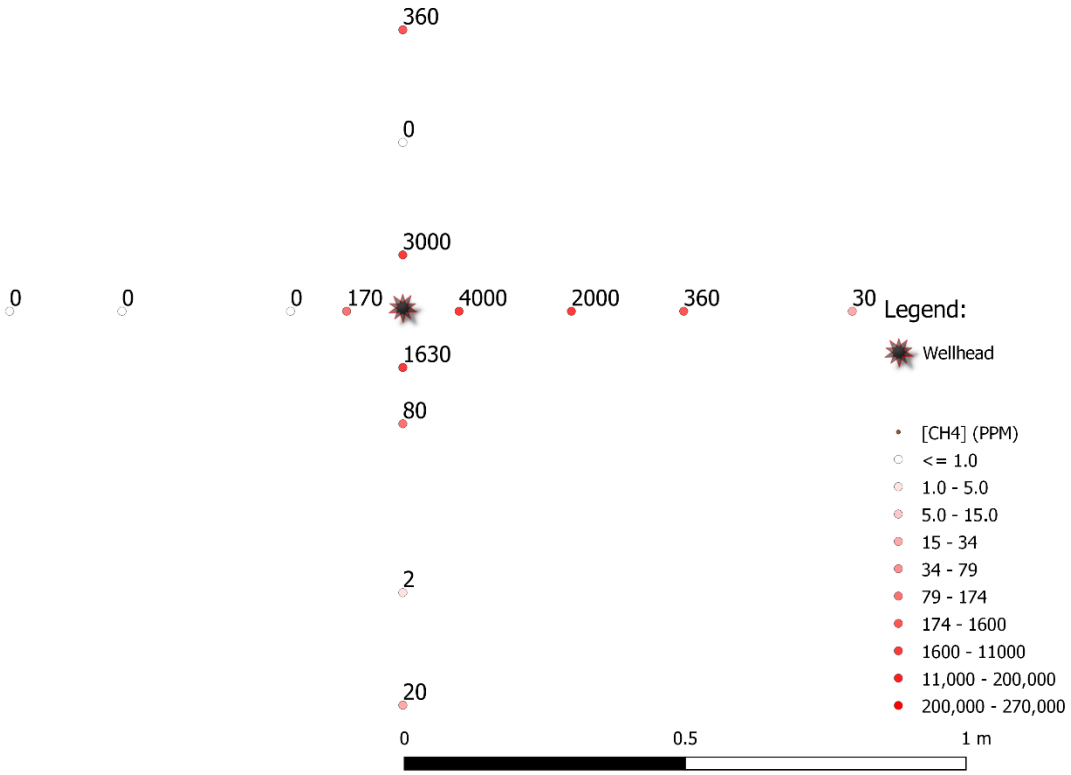

Figure E. 2.7 2019-06-07 soil-surface methane gas concentrations as ppm CH_4 above background levels.

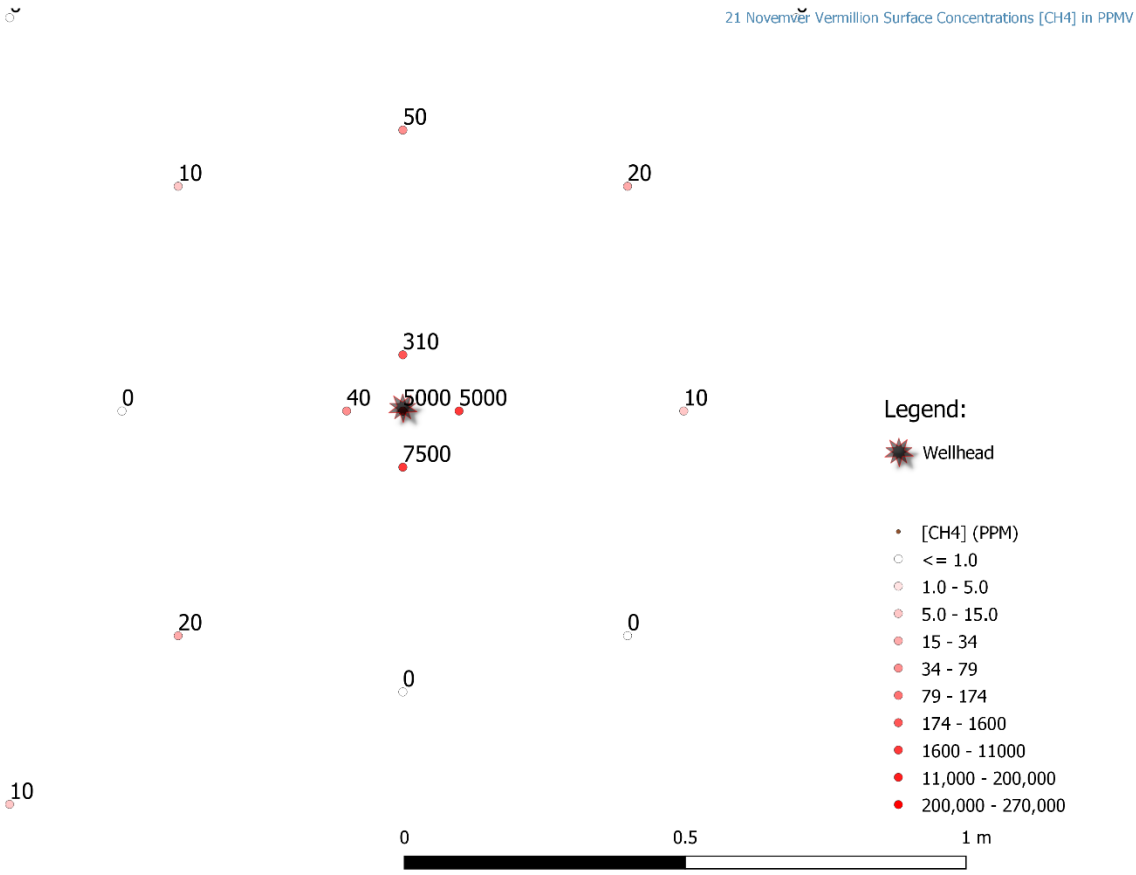

Figure E. 2.8 2019-07-09 soil-surface methane gas concentrations as ppm CH_4 above background levels.

F

Barometric efficiency applications to migrating free-phase gas monitoring

Abstract

Barometric efficiency is the relationship between a change in barometric loading on an aquifer and the observed water level response in piezometers in this aquifer. This parameter is commonly used to infer the storage properties of the aquifer since the compressibility of the aquifer generally depends primarily on the compressibility of the aquifer matrix. Barometric efficiency will also be affected by the content of free-phase gas within an aquifer. Therefore, if aquifer matrix compressibility is assumed to be constant spatially, observed variations in barometric efficiency can be interpreted to be due to variations in free-phase gas saturation. The data presented here are from case-study observations of water level over the winter months in four piezometers, all completed in a silty-sand unconfined aquifer around a petroleum well with gas migration outside the surface casing. The results indicate a plausible explanation for spatially variable barometric response due to differences in subsurface free phase gas content. These findings indicate a potential for future application of barometric efficiency as a measure of spatial and temporal variations in subsurface free phase gas content around wells with migrating gas.

Introduction:

Background of Barometric loading:

When a barometric load is applied to an aquifer, for example due to increased atmospeheric pressure during a passing high-pressure weather system, the change in total stress on the formation is partially borne between the formation matrix and the fluid, causing slight compression of the formation and a rise in pore pressure (Heim, 2016). Conversely, the

barometric load in a well or piezometer that is open to the atmosphere is transferred entirely to the water surface, resulting in an immediate rise in total downhole pressure measured in the piezometer (Figure F1). This loading causes an imbalance in pressure between the well and aquifer water pressure, which is eventually equalised through water flow from the well to the formation. The end result of this equalisation is a lower water level and a lower apparent piezometric pressure after the water levels have been barometrically compensated (for example, by subtraction of barometric pressure from total logger pressure in Solinst Levelogger software). Following a loading or unloading event, the ratio between water and barometric pressure changes is described by the barometric efficiency, BE, defined as:

$$BE = \frac{\Delta_{Water\ Level}}{\Delta_{Barometric\ Pressure}}$$

The BE typically ranges from 20 to 75% in confined aquifers, and between 80 to 100 % in unconfined aquifer (solinst.com). Related to BE, the Barometric Loading Efficiency:

$$\bar{B} = 1 - BE$$

is obtained from the barometric efficiency, and indicates the proportion of the barometric pressure load that is borne by the formation. A perfectly elastic formation would transfer all barometric pressure to a pore fluid rise and therefore $\bar{B} = 0$.

In addition to the compressibility of the formation, the compressibility of the pore fluids will also impact barometric efficiency. A more compressible pore fluid (such as one containing a higher volume fraction of free-phase gas) will have a lower pore pressure rise in response to a loading event in comparison to an aquifer with a less compressible fluid. In return, the aquifer

with the more compressible pore fluid will have a greater water level change in the well following a loading event, and therefore a higher barometric efficiency (Figure F1).

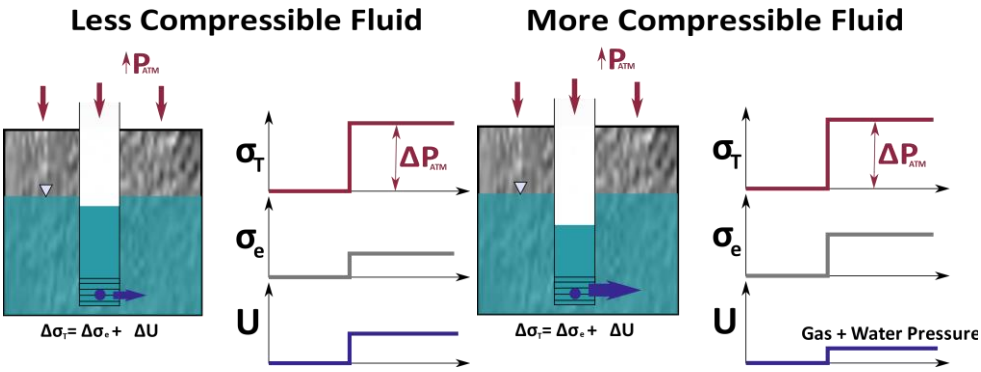

Figure F1 Conceptual response to water level in two piezometers immediately following an increase in atmospheric pressure (P_{ATM}). The increase in atmospheric pressure initiates an increase in total stress, σ_T, which then causes an increase in both the effective stress, σ_e and aquifer pore pressure, U. Conversely, the pressure in the well increases to the full extent of the atmospheric pressure increase. Water flows out of the well to equalize the lesser increase in pore pressure in the formation. Differences in this barometric response exist due to differences in aquifer properties, including the content of free-phase gas. Conceptual diagram after Heim, 2016.

Previous Work:

Previous researchers have used water well response to loading events such as barometric pressure variations, or atmospheric, earth, or ocean tides, to estimate properties of the subsurface through the relationships between the loading and observed subsurface pressure changes (Jacob, 1940; Rojstaczer, 1988; Bailey, 2017). The parameter that describes storage in an aquifer (specific storage) is a function of the aquifer compressibility, and is a common application of calculated barometric efficiency relationships in confined or semi-confied aquifers (Turnadage et al., 2019). Other parameters (such as pneumatic and hydraulic diffusivities) can also be calculated by using frequency-dependant responses to loading (Rojstaczer, 1988). One accepted

method for barometric efficiency analysis is the Fourier analysis method, which is relatively simple and allows for spatial comparisons between wells (Turnadage et al., 2019).

Unconfined or shallow aquifers can exhibit a water level response to barometric pressure variations, similar to confined aquifers (Peck, 1960). Hare and Morse (1977) saw this phenomenon and attributed it to the presence of a clay cap within an isolated portion of the aquifer, causing artificial confinement of the aquifer and barometric efficiencies of 93% despite shallow depths. Turk (1975) observed daily water table variations on the order of 1-6 cm/day in a fine-grained sediment unconfined aquifer, and attributed these variations to diel atmospheric pressure variations acting on compressible air entrapped within the capillary fringe. The presence of entrapped (and compressible) gases allows for significant water table variations in response to barometric responses changes, even in the absence of a confining layer, a phenomenon which has been further tested in a laboratory setting (Peck, 1960, Turk, 1975). The size of entrapped air bubbles in the capillary fringe will vary with overlying water and air pressures as a linear response defined by the ideal gas law, as demonstrated by a lab and modelling experiment using compacted silt (Marinas & Roy, 2013).

In natural systems, the presence of free gas within shallow aquifers, introduced through entrapment, varying water levels, or geochemical reactions, has important physical and geochemical implications. Gases may also be introduced by anthropogenic processes, either intentionally (e.g., through air sparging) or accidentally (as in the case of gas migration). The presence of gas within formation pore space will modify the effective hydraulic conductivity of the upper aquifer unit and cause it to behave as a semi-aquitard with preferentially vertical flow

through the gas-saturated zone (Ryan et al., 2000). Free gas will also dissolve and potentially induce geochemical changes (Van de Ven & Mumford, 2020; Roy et al., 2016).

Since the storage parameter of an aquifer is a function of both the compressibility of the reservoir matrix and the fluid (and the solid particles to a negligible amount), some researchers have used the loading response derived storage estimate to determine gas saturation. Sato (2006) used earth-tide pressure responses in a reservoir for carbon dioxide sequestration to estimate the free gas saturation. Heim (2016) proposed that these methods could also be used to estimate gas saturation for other applications such as air sparging or other situations where gas is injected into the subsurface. This method was demonstrated for a deeper petroleum well subject to ocean tide loading, with higher gas saturation, and a terrestrial well with barometric loading only (and limited estimated gas saturation; Heim, 2016).

Motivation:

Four shallow monitoring wells were hand-installed at a gas migration research site for the purposes of shallow groundwater sampling. All wells were completed within the upper silty-sand aquifer at a 1 m depth, with variable distance from a subsurface free-phase methane gas source caused by gas migration outside the casing of a petroleum well. Water levels were recorded hourly using automated loggers for determination of water table depth changes seasonally. Strong quasi-diurnal and multi-day cyclic fluctuations in piezometer water levels, with magnitudes up to several cm, were observed in all four piezometers (Figure F2). Literature review and preliminary data analysis attempting to explain these fluctuations led to indications that the interaction of subsurface free-phase-gas and barometric pressure changes may be causing the observed variation. Subsequent data analysis, presented here, then investigated the hypothesis

that difference between the wells in relative barometric efficiency may be related to spatial variations in subsurface free-phase-gas contents which had entered into the shallow aquifer as a consequence of gas migration. This appendix section presents the methods and outcomes of this investigation, and relates findings to potential for future study.

Methods

Field Data

Water levels were recorded hourly from 2019-12-13 to 2020-02-07 at four different shallow monitoring wells at the gas migration field research site. Wells were completed with 45 cm screens centered at 1m depth below ground surface (BGS). The monotiroing well locations were 1.25 m South of the petroleum well, 10m South, 10m North, and a ‘Background Location’ approximately 42 m NW at the corner of the well pad. Previous slug testing and permeameter analysis determined the horizontal hydraulic conductivity to be $3 * 10^{-6}$ m/s (Table E.1, E.2) in this silt and fine-sand unconfined aquifer.

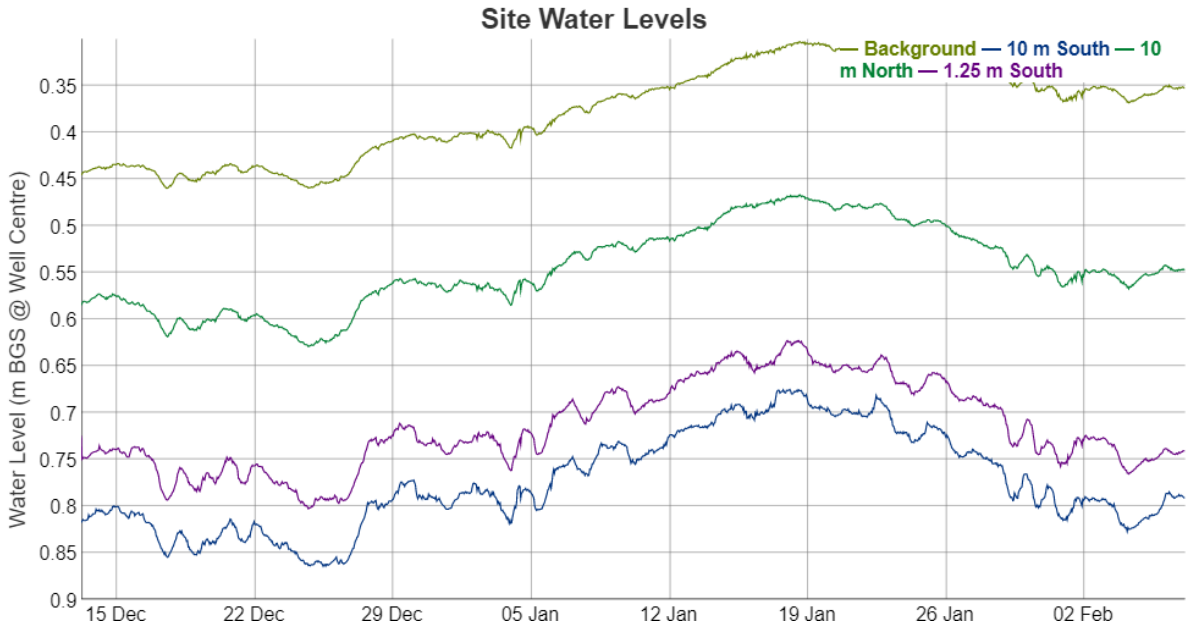

Figure F2 Wintertime water levels showing the shallow water table and periodic variations on the order of 2-3 cm

Data Analysis Methods

Data was imported from barometrically compensated level logger and barologger data (Solinst). Barometric compensation was completed in Solinst Levellogger 4.4.0 using the built-in procedure which subtracts the measured atmospheric pressure from the level-logger pressure at each hourly measurement point, leaving only the pressure due to the height of water above the logger in the well. Raw pressure measurements were all converted to equivalant pressures as meters of fresh water. Water levels were compared to ground surface elevation datum at the location of the petroleum well (Figure F2).

Equivalent water pressure measurements were all normalised to show the relative pressure above or below the average of the first five measurements, thereby converting all time series to the same scale centered on zero m water pressure. Next, the Fast Fourier Transform function (FFT) was used to convert each time series into the frequency domain (Turnadage et al.,

2017). Short term time series fluctuations (noise) and long-term variations (ostensibly due to seasonal changes and longer-term meteorological events) were removed through the application of a band pass filter between the frequencies of 6 hours and 5 days. The reverse FFT function then reverted the data back to the time domain. This filtering procedure was applied to all four barometrically compensated water level time series and the barometric pressure time series. The barometric loading pressure was then cross plotted against the piezometer water pressure for each of the wells. These plots were fitted with a linear best-fit line, where the slope is equal to the barometric efficiency (Robinson & Bell, 1971).

Using a method outlined by Heim (2016), based on methods by Jacob (1940) and Chen et al. (1995), the gas saturation was then calculated using reasonable assumptions of the matrix compressibility (Table F1). These methods rely on the fact that barometric loading efficiency is a function of the compressibility of the formation which is in turn a function of the compressibility of the formation matrix, and formation fluid (including both the water and gas components). The compressibility of the solid grains is assumed to be negligible.

Firstly, the compressibility of the soil matrix, C_p' is calculated using assumed values for the confined modulus of elasticity.

$$C_p' = \frac{1}{n * B_b'}$$

Where n is the porosity and B_b' is the confined modulus of elasticity, calculated with:

$$B_b' = \frac{3(1-\gamma)}{1+\gamma} B_b$$

Where γ is the Poisson's Ratio and B_b is the soil elastic modulus.

The barometric efficiency (BE), determined as the slope of the cross-plot of filtered barometric vs. hydraulic pressure, is used to determine the barometric loading efficiency, $\bar{B}$, with an assumption of incompressible solid grains (C_s=0; Jacob, 1940).

$$\bar{B} = 1 - BE$$

The compressibility of the formation fluid, C_f, is then calculated using the measured barometric loading efficiencies and the calculated matrix compressibility.

$$\bar{B} = \frac{C_p'}{C_p' + C_f}$$

Which is re-arranged to:

$$C_f = \frac{C_p'}{\bar{B}} - C_p'$$

Where $\bar{B}$ is the barometric loading efficiency, C_f is the compressibility of the pore fluid (Pa^{-1}), and C_p' is the compressibility of the formation matrix (Pa^{-1}).

The gas saturation, S_g, is then calculated using standard literature values for the compressibility of water and the compressibility of gas (Table F1).

$$S_g = \frac{C_f - C_w}{C_g - C_w}$$

The specific storage of the formation was also calculated using the calculated fluid and matrix compressibility (Fetter, 2001)

$$S_s = \rho_w g\left(C_b' + nC_f\right)$$

Where ρ_w is the water density (assumed to be 1000 kg m^{-3}), g is the acceleration due to gravity (9.8 m s^{-2}), and C_b' is the bulk matrix compressibility (Pa^{-1}), n is the assumed porosity, and C_f is the fluid compressibility.

Results and Discussion

The barometrically compensated water levels indicate a higher water table at the 10N and 'Background' wells, suggesting a primarily southward hydraulic gradient and groundwater flow direction. Wintertime temperatures were consistently below freezing, suggesting precipitation would be stored as snow, with consequently negligible recharge into the aquifer. Electrical conductivity and temperature measurements were used to verify that the loggers were measuring the pressures of liquid water within the piezometers over the monitoring period. All wells froze later in the winter season. Unfiltered barometrically compensated water levels varied on quasi-daily cycles and on longer-term trends (Figure F2). Following the FFT filtering procedure, the resultant filtered water level series showed smaller pressure variations which cyclically varied with a more consistently apparent inverse relationship to barometric pressure (Figure F3).

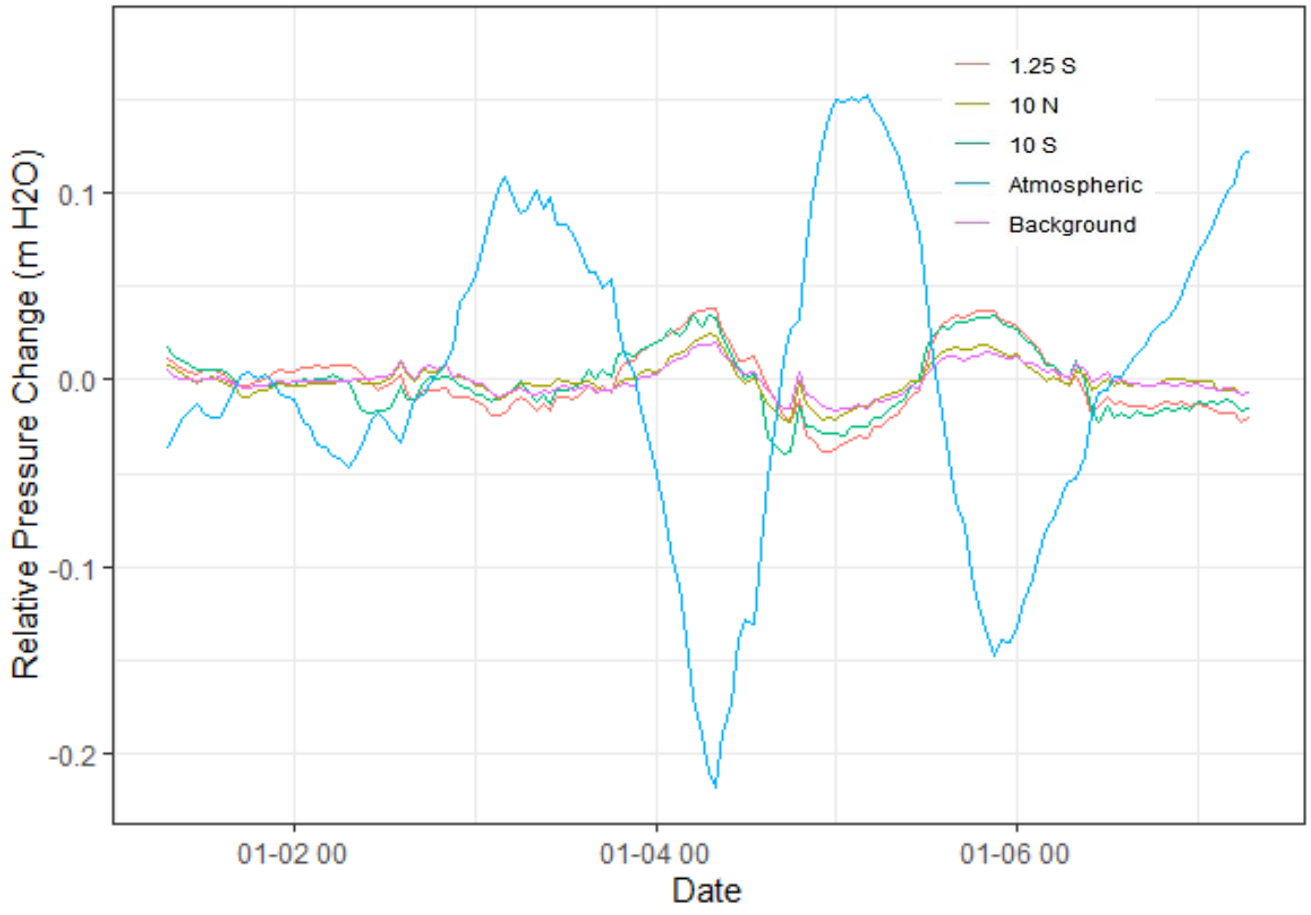

Figure F3 Time series water levels following band pass filtering, showing barometric pressure variations (blue) in comparison to piezometric pressures. Vertical lines show 24 hour increments.

Subsequent cross-plotting of the filtered hourly data show a relatively linear relationship between rising barometric pressure and lower measured water levels (Figure F4). Best-fit linear trendlines indicate a calculated barometric efficiency ranging from 0.39 to 0.17, with a higher barometric efficiency (i.e. steeper regression relationship between P_{ATM} and water pressure) closer to the wellhead with measured gas migration.

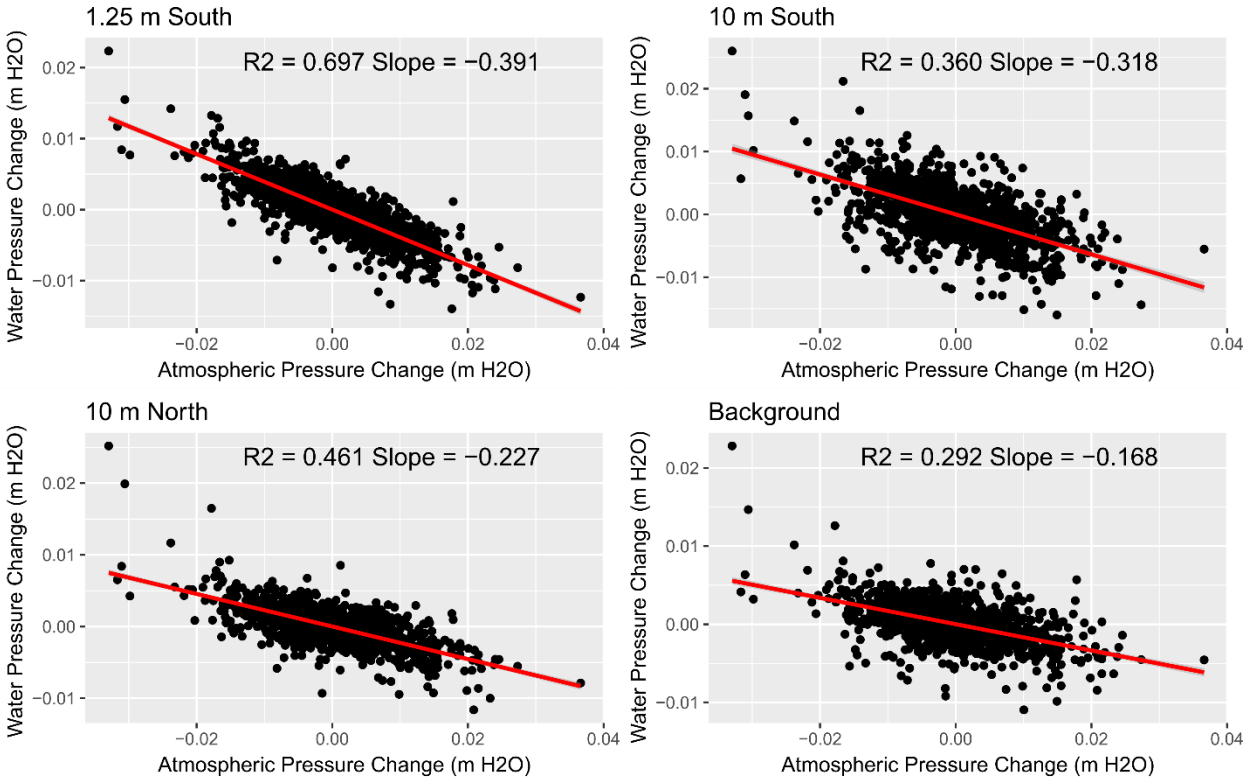

Figure F4 Atmospheric pressure change vs. water level pressure change for four monitoring wells, fitted with a least-squares fit linear regression.

The assumed aquifer and fluid parameters were kept constant when calculating the gas saturation for the four different wells across the well pad (Table F1). Considering the calculated barometric efficiencies and the assumed soil properties, the computed gas saturations in the shallow aquifer were between 2.8-3.4%, with higher saturations closer to the petroleum well (Table F2). Computed specific storage ranged from 2.3 to 2.6 $*10^{-3}$ m^{-1}, which is within the range of literature values for a loose sand (considered equivalent to the unconsolidated silty sand observed on-site; Batu, 1998).

Table F1 Calculated and assumed input parameters used in the gas saturation calculations.

Assumed Parameter		Value	Units	Source
Poisson's Ratio	γ	0.3	~	Silty Sand: Structx.com https://structx.com/Soil_Properties_004.html
Soil Elastic Modulus (Young's)	B_b	10	MPa	5-20 Mpa for silty sand: from https://structx.com/Soil_Properties_003.html
Porosity	n	0.35	~	Site estimate using Hydraprobe soil moisture content
Water Compressibility	C_w	$4.60 * 10^{-10}$	Pa^{-1}	(Engineering Toolbox)
Gas Compressibility	C_g	$7.65 * 10^{-6}$	Pa^{-1}	(Engineering Toolbox)
Solid Grain Compressibility	C_s	0	Pa^{-1}	Assumed. (e.g., Fetter 2001)
Porosity	n	0.38	cm^3/cm^3	Based on Hydraprobe soil moisture measurements with assumed full saturation
Barometric loading efficiency	$\bar{B}$	0.61-0.83	m/m	Filtered linear best-fit of atmospheric and water pressure field data.

Table F2 Calculated parameters including barometric efficiencies and free gas pore saturations at four groundwater monitoring well locations around the gas migration case study wellsite.

Well Location	Barometric Efficiency, BE	Barometric Loading Efficiency, $\bar{B}$	Compressibility of the Fluid (Pa^{-1})	Gas Saturation (%)	Specific Storage (m^{-1})
1.25 S	0.39	0.61	$2.90 * 10^{-7}$	3.8	$2.59 * 10^{-3}$
10 S	0.36	0.64	$2.76 * 10^{-7}$	3.6	$2.54 * 10^{-3}$
10 N	0.23	0.77	$2.30* 10^{-7}$	3.0	$2.38 * 10^{-3}$
43 NW	0.17	0.83	$2.13* 10^{-7}$	2.8	$2.32 * 10^{-3}$

A brief sensitivity analysis on the assumed literature values for the Young's Modulus for the silty sand soil demonstrated a large range in potential gas saturations between the end

member literature values of 5 to 20 MPa (Table F3). The range in gas saturations between 1.3% and 7% demonstrates that the varying barometric efficiencies could plausibly be caused by spatial differences in soil elastic modulus instead of the free gas content. However, the spatial distribution in barometric efficiencies and resultant free gas content is consistent with the expected spatial distribution of gas within the aquifer based on measured effluxes, gas concentrations, and the literature understanding of free gas accumulation in subsurface (Steelman et al., 2017; Van de Ven and Mumford, 2020; Fleming et al., 2021).

Table F3 Sensitivity analysis of variable assumed soil elastic modulus (B_b) on resulting calculated free gas pore saturations considering the calculated barometric efficiencies at each well.

	B_b (Mpa)	
	5	20
Well Location	**Sg (%)**	
1.25 S	7.0	1.7
10 S	6.6	1.7
10 N	5.5	1.4
43 NW	5.1	1.3

Conclusion

Briefly, from the analysis presented here it can be concluded that that:

i) Barometric efficiency techniques applied to water level-barometric response variations at this research site, reasonably explain the measured hourly-to-daily time-series variations groundwater pressure variations.

ii) Using published techniques and assumed fluid and aquifer parameters (which were also assumed not to vary spatially), the free phase gas saturation values estimated from the calculated barometric efficiencies ranged from 2.8% to 3.8%.

iii) The potentially large sensitivity to assumed parameters using literature values, and further refinement (or field determination of these values) would be required for more accurate estimation of gas saturation.

iv) The estimated spatial distribution with higher gas saturations near the petroleum well was consistent with expectations based on previous site characterization.

Future work developing this method may show potential for spatial free-phase gas assessment or minimally intrusive long-term monitoring of free gas contents and migrating gas extent within the shallow subsurface.

Additional References for Appendix E

Bailey, B. 2017. Assessing the utility of barometric response functions in estimating hydrogeological parameters of the High Plains Aquifer (Doctoral dissertation, University of Kansas).

Batu, V. 1998. Aquifer hydraulics: a comprehensive guide to hydrogeologic data analysis. John Wiley & Sons. pp 59

Marinas, M., Roy, J. W., Smith, J. E. 2013. Changes in entrapped gas content and hydraulic conductivity with pressure. *Groundw*. 51(1), 41-50.

Hare, P. W., Morse, R. E. 1997. Water-level fluctuations due to barometric pressure changes in an isolated portion of an unconfined aquifer. *Groundw*. 35(4), 667-671.

Heim, V. L. 2016. Feasibility of Using Ambient Fluctuations of Pore Pressure to Characterize Gas Saturation and Other Formation Properties (Masters dissertation, Clemson University).

Jacob, C. E. 1940. On the flow of water in an elastic artesian aquifer. *Eos, Transact. Am. Geophys. Union*. 21(2), 574-586.

Peck, A. J., 1960. The water table as affected by atmospheric pressure, *J. Geophys. Res.* 65, 2383–2388,

Rojstaczer, S. 1988. Determination of fluid flow properties from the response of water levels in wells to atmospheric loading. *Wat. Resour. Res*. 24(11), 1927-1938.

Rosenberry, D. O., Glaser, P. H., Siegel, D. I., Weeks, E. P. 2003. Use of hydraulic head to estimate volumetric gas content and ebullition flux in northern peatlands. Wat. Resources Research, 39(3).https://doi.org/10.1029/2002WR001377

Ryan, M. C., MacQuarrie, K. T. B., Harman, J., McLellan, J. 2000. Field and modeling evidence for a "stagnant flow" zone in the upper meter of sandy phreatic aquifers. *J Hydrol.* 233(1-4), 223-240.

Sato, K. 2006. Monitoring the underground migration of sequestered carbon dioxide using Earth tides. *Energy Conversion Manag.* 47(15-16), 2414-2423.

Turk, L. J. 1975. Diurnal fluctuations of water tables induced by atmospheric pressure changes. *J Hydrol.* 26(1-2), 1-16. https://doi.org/10.1016/0022-1694(75)90121-3

Turnadge, C., Crosbie, R. S., Barron, O., Rau, G. C. 2019. Comparing Methods of Barometric Efficiency Characterization for Specific Storage Estimation. *Groundw.* 57(6), 844-859.

Weeks, E. P. 1978. Field determination of vertical permeability to air in the unsaturated zone (No. 1051). Department of the Interior, Geological Survey.